Winter 2023

# Visual characteristics of walleye pollock and Chinook salmon: Modeling theoretical visual space and target contrast of trawling materials in the Bering Sea

Rebecca Haehn
*Western Washington University*, rebecca.haehn@noaa.gov

**Visual characteristics of walleye pollock and Chinook salmon: Modeling theoretical visual space and target contrast of trawling materials in the Bering Sea**

By

Rebecca Haehn-Tam

Accepted in Partial Completion
Of the Requirements for the Degree
*Master of Science*

ADVISORY COMMITTEE

Dr. Kathryn Sobocinski

Dr. Ellis Loew

Dr. Leo Bodensteiner

GRADUATE SCHOOL

David L. Patrick, Dean

**Master's Thesis**

In presenting this thesis in partial fulfillment of the requirements for a master's degree at Western Washington University, I grant to Western Washington University the non-exclusive royalty-free right to archive, reproduce, distribute, and display the thesis in any and all forms, including electronic format, via any digital library mechanisms maintained by WWU.

I represent and warrant this is my original work and does not infringe or violate any rights of others. I warrant that I have obtained written permissions from the owner of any third-party copyrighted material included in these files.

I acknowledge that I retain ownership rights to the copyright of this work, including but not limited to the right to use all or part of this work in future works, such as articles or books.

Library users are granted permission for individual, research, and non-commercial reproduction of this work for educational purposes only. Any further digital posting of this document requires specific permission from the author.

Any copying or publication of this thesis for commercial purposes, or for financial gain, is not allowed without my written permission.

Rebecca Haehn-Tam

# Visual characteristics of walleye pollock and Chinook salmon: Modeling theoretical visual space and target contrast of trawling materials in the Bering Sea

A Thesis
Presented to
The Faculty of
Western Washington University

In Partial Fulfillment
Of the Requirements for the Degree
*Master of Science*

By
Rebecca Haehn-Tam
June 2023

**Abstract**

Walleye pollock (*Gadus chalcogrammus*) and Chinook salmon (*Oncorhynchus tshawytscha*) are important economic and cultural resources in the Alaska large marine ecosystem (LME). Chinook salmon bycatch is a large concern within the pollock fishery. Current strategies to reduce salmon bycatch include modifying trawl gear by implementing artificial light near or on escapement panels to increase salmon escapement from the net. The visual systems among fish species are known to have different spectral sensitivities and classes. The visual characteristics of pollock and Chinook salmon, which are caught together in the pollock fishery were investigated in an effort to understand differences in the way trawl gear is perceived. The visual pigments of each species were measured using microspectrophotometry (MSP)Walleye pollock were dichromats with spectral sensitivity ranging from 449nm–518 nm and Chinook salmon were trichromats with sensitivity ranging from 436 nm–545 nm. Chinook salmon spectral sensitivity spans a larger range than pollock due to a third visual pigment with maximum absorbance in the 545 nm (green) spectral band located in single and non-identical twin cones. The green opsins within Chinook salmon will activate when stimulated by wavelengths that are outside of the spectral sensitivity of pollock. Blue and blue-green spectral classes were present in both species. Walleye pollock and Chinook salmon photoreceptor classes included single cones, non-identical twin cones, and rods. Microspectrophotometry data defining pollock and Chinook salmon visual pigments, spectral irradiance data from the Bering Sea, and spectral reflectance of commonly used trawl components were input into two visual models, VPModel® and the R package *pavo*. Visual models predict how the organism's visual system responds to visual stimuli. Modeling the spectral distribution and physiological visual characteristics provides an avenue to predict how fish interact and adapt to the changing light environment. Blue targets had the deepest and longest-range critical threshold values. Spectral irradiance availability generally decreased with depth and increasing chlorophyll a concentration. Target contrast against the background space light was dependent on the light environment characteristics including depth. Using the physiological data and theoretical model output allows spectral range and intensity limitations to be considered in future behavior experiments and escapement trials to increase the escapement potential of Chinook salmon in the walleye pollock trawl fishery in the Bering Sea.

**Acknowledgments**

I would like to thank Dr. Kathryn Sobocinski, who chaired my committee, for her unending support, encouragement, and understanding throughout the entire program. I would not have believed it possible to complete a degree while working, get married, and renovate a home without the down-to-earth conversations that we shared during our progress meetings. Special thanks go to Dr. Ellis Loew for agreeing to be on my committee from all the way in New York and for unstintingly sharing his insight and knowledge which guided me through this research. When are you coming back out to Seattle? We will be sure to go out for fried chicken gizzards. Thank you to Dr. Christina Wahl and Marina Loew for opening your home to me while I was working with Ellis. I learned that I love your homemade lemon pickle amidst the myriad of scientific knowledge I gained that week! I am grateful to Dr. Leo Bodensteiner for his participation on my committee and for coming up with great questions and ideas for me to ruminate over. Dr.'s Lyle Britt and Noëlle Yochum provided me with so much inspiration and help throughout the entire process from conception to implementation. Lyle- I would not have discovered the world of visual ecology without you. Thank you to my college Chris Anderson for assisting with the spectral reflectance data collection. He is much more adapted to chilly winter weather than I am. Dr. Alison Deary was always on hand to talk with or practice talks. She reminded me every day that I could complete this program and what were reasonable expectations for myself. Within the AFSC-GAP group, Dr.'s Sean Rohan and Duane Stevenson deserve recognition for making themselves available for discussion and I did plenty of book borrowing from Sean's library. My participation in this program was made possible through funding provided by the NOAA Fisheries Academic Studies Program.

My completion of this project would not have been possible without the love and support of my family. I'm grateful to Lawrence Tam and Ashe for understanding why I was away from home every week for 3 quarters and for the weekends when I was at home, but really I'd be at the office working for a few hours in the morning trying to finish up schoolwork. My mom and dad always asked about my progress, cheered me on, and listened to my complaints when I couldn't find enough hours in the day. My family always believed in me even when I wasn't sure I could believe in myself. Special thanks to all my friends for picking our friendship back up after I spent 2 years not having enough mental bandwidth to even text you back (although you all should have received New Year's cards). Now we can check this thesis off my list!

## Table of Contents

## List of Figures and Tables

## Introduction

*Bering Sea walleye pollock fishery and Chinook salmon bycatch*

Walleye pollock (*Gadus chalcogrammus*) is an important economic resource in the Alaska large marine ecosystem (LME). Chinook salmon (*Oncorhynchus tshawytscha*) is an economically beneficial resource, significant cultural icon, and subsistence fishery for the Alaska Native peoples within the same LME. Chinook salmon and pollock spatially overlap in the southeast portions and outer shelf edge of the Bering Sea where the pollock fishery operates (Stram and Ianelli 2009). A large concern within the pollock fleet and fisheries management is the bycatch of Chinook salmon.

Bycatch reduction efforts in fisheries are mandated by the Magnuson-Stevens Act (MSFCMA, 2007). The reduction of salmon bycatch in the pollock fishery has been a priority of fishing and conservation engineering groups since 2002 (Stram and Ianelli 2015). Fishermen and conservation engineers have worked to support management efforts by designing additions to fishing gear that attempt to reduce salmon bycatch. The design and development of excluders on trawl nets provide salmon with a way to clear the net before being landed. Current designs rely on water flow, direction, and speed to direct salmon toward escapement panels (Yochum et al. 2021). These methods ae not 100% effective, prompting research and design of alternative approaches

The Eastern Bering Sea pollock fishery comprises approximately 40% of the global pollock catch. Fishing effort is generally distributed on the southeast area of the shelf during the winter fishing season and on the shelf edge during the summer season (Stram and Ianelli 2009, 2015,

Ianelli et al. 2021). While the overall bycatch rate for all species is small (~1.2% by weight) within the pollock fishery, the overall impact on species collected as bycatch is large due to the sheer number of metric tons caught by the fishery (2017-2021 average of  1.23 million metric tons; “NOAA Fisheries: Landings” 2023). Chinook salmon bycatch in the pollock fishery peaked in 2007 (116,329 individuals) and has mostly remained below 30,000 individuals since that time; exceptions were in 2017 when 30,078 Chinook salmon were caught as bycatch and in 2020 when 32,204 individuals were caught (Ianelli et al. 2021).

In the eastern Bering Sea, pollock abundance is concentrated north of the Pribilof and Zemchug Canyons and east of Pervenets Canyon (McCarthy et al. 2020). Walleye pollock are broadly distributed between the 50 and 200 m isobath (Stienessen et al. 2022). Pollock’s mean depth from the surface was 85 m in the area east of 170°W and 96 m west of 170°W; however, vertical distributions have varied over the years (Honkalehto and McCarthy 2015). The mean vertical distribution for 93% of adult pollock was within 50 m of the benthic substrate (Honkalehto and McCarthy 2015).

Chinook salmon inhabit a large spatial area from northern California to the Chukchi Sea in Alaska. During the winter, evidence of Chinook salmon inhabiting the Bering Sea near the Alaska Peninsula and slope edge is provided by the catch data within the commercial pollock fishery and one  archival tag from a Chinook salmon placed in 2002 and recovered in 2004 (Walker and Myers 2009). Studies investigating vertical distribution data from Chinook salmon using archival tags are data-limited due to low sample sizes, thus inferences must be made with care. The reported maximum depth during the day was 125 m and the maximum depth at night

was 84 m (Walker et al. 2007). Movement during the day was characterized by vertical motion throughout the water column, whereas nocturnal movement was at a relatively stationary depth (Walker et al. 2007). These data suggest the vertical pelagic distribution of pollock overlaps with adult Chinook salmon, particularly during hours of daylight. This conclusion was supported by anecdotal evidence obtained from fishermen actively participating in the pollock fishery (S. Harrigan, *pers. comm.*).

Populations of West Coast Chinook salmon, including populations in Alaska, have dramatically decreased since the 1980s, and there is limited understanding of survival during the marine phase (Welch et al. 2021, Beamish 2022). Recent conservation management measures include changing the spatial distribution of the fishing fleet to avoid salmon bycatch, enumerating and tracking 100% of the salmon bycatch, redistributing the fishing fleet's total allowable catch (TAC), implementation of an industry-proposed incentive program, and prohibited species catch limits that close the fishery when reached (Ianelli et al. 2021). Since 2011, nearly 100% of pollock fishery operations are monitored by a scientifically trained observer (Ianelli et al. 2022). The pollock fleet actively participates in these mitigation measures to reduce the impact of Chinook salmon bycatch on regional stock groups.

Chinook salmon is a highly valued bycatch species and thus protection of regional stock groups is a priority for managers. Bycatch impacts are evaluated primarily through biological and catch data collected through the AFSC Fisheries Monitoring and Analysis Division. The impact assessment of Chinook salmon bycatch has been re-evaluated as more genetic data have become available. The data indicate that reductions in bycatch since 2008 have decreased impacts on

western Alaska Chinook salmon stocks (Ianelli and Stram 2015). Genetic analysis reveals that the majority of Chinook salmon captured in the pollock fishery originate from coastal Western Alaska (40%) and British Columbia stocks (25%) (Guthrie III et al. 2021). The remaining proportion is divided relatively equally between North Alaska Peninsula and West Coast U.S. stocks. The sustainability of individual regional groups is a management challenge for mixed-stock species, such as Chinook salmon.

At-sea conservation measures that target the salmon bycatch in commercial fisheries focus on shifting spatial areas and gear avoidance or reduction devices. Integrating mechanistic physiology and behavioral drivers is a critical link to understanding fishes within their environments and how they interact with fishing gear. Visual sensing of trawl gear can affect the behavioral responses, such as changes in speed or direction, of fishes in the trawl path (Zhang and Arimoto 1993, Glass and Wardle 1995, Ryer and Olla 2000, Liao 2007, Arimoto et al. 2010). Incorporating mechanistic drivers, like fish visual ecology at a species-specific level into fisheries science can provide insight into fish behavioral responses to changes in their environment (Horodysky et al. 2015) and increase conservation effectiveness. Bycatch reduction of Chinook salmon by the pollock fishery continues to be critically important as declines in West Coast and Alaska stocks persist. Applying visual system principles and species-specific physiology to bycatch reduction efforts could potentially increase the effectiveness of conservation measures implemented within the pollock fleet by using high or low-contrasting materials that can be detected by the Chinook salmon visual system.

*Fish vision*

Light is defined as that part of the electromagnetic spectrum that stimulates the visual system. Most fish visual systems have developed and adapted responses to the photic properties of the underwater environment. Visual systems are an important component in investigating fish behaviors such as communication (Wilkins et al. 2016), mating or territory defense (Whitney 1969, Kodric-Brown 1998), foraging, and survival (Aksnes and Giske 1993, Ryer and Barnett 2006). Fishes that rely on vision for survival mechanisms such as foraging and predation avoidance are constrained by the light intensity and spectral range within their environment (Loew and McFarland 1990, Beauchamp 1994, Beauchamp et al. 1999, Partridge and Cummings 1999, Marshall et al. 2003). Fish response to the changing visual environment can impact spatial distribution and fine-scale patterns in habitat selection. Thus, understanding the mechanisms of fish physiology links environmental conditions to behavior and survival (Horodysky et al. 2015).

*Light environment*

Light is the portion of the electromagnetic spectrum that stimulates the visual system. Light level (intensity) and wavelength availability (chromaticity) are drivers of the evolution of vision underwater. Light intensity and wavelength range are directly affected by habitat characteristics, such as turbidity, dissolved organics (gelbstoff), zooplankton composition and abundance, phytoplankton composition and abundance (e.g., chlorophyll), and depth. Visual adaptations of fishes to light intensity and wavelength are evidenced in morphology (eye placement and size), retinal histology (receptor types, number, and size), and physiology (photoreceptor type and visual pigments; Martinez et al. 2021).

The spectral distribution of light underwater is determined by scattering and absorption as the solar radiance moves through the water column (Jerlov 1968). In general, as depth increases the intensity decreases and the bandwidth narrows. Light is usually available to fishes at depths greater than 100 m (Levine and MacNichol 1982), but the distribution of wavelengths with depth or horizontal distance depends on the water's characteristics. For clear oceanic waters, the resulting bandwidth is centered in the blue wavelength region, and for freshwater containing dissolved organics and/or phytoplankton, the resulting bandwidth shifts towards longer wavelengths. Wavelength-specific spectral property data for water bodies in polar regions are scarce as well as spatially and temporally dependent on when the data were collected. Optical properties of Arctic water bodies have focused on clarity, intensity, and surface reflectance (Naik et al. 2013, Hirawake et al. 2021, Krapivin et al. 2021, Rohan et al. 2021). Spectral property data have been collected on chromophoric (colored) dissolved organic matter and compared to the spectral characteristics in Bering Sea water (Sasaki et al. 2001, Yao et al. 2022) to yield an understanding of the optical properties of the visual environment where pollock and Chinook salmon are found together. Understanding the characteristics of the spectral properties of underwater arctic environments within a fisheries context will add a valuable parameter to fish visual models as well as behavior studies.

*Fish visual physiology*

Fish visual physiology investigations include the identification of photoreceptor cells and visual pigments. Photoreceptor cells are the first step in the visual process; they are cells that absorb light and transmit information through the visual pathway to the brain. Photons absorbed by visual pigments, which are molecules in the photoreceptor cell outer segment, stimulate a

neuronal signal that moves through the retina and ultimately to the visual centers of the brain. Except for some deep-sea fishes, there are two types of photoreceptors found in marine teleost fishes (Douglas, 2001): rods are highly sensitive and subserve black and white or luminosity (scotopic) vision, and cones are less sensitive to intensity and subserve color or chromatic (photopic) vision. The limits of color vision are set by the visual pigments within the photoreceptors. To have color vision, there must be at least two distinct cone classes with overlapping spectral sensitivities.

The spectral sensitivity of individual photoreceptors is determined by the visual pigments contained in the outer segment. Visual pigments are composed of a protein moiety (opsin) and a bonded molecule of vitamin A aldehyde (chromophore). The chromophore is either $A_1$ or $A_2$. The $A_2$ form shifts the spectral sensitivities of the visual pigment toward longer wavelengths at the expense of photosensitivity and increased thermal noise (Bridges 1972). The absorption of a photon of light causes a change in the configuration of the visual pigment, ultimately leading to a change in the photoreceptor cell membrane potential. Each visual pigment is characterized by its wavelength at maximum absorbance ($\lambda_{max}$) and the shape of its normalized absorbance spectrum. Dartnall (1953) proposed that when plotted on a frequency as opposed to a wavelength scale, all visual pigments can be described by a common template, which was later refined and validated (Govardovskii et al. 2000). The shape of the absorbance spectrum is Gaussian and becomes leptokurtic at wavelengths with less than 30% of the peak absorbance (McFarland and Munz 1975). This curve is the probability that a visual pigment molecule will absorb a photon at a given energy. Microspectrophotometry is a technique that measures the absorption spectrum of the visual pigment(s) within individual photoreceptor cells. The absorption spectrum of the

visual pigment(s) can be incorporated into visual models that predict the visibility of relevant targets in the photic environment in which the animal is performing relevant behaviors (Loew and Lythgoe 1978, Lythgoe 1984).

Vision, as opposed to simple photoreception, depends on the contrast between a target and the background against which it is being viewed. When the background is part of the water column and the light is evenly scattered, this is defined as spacelight. The spectral placement of visual pigments for a given animal is determined by the background spacelight and the spectral reflectance of relevant targets. This concept has fostered two hypotheses: 1) the sensitivity hypothesis states that the best visual pigment for discriminating an object against a background based on brightness is one that is matched to the spectral distribution of the background spacelight; 2) the contrast hypothesis suggests that to discriminate objects based on their spectral reflectance at least two visual pigments would be needed – one matched to the background and the other offset from the background (Lythgoe 1972, McFarland and Munz 1975, Sabbah and Hawryshyn 2013). The contrast and sensitivity hypotheses were tested within two groups, Indo-Pacific inshore coral reef fishes and tropical pelagic fishes. Researchers concluded that although the hypotheses were not mutually exclusive, the optimal detection of an object was to have a scotopic visual pigment matched to the background (Muntz and McFarland, 1973).

Much of the early (1950s–1970s) visual pigment work assumed that scotopic visual pigments were the most abundant in a retinal extract containing visual pigments. This extraction technique created a retinal extract combining visual pigments from all the photoreceptor cells in the retinal sample. Extraction techniques involved washing the retina, sonic disruption, centrifugation, and

rewashing to separate the opsins from other cellular material. The extracts were then exposed to a spectrophotometer for wavelength absorption analysis. These retinal extracts were a mix of primarily rod and some cone visual pigments since there was no known method to separate the two types of photoreceptors. Retinal extraction was the precursor to microspectrophotometry (MSP). The development of microspectrophotometry has allowed investigations into visual pigment on a much smaller (cellular) scale (Liebman 1972). The ability to differentiate between visual pigments on a cellular level sets the stage for investigations into the visual tasks of the photopic portion of the visual system. The technological advancement of MSP inspired McFarland and Muntz (1973) to reframe Lythgoe's original contrast hypothesis (1966) within the framework of the photopic visual system.

Photopic, or color vision, provides an animal with more information about its visual environment and supports visual tasks associated with behavior. The proposed evolutionary driver behind the development of color vision was to produce the highest possible contrast between an object, or group of objects, and the background by matching or offsetting visual pigments from the spectral distribution of light within the environment (Wallace 1891, Walls 1942, Lythgoe 1966, 1968, McFarland and Munz 1975). Characteristics, including clarity and depth of the photic environment, impose limitations on environmental spectral availability and light intensity. Studies exploring the relationship between visual pigments and underwater spectral characteristics suggest a correlation between cone pigments and water spectral signatures (McFarland and Munz 1975, Loew and Lythgoe 1978, Levine and MacNichol 1979, 1982, Lythgoe et al. 1994). Evolutionary development of matching or offset pigments was dependent on what type of visual task needed to be accomplished: is a dark or reflective target more

important? Clear open oceanic waters contain fish with more short-wave sensitive cone pigments while nearshore fishes have longer wavelength pigments in response to the spectral signatures of their more dynamic environments (Lythgoe et al 1994). As the spectrum and intensity of light narrow, offset pigments were evolutionarily selected to contrast a target against an almost monochromatic background (McFarland and Munz 1975). In highly productive LMEs, such as those within Alaska, midwater and benthic fishes may exhibit offset photopic visual pigments (Loew and Lythgoe 1978).

A secondary aspect to consider when relating pigments and environment is task performance. Visual tasks associated with target recognition, such as prey location, mate recognition, and schooling are related to the spectral range of visual pigments of a fish species at various life stages and its evolutionary history. Using visual pigment range and spectral distribution within the environment to incite responses to visual tasks like prey location and predation avoidance could be beneficial to elicit target approach or repellent behaviors to trawl gear.

*Color detection and discrimination models in visual ecology*

To determine the potential visibility of a particular target to a given animal, three pieces of information must be available. The first is the nature of the light available to irradiate the target. This is best described by the scalar spectral irradiance measured or modeled for the space in which the object is being viewed. The second is the optical characteristics of the target, that is, how it interacts with the scalar irradiance. Combining these two pieces of information allows the calculation of the light available to a visual system ”looking” in the direction of the object using an equation of radiant transfer (Zhang 1997). The third piece of information is the nature of the

”receiver”, that is the eye. Several models that aim to predict what visual pigments would maximize the visibility of objects in a given photic environment are available. Predictive color vision models include the most utilized Receptor Noise Limited (Vorobyev and Osorio 1998), VPModel® (Zhang 1997, Loew and Zhang 2005), bee color hexagon (Chittka and Menzel 1992), Goldsmith tetrahedron (Goldsmith, 1990), and more (see the full review in Renoult *et al*. 2017).

Species-specific photoreceptor sensitivities are potentially correlated with the available environmental light. As might be expected from an evolutionary development perspective, the spectral sensitivity of photoreceptors will overlap with the available spectral distribution of the photic environment. For example, deep-sea fishes have visual pigments confined to the blue part of the spectrum which is congruent with the narrowed spectrum of available light and the reduced intensity characteristic of increasing depth (McFarland and Munz 1975, Loew and Lythgoe 1978, Lythgoe 1984, Bowmaker 1995, Bowmaker and Loew 2008).

Fish visual systems are designed to perform basic visual tasks in the underwater environment but also play a role in susceptibility to fishing gear in commercially harvested species. Trawl gear is a recent addition to the environment within an evolutionary context. Recognition of “new” anthropogenic objects, such as trawl gear, is unlikely to produce an evolutionarily-dictated behavioral response. However, the visual system of some fishes is physiologically capable of detecting luminous or chromatic contrast of different gear materials from the other materials or the background spacelight. Previous studies measured the apparent contrast of trawl gear in tanks to generate equations to predict the visibility of different parts of the gear (Kim and Wardle 1998a). These equations were used in a study modeling underwater radiance of the background

generated by a net (sand cloud) to estimate the theoretical fish visual stimulus field (Kim and Wardle 1998b). Another study examined color effects on the underwater visibility of monofilament. The appearance of monofilament varies with color and angle relative to the sea surface (Wardle et al. 1991). By modeling photoreceptor responses to underwater spectral reflectance of trawl components, fish responses to depth, distance, intensity, and color can be estimated.

*Research questions and hypothesis*

This study is divided into 4 main questions. The first 3 are:

1. What visual pigments are present in the photoreceptor cells of walleye pollock and Chinook salmon?
2. What is the spectral signature (radiance) of trawl gear at depths in the Bering Sea?
3. What are the spectral irradiance characteristics of Bering Sea waters at sites relevant to walleye pollock and Chinook salmon?

The results from these 3 questions will be used as factors in addressing the 4$^{th}$ question:

4. Can walleye pollock and Chinook salmon discern trawl gear underwater?

Using the photoreceptor data, target radiance (trawl material spectra), and background irradiance (water spectra), I use existing visual systems models, the R package *pavo* and VPModel®, to calculate the best pigment pairs and contrast values for the detection of trawl materials by walleye pollock and Chinook salmon. VPModel® maps a 2-D chromatic contrast of targets (spectral reflectance) within the provided environmental and visual-receiver (photoreceptor visual pigments and scotopic/photopic sensitivity) parameters. The critical thresholds of range

and depth are calculated using the parameters provided. An iterative process then produces the 'best' visual pigment pair suited to detect the target. The R package *pavo* collates a framework for analyzing and visualizing spectral data. This package supports multiple spectral curve file types and simplifies exploring, aggregating, smoothing, and visualizing these types of data. Secondarily, *pavo* integrates visual system modeling which produces theoretical color space and color distance (contrast) that incorporate the visual system of the receiver, which in this study are walleye pollock and Chinook salmon, using user-defined data inputs. The output data can be used as physiological inputs to designing trawl gear bycatch reduction trials aimed at reducing Chinook salmon incidental catch in the pollock fishery.

## Methods

### *Microspectrophotometry (MSP)*

#### Data collection

Juvenile and adult walleye pollock specimens were collected during a NOAA mid-water trawl survey using a four-seam Aleutian wing trawl (AWT) with a 90-meter headrope from the Shelikof Straight region of Alaska in March 2018. Wild adult Chinook salmon were caught during the same survey. Hatchery-raised adult Chinook salmon specimens were provided by the Northwest Fisheries Science Center Manchester Research Station in April 2019. Hatchery Chinook salmon were held in 5-m diameter, flow-through tanks supplied with filtered (to 20 μm) seawater and fed commercial fish feed. Landed wild fish were immediately removed from the cod end and placed on ice in a lightproof container. Raised salmon were removed from tanks and transferred to a lightproof container. The container was placed in a refrigeration unit to allow the fish eyes to dark adapt. The dark adaptation allows visual pigments to regenerate and provide a

maximum signal for MSP. Fish eyes were dark-adapted for a minimum of 2 hours on ice. Whole specimens were euthanized by severing the spinal cord at the base of the head, and the eyes were enucleated under dim red-light conditions. Infrared light and night vision goggles were used in conjunction with a dissecting scope to hemisect the eye and separate the cornea and lens. The retinas were carefully detached from the retinal pigment epithelium (RPE) and moved onto a slide with hypertonic buffer (~6% sucrose). Small pieces of the retina were transferred onto a coverslip and macerated to aid in the separation and dispersion of photoreceptors. The retina sample was covered by a second coverslip edged with silicon grease and placed on the MSP stage.

MSP is used in the field to acquire the physiological spectral sensitivity of a photoreceptor cell. The computer-controlled single beam of light is passed through the sample and into the photomultiplier tube (PMT). The PMT counts the photons transmitted through the sample at each wavelength. The photomultiplier output data was transferred to the computer using a current-to-voltage transducer and an A/C converter. A halogen lamp was the light source. The condenser was a 40X Zeiss Ultrafluor and the objective was a 100X Zeiss Ultrafluor. Measuring wavelength was controlled with a computer-driven monochromator and stepper motor. Photoreceptor cell types were identified by morphology. Rod outer segments were long and cylindrical. Single cones were piriform where the outer segment was located on the smaller diameter end of the inner segment. Twin cones were similarly shaped, with 2 outer segments adjacent to one another on the same end of the piriform. Single and twin cones differed in size for both walleye pollock and Chinook salmon. The outer segment of rod and cone photoreceptors were bidirectionally scanned using the halogen light source from 750–350 nanometers, in 1 nm

increments, to generate an absorbance spectra curve (Loew 1982, 1994). The MSP absorbance curves were accurate to ±1.00 nm.

### Data Processing

The wavelength at peak absorbance ($x_{max}$) for each curve was determined by initially filtering the data ('smooft' routine in Pascal; Press et al., 1987) followed by normalization of the optical density using an MSPA (microspectrophotometry analysis) program created using LabView (E. Loew, Cornell University, pers. comm.). The absorbance curves were then fit to known templates. The templates are based on the premise that a normalized absorbance spectrum has a standard shape for vitamin A1 or A2 chromophores when wavelength is converted to frequency (Dartnall 1953). The templates have been updated and are described mathematically by Lamb's formula (1995) and incorporate a modified version of the Mansfield-MacNichol transform (Govardovskii et al. 2000). These latest iterations are considered the universal absorbance and spectral sensitivity curve templates for A1 and A2-based visual pigments when wavelength ($\lambda$) is greater than 330 nm.

Data records with absorbance curves with a clear Gaussian distribution were selected for analysis. Vessel pitch and roll affected sample processing, resulting in records of poor quality. Specifically, vessel motion caused the light filament to move, which resulted in the MSP beam shifting outside of the cell resulting in poor quality or inaccurate records. Approximately 57% of records were considered poor quality or inaccurate and were not used in the analysis.

The $x_{max}$ was generated using the mean of the 40 data points centered at the peak of the curve (20 on the right limb and 20 on the left limb), fit to a Gaussian distribution, and divided by the correction factor for rhodopsin to transform proportion into an equation to establish peak wavelength (Govardovskii et al. 2000). The curves were normalized to the peak wavelength value. The absorbance curves were fit to pure A1 and A2 templates. The goodness of fit was determined by calculating the least-squares straight line distance for 70% and 30% of maximum absorbance for the long-wave limb between the absorbance and the template curves (MacNichol 1986). The $x_{max}$ for each species-specific photopigment type were averaged to obtain a single value to represent the cell type and spectral class for each photoreceptor class. The MSP wavelength error is approximately ± 1 nm; therefore, values were reported as whole numbers. Due to the data quality of samples taken on board the vessel, visual pigments were reported as $x_{max}$, as opposed to $\lambda_{max}$ values. The $x_{max}$ values represent the wavelength of maximum spectral absorbance is the peak of the normalized curve, whereas $\lambda_{max}$ is the peak of the best-fit spectral template curve on the raw data

Non-metric multidimensional scaling (NMDS) ordination was chosen to search for grouping patterns in the spectral absorbance data. NMDS is suited for small sample sizes. NMDS plots were used to evaluate differences in photoreceptor cell type and visual pigment complex between adult versus juvenile life stages of walleye pollock and hatchery versus wild Chinook salmon populations using the R package vegan (Oksanen et al. 2022). The NMDS data frame includes absorption values at each wavelength (350-750 nm) for each observation. A dissimilarity matrix was calculated with the wavelength absorption data for each species. NMDS parameters included a selection of 2 dimensions, Euclidean distance measure, and 20 iterations to reach the best

solution. A PERMANOVA (*vegan::adonis2,* Oksanen et al., 2022) was used to calculate the test statistics between pollock life stages and Chinook habitat types as well as cell class. Group sample sizes were unequal, and the number of comparisons was small, therefore the Bonferroni pairwise posthoc test was run on Chinook salmon cone color classes to test for differences among group means.

*Spectral reflectance*

Definition of color categories

The color descriptors used are the qualitative human-subjective categories previously described for reef fishes (Marshall 2000). The categories are based on the human interpretation of color and do not reflect how a fish's visual system may process color. Evidence suggests color interpretation by fish varies among species (Bowmaker 1990).

Data collection

Fiber optics reflectance spectroscopy (FORS) readings for trawl gear materials were collected during February 2023. Trawl net material and line were provided by 10 manufacturers (Appendix B). Line and trawl netting sample materials were constructed from nylon or polyethylene twine with a twisted or braided structure, a polyethylene/polypropylene copolymer, or an ultra-high-molecular-weight polyethylene fiber with a braided construction (Dyneema). The spectrum of light reflected from the material's surface was sampled with a Pembrook Q-mini (model AFBR-S20M2WU) spectrometer. The Q-mini measures spectra from 225-1000 nm wavelengths with a spectral resolution of 1.5 nm. The entrance slit of the spectrometer was 4 μm. The sampling area of the fiber optic cable attached to the Q-min was approximately 0.3 $mm^2$.

The end of the fiber optic cable was placed close to the color patches of each component of net material at a 35-45° angle, measured, and recorded as a .spz file using Waves software (RGB Photoronics GmbH 2020). Line and netting reflectance values were collected in 1-nm increments for 350-750 nm wavelengths. Each color patch was measured 3 times for the line and netting samples. For multi-colored materials, samples were taken for each color if the sample area was larger than 1 $mm^2$. A white gypsum standard sample was recorded to calibrate for 100% reflection in all environments.

### Data processing

The R package pavo was used to process and analyze the line and netting spectral reflectance data (Maia et al. 2019). Data were restricted to 380-650 nm wavelengths, which correspond with the range of biologically appropriate spectral limits inclusive of both pollock and Chinook salmon. Three line and net color patch sample curves were averaged to obtain mean reflectance values at 1 nm increments for each color patch. The small-scale measurements generated a large dataset desirable to perform a flexible statistical smoother. Local regression smoothing (LOESS) was used to reduce the minor electrical noise in the sample curves. LOESS was ideal because only the degree of the local polynomial needs to be provided and it does not require a specific function to fit the model. The original spectral curve was preserved by applying the minimum amount of smoothing (degree = 2, $\alpha = 0.2$). The minimum value of each smoothed curve was subtracted from all wavelengths, standardizing the minimum reflectance to 0. All reflectance values in the sample were then divided by the maximum reflectance of the sample. These values were divided by the white reflectance value of the corresponding wavelength to normalize the reflectance curves.

The hue (color) for each color patch was described as peak wavelength and the spectral location of maximum reflectance. Hue was calculated with the *pavo::summary()* function using the formula:

$$H = \lambda_{Rmax}$$

A principal component analysis (PCA) reduced the dimensionality of the highly correlated reflectance values at each wavelength (271 observations within 145 reflectance spectra; Cohen 1964). This technique uses each measured wavelength as a variable, and the reflectance curve, the spectrum as a whole, is the observation. The eigenvectors provide scores for each observation which maximized the variance of the variables (Endler 1990). The data were centered to a mean reflectance of 0 to eliminate brightness as the dominant variable. Due to the relatively consistent shape of reflectance curves, the majority of the variance is likely to be explained by the first four principle components (unpublished data within Endler 1990). The PCA revealed clustering between the color patch and trawl components.

*Spectral irradiance of Bering Sea waters*

Data collection

Spectral irradiance data for the water column were collected in the Bering Sea during May–July 2014. Areas selected for analysis corresponded to commercial pollock fishing areas in the Bering Sea that have recorded Chinook salmon bycatch (Figure 1, *pers. comm.* D. Stevenson, NOAA AFSC).

Data were collected with an autonomous spectral irradiance logger (SIL) developed by NOAA AFSC. The SIL measured the overall intensity and spectral distribution of ambient light during

clear and overcast weather conditions. The SIL was integrated with a TriOS optical sensor RAMSES ACC UV/VIS (Article-Nr. 40S121010) hyperspectral radiance and irradiance sensor. The RAMSES radiometer utilizes an internal miniature spectrometer with a wavelength measurement range of 280-720 nm, primarily used to measure upwelling radiance and downwelling irradiance. Within the SIL, the radiometer measured the intensity and spectral distribution of light of downwelling irradiance while attached to the gear facing up toward the surface. The SIL was mounted on the head rope of the bottom trawl net used on the AFSC Eastern Bering Sea shelf survey. Data were collected during each 30-minute survey tow from the surface to the benthos, throughout the bottom tow, and back to the surface. The data for each cast or haul were filtered to include only measurements from the upcast. The upcast period is from the time of haulback until the net reaches the surface. Measurements during the upcast were more stable than measurements recorded during the downcast.

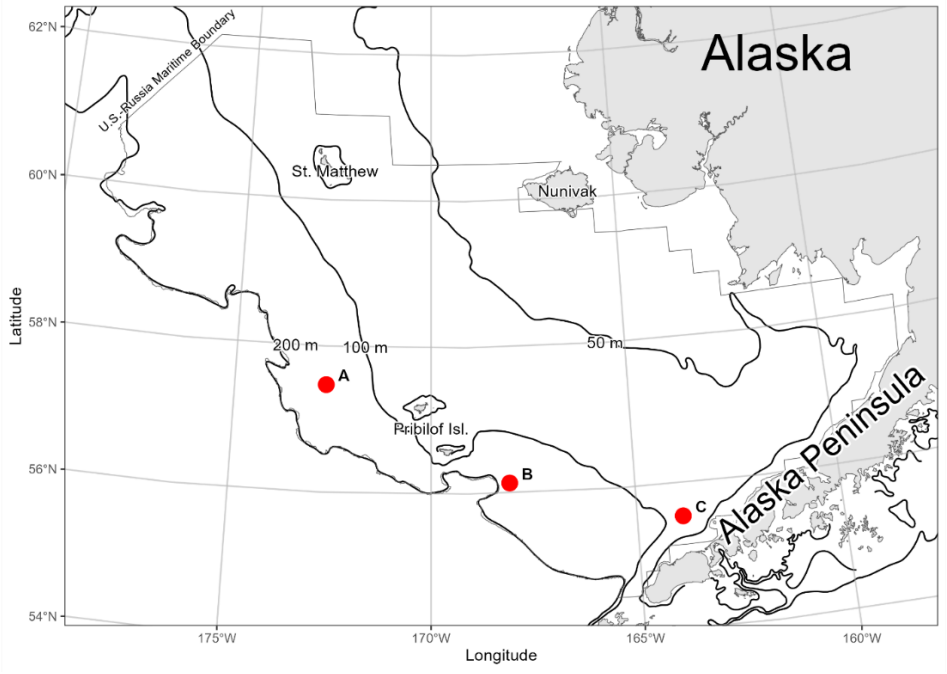


Figure 1. Site map of spectral irradiance stations. Stations were selected based on high bycatch numbers of Chinook salmon in the pollock fishery.

Data processing

Spectral irradiance data points were measured in $W/m^2/sec$ and then plotted on a natural log scale. Plotted wavelengths were limited to the known visual spectra perceptible by these fishes (380-650 nm). Just-below-surface irradiance was filtered from the data for use in VPModel® and plotted to determine wavelength at maximum irradiance for each site. Data were further reduced to focus on depths inhabited by pollock and Chinook salmon. During 2014, the majority (~93%) of adult pollock were within 50 m of the bottom (Honkalehto and McCarthy 2015). Data were filtered to focus on 2 distinct light environments at the 40-50 m and 90-100 m depths. The irradiance in the maximum depth bin available for each station was analyzed as well. These spectral data are spatially and temporally variable. The data collected and analysis conducted provided a snapshot view of the spectral conditions in spatially relevant locations and depths where pollock are fished and Chinook salmon bycatch was greater than in surrounding areas.

*Theoretical visual models*

Visual models were used to predict how the organism's photoreceptors responded to visual stimuli or reflectance of a target. The color space produced by the model is constructed from information about an organism's visual physiology. The location of the target in the color space is determined by the model output. VPModel® and the *pavo* R package are classified as basic physiological visual models. The next step is to incorporate behavioral responses to targets. These psychophysical color space models predict visual responses to a target based on the physiological capabilities of the organism, environmental viewing conditions, and characteristics of a target (Renoult et al. 2017).

VPModel®

General assumptions made by the VPModel® modules included: 1) the source of light was directly overhead, 2) the water properties were the same at distances and depths specified in the module, and 3) the large particles did not scatter the light (Loew and Zhang 2005). VPModel® contains two modules. The first module calculated downwelling irradiance taking into consideration chlorophyll a and dissolved organic material (DOM) concentrations. Irradiance data collected from just below the surface for each station was input into this module. The chlorophyll and DOM concentration data at each site were unknown at the time of spectral irradiance data collection in 2014. Estimated chlorophyll a concentrations were produced for July 2014 using monthly composite data from the NOAA Polar Watch data catalog (NOAA 2023). Chlorophyll concentrations determined from the 2014 dataset set for stations A, B, and C were 4.0, 5.0, and 6.5 $mg/m^3$, respectively. VPModel® generated the available irradiance spectra at decreasing depths utilizing the just-below-surface irradiance data which used the same irradiance file to model chromaticity discrimination of the same targets under more current chlorophyll a conditions. Chlorophyll concentrations from July 2022 were compiled from the same dataset as the 2014 records for comparison. Dissolved organic matter (DOM) values were unavailable for the Bering Sea. The average concentration of DOM in seawater is <1.0 mg/L (Catalá et al. 2021), so values conforming to this average were used in the first module. The first module calculated downwelling irradiance based on the near-surface irradiation data with the associated parameters of DOM and chlorophyll a. The depths at which pollock and Chinook co-occur (>50 meters) suggest the unnecessary inclusion of an upwelling parameter. The product of the module was a graphical representation of irradiance (photons/$m^2$/nm) by wavelength as depth

increases. The irradiance results of this module were used as the irradiance-at-depth data for the second module.

The second module calculated target radiance and background radiance as viewed by a visual system in a specified direction and depth. Inputs to this module included spectral irradiance from "just-beneath-surface" for each station, visual pigment sensitivity ranges from each species, spectral reflectance of the averaged color patches as the targets, environmental parameters, and scotopic and photopic thresholds. These thresholds are a measure of the minimum luminescence required to stimulate a signal from the photoreceptors in low light (scotopic vision) and high levels of illumination (photopic vison). The scotopic threshold input for pollock was $4.348 \times 10^{-4}$ $W/m^2/sec$ (Olla et al. 1997a), and the photopic threshold was 3 natural log units times the scotopic threshold (Dartnall 1975). Using these inputs, the luminosity and chromaticity, contrasts between the targets and background spacelight were calculated at each site and depth. The final module output predicted the best visual pigment pair for detecting the targets using an iterative process (Loew and Zhang 2005).

The color thresholds from the model results are predicated on the assumption that a fish's visual pigments are optimized for ecologically relevant target discrimination within a specific spectral environment (Zhang 1997) and that chromaticity is independent of luminosity. Color thresholds are the value at which the chance of perceiving the target against the background is equal to 50% (Stiles 1959). The models attempt to determine if a given color (target) would stimulate the available photoreceptor cells, how the target is perceived (chromatic/luminous contrast

thresholds), provide visual system information, and guide future studies investigating behavioral thresholds.

Pavo

The functions within the *pavo* package estimate relative photoreceptor quantum catch (*vismodel*), convert points into a defined color space (*colspace*), and estimate color distances between points (*coldist*). The spectral analysis conducted within this portion of the study used the R package *pavo2* (Maia et al. 2019) in R version 4.2.3 (R Core Team 2023). Visual pigment absorbance curves were generated using *sensmodel,* and peak absorbance value inputs were the mean pigment values from cones using microspectrophotometry. The relative quantum catches were calculated in *pavo* using the equation from Vorobyev et al. (1998):

$$Q_i = \int_{\lambda} R_i(\lambda) S(\lambda) I(\lambda) d\lambda$$

where $i$= 1,2,…n, $Q_i$ is the quantum catch of the receptor, λ represents the wavelength, $R_i(\lambda)$ is the spectral sensitivity of the receptor defined by the visual pigments, $I(\lambda)$ is the illuminant spectra, and integration is over the range of the spectrum.

The time interval for the collection of the illumination varied. Samples were collected when a change in light availability was detected. Data were binned and averaged into 10-m depth bins to ensure data at all investigated depths. The averages were converted from $W/m^2/sec$ to $\mu mol/m^2$ for use in *vismodel*. Spectral irradiance values from 40-50m, 90-100m, and the deepest depth measurement at each station were selected for analysis.

The model did not take into consideration rod sensitivity (luminance) or possible filtering of wavelengths by ocular media. Assumptions were: 1) the photon catch metric is a product of receptor spectral sensitivity, reflectance, and illumination at each wavelength, 2) the background spectrum does not influence reflectance wavelengths, and 3) the von Kries transformation is not implemented. In water more than 1 m deep, the von Kries transformation failed to model color consistency for color changes over varying distances (Vorobyev et al. 2001); thus, the background spacelight spectrum was not included as a parameter. The resulting values from *vismodel* were converted into a location in color space *(colspace*). The greater the distance between targets in the color space, the more contrast between the targets under the spectral irradiance conditions specified in each model.

The hue determined by the maximum reflected wavelength of the spectral reflectance for each color patch sample was used to assign a color to the sample. Reflectance curves of samples with identical colors were averaged to create one spectral reflectance curve for each color patch to reduce the number of targets plotting within a color space. Color discrimination of targets was modeled using three irradiance profiles for all sites: daylight (D65), 40-50 m, and 90-100 m depth. Targets at stations A and B were also modeled using the irradiance profiles from the deepest depth bin available, 120-130 m and 140-150 m, respectively. The spectral curves of the trawl components were projected as targets into the dichromatic and trichromatic color space of walleye pollock and Chinook salmon.

Di- and tri-chromatic color space was represented as a segment or equilateral triangle (MacLeod and Boynton 1979). Each end of the segment's color space represents short or long wavelengths

as defined by the visual pigment absorbance range of walleye pollock. The vertices of the triangle color space are representative of short, medium, and long wavelengths limited by Chinook salmon visual physiology. Within these color spaces, similar targets will group together. The further apart the targets are from each other, the greater the contrast between them.

The averaged color patch reflectance spectra were plotted in dichromatic color space (segments) using the spectral sensitivities of walleye pollock and trichromatic color space (triangles) for Chinook salmon visual pigment ranges. Averaged color patch reflectance spectra were characterized as targets within the color space.

Chromatic contrast (ΔS) was calculated using non-weighted Euclidean distances between color patches with *pavo::coldist*. Non-weighted distances were chosen because photoreceptor densities for pollock are unknown and calculating the theoretical signal-to-noise ratio was not within the scope of this project. Here, the threshold of discrimination, or just noticeable difference (JND) was correlated with $\Delta S > 1$.

**Results**

*Microspectrophotometry*

Using MSP, 2 visual pigment spectral classes were identified in walleye pollock and 3 for Chinook salmon. Photoreceptor cell absorbance was measured from 2 adult and 3 juvenile walleye pollock obtained during the midwater survey. A total of 165 pollock samples were collected from 4 fish and 66 Chinook salmon MSP records were collected from 5 adult fish (3 wild, 2 hatchery-raised). The MSP instrument accuracy is high with little variation. A

PERMANOVA was conducted between specimens to test for differences between cell types and among spectral groups ($F_{5,82} = 2.024$, $p = 0.176$) (Appendix A). Of those records, 77 were high enough quality to be analyzed. High quality records of vertically stacked outer members on twin cones could not be used as an individual record of an outer segment and thus were not included in the analysis of either species. The remaining 62 records representing 9 rods, 30 single cones, 13 non-identical twin cones, and 10 detached twin cone outer segments, were analyzed. Of the 66 Chinook salmon photoreceptors sampled, 37 were included in the analysis, representing 6 rod cells, 18 single cones, 5 non-identical twin cones, and 8 twin cone unmatched outer segments (Table 1). A PERMANOVA tested for differences in the $x_{max}$ values within the same spectral class among specimens ($F_{5, 41} = 2.368$, $p = .079$) and no difference was found between fish (Appendix A). No differences were determined between adult/juvenile walleye pollock life stages and hatchery/wild Chinook salmon fish.

NMDS ordination was used to visually assess for dissimilarity between adult and juvenile pollock photoreceptor absorbance. The walleye pollock NMDS ordination indicated no separation between adult and juvenile samples (stress = 0.073). A PERMANOVA was conducted and no significant difference was found between pollock life stages ($F_{1, 81} = 1.034$, $p = 0.336$). A second NMDS assessed differences between hatchery-raised and wild-caught Chinook salmon absorbance. The NMDS between hatchery-raised and wild Chinook salmon indicated no differences between the rearing types and was confirmed with PERMANOVA (stress =0.048, PERMANOVA: $F_{1, 40} = 1.904$, $p = 0.167$) (Figure 3).

Rods, single cones, and twin cones were present in the retinas of walleye pollock and Chinook salmon. Peak wavelength for rods ranged from 502 to 520 nm (μ= 509, n =9) for walleye pollock and 496 to 519 nm (μ = 507, n = 3) for Chinook salmon (Table 1). Medium wavelength and short wavelength opsins were measured in single and twin cones in both species. Walleye pollock had one medium-wave cone (MWC) opsin. The MWC ranged from 503 to 522 nm (n = 24).. Identical twin cones were not detected in juvenile and adult pollock, although previously single and twin identical cone morphology and spectral class were present in larval walleye pollock (Britt et al. 2001, Britt 2009). SWC (short-wave cone) in pollock ranged from 447 to 521 nm (n = 44). Chinook salmon had 2 MWC opsins. These ranged from 512 to 527 nm (n = 9) and 538 to 552 (n = 13) in single cones nm and 512 to 527 nm (n = 4) and 535-554 (n = 4) nm in twin cones. SWC ranged from 433 to 439 nm in single cones (n= 5) and 432 in twin cones (n = 1). The values for both cone morphologies were consistent with MSP analysis on the blue photoreceptor class of smolt and parr stage Chinook salmon (Novales Flamarique 2005). Red and UV photoreceptor classes were not detected in this study's oceanic phase juvenile Chinook salmon.

Adult and juvenile walleye pollock were dichromats producing 2 cone wavelength sensitivities and Chinook salmon were trichromats possessing 3 cone wavelength sensitivities (Table 1). Both Chinook salmon and walleye pollock possess non-identical twin cones and single cones. Sets of twin cones are characterized by 2 structurally identical outer segments (i.e., twins vs. double). However, the visual pigment contained in each segment is different (i.e., non-identical, E.R. Loew and Lythgoe, 1978). The twin cones were maximally sensitive to mid-wave wavelengths, while the single cones were smaller and sensitive to both mid- and short-wave wavelengths. Both

species had predominantly non-identical twin cones in the blue-green spectral class and both species lack longer wavelength cone pigments.

Table 1. Microspectrophotometry visual pigment results for walleye pollock (*G. chalcogrammus*) and Chinook salmon (*O. tshawytscha*) photoreceptor cells. Morphological cell types include single cone (c), non-identical twin cone (t), and rod (r). Spectral groups are classified as short-wavelength cone (SWC), mid-wavelength cone (MWC), and rod.

| **Species** | **Cell type** | **Spectral group** | **Mean $x_{max}$** | **Standard deviation** | **Min $x_{max}$** | **Max $x_{max}$** | **Spectral class** | **Number of samples** |
|---|---|---|---|---|---|---|---|---|
| *Gadus chalcogrammus* | c | SWC | 449.33 | 2.66 | 447 | 454 | blue | 6 |
| | c | MWC | 518.87 | 3.85 | 503 | 522 | blue-green (cyan) | 23 |
| | t | MWC | 515.63 | 3.61 | 506 | 521 | blue-green (cyan) | 38 |
| | r | rod | 507.62 | 5.66 | 502 | 516 | blue-green (cyan) | 8 |
| *Oncorhynchus tshawytscha* | c | SWC | 436.40 | 2.41 | 433 | 439 | blue | 5 |
| | c | MWC | 519.44 | 5.55 | 512 | 527 | blue-green (cyan) | 9 |
| | c | MWC | 545.00 | 5.77 | 538 | 552 | green | 4 |
| | t | SWC | 432.00 | | 432 | 432 | blue | 1 |
| | t | MWC | 519.00 | 5.12 | 512 | 530 | blue-green (cyan) | 13 |
| | t | MWC | 545.75 | 7.93 | 535 | 554 | green | 4 |
| | r | rod | 507.00 | 7.80 | 496 | 519 | blue-green (cyan) | 6 |

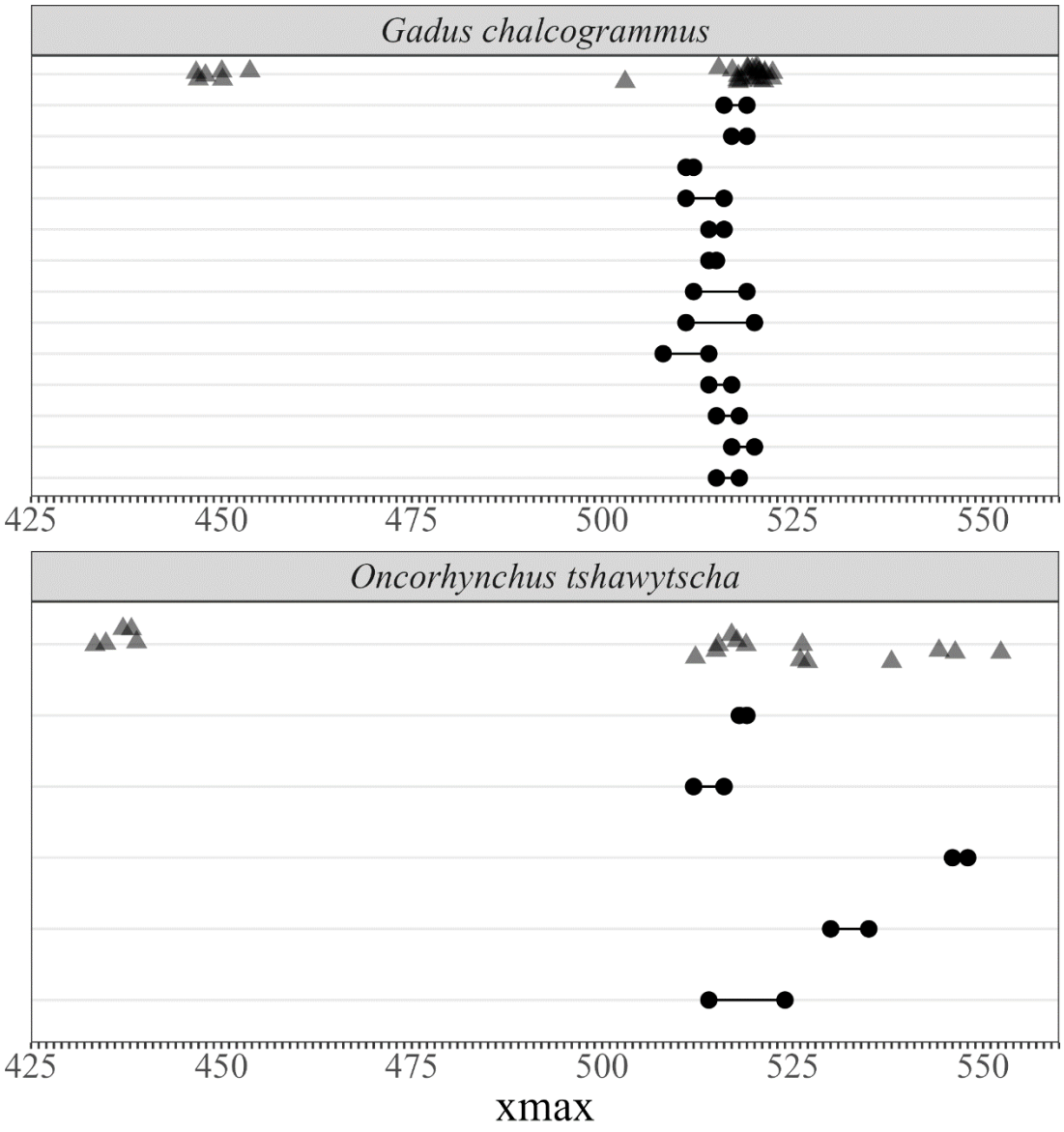


Figure 2. Distribution of the $x_{max}$ of single and twin cone visual pigments. Circles connected with a line represent the 2 adjacent outer segments of each twin cone where both outer segments were sampled using MSP. Triangles represent single cone $x_{max}$ values. The differences in visual pigment peak absorbance between the outer segments of twin cones ranged from 2 to 10 nm.

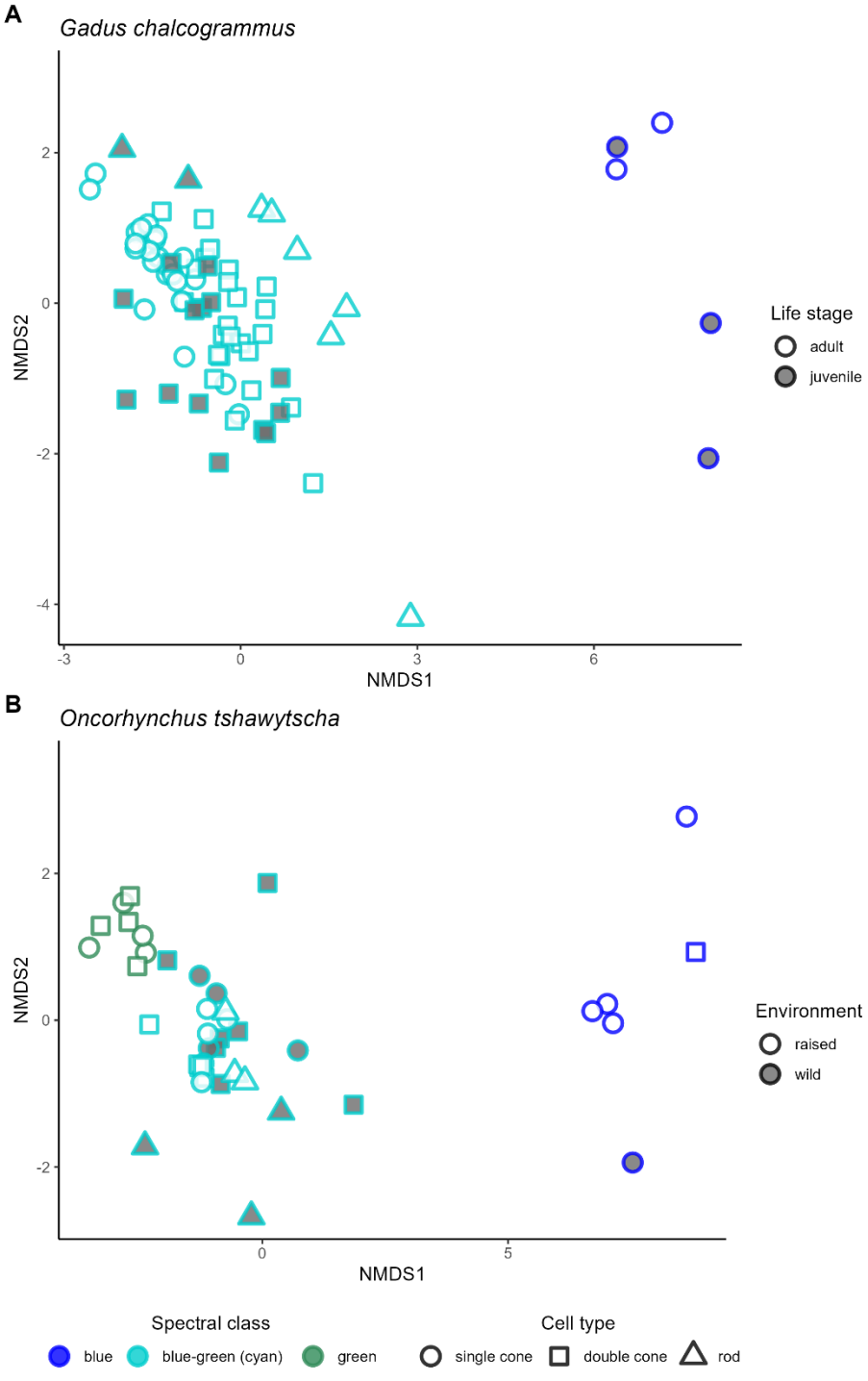


Figure 3. NMDS ordination plot showing the distribution of spectral classes for wild adult and juvenile walleye pollock (panel A) and hatchery and wild adult Chinook salmon (panel B).

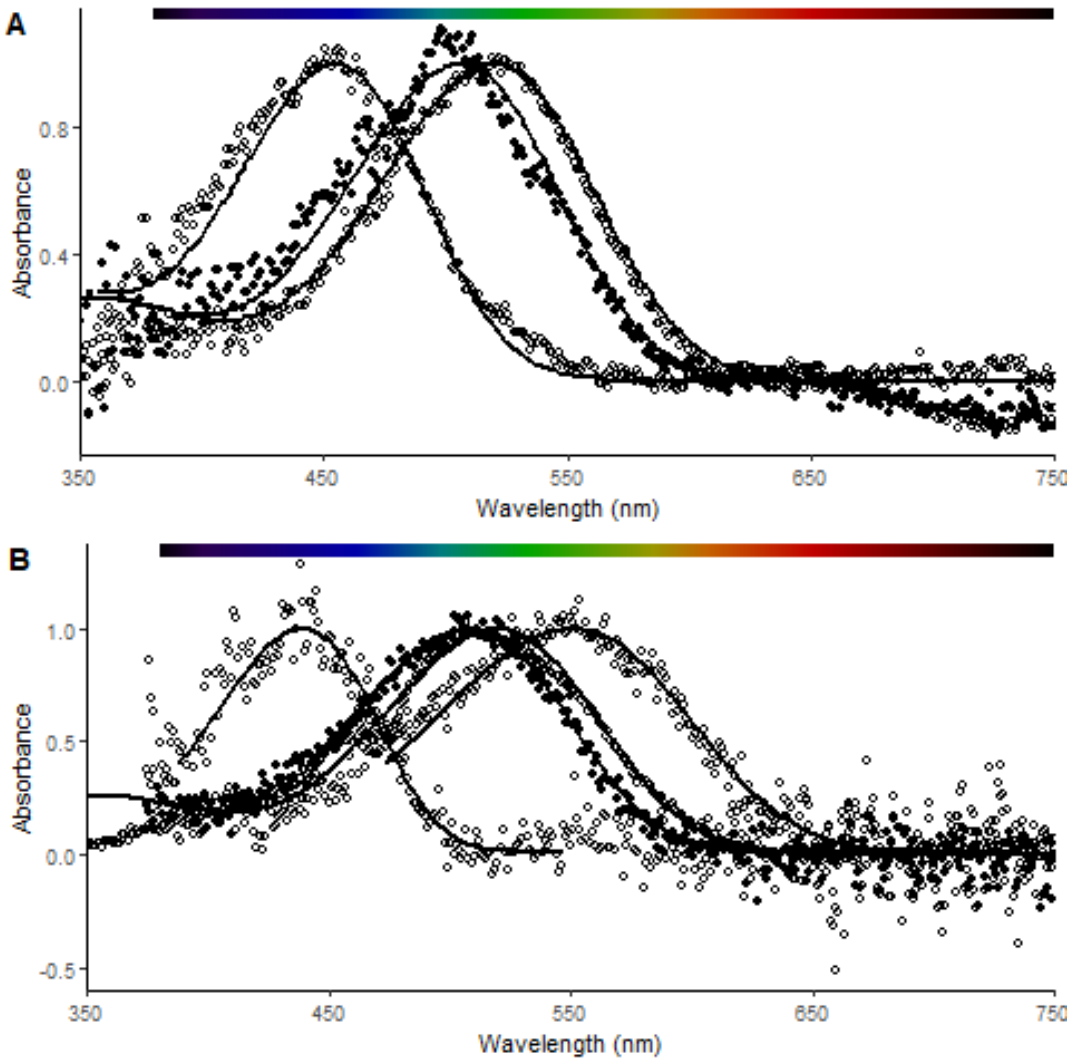


Figure 4. Visual pigment absorbance curves for walleye pollock (panel A) and Chinook salmon (panel B). Open circles represent absorbance values for cone visual pigments. Solid circles represent absorbance values for rods. The solid lines are vitamin A1 visual pigment templates fitted to each measurement (Govardovskii et al. 2000).

*Spectral reflectance*

Spectral reflectance data were collected from 44 types of new and used netting as well as 32 types of line. Some line and netting contained multiple colors, resulting in a total of 145 color patches (Appendix B.

Maximum reflected wavelength (MRW) values of green and yellow color patches spanned the widest range (Figure 5). Hue was the wavelength at maximum reflectance (Andersson 1999). Hues of the color patches ranged from 381 nmto637 nm (Table 2). The range of hues for red and orange as well as brown and yellow color patches overlapped. The green and blue color patches data had greater ranges of hue at maximum reflectance covering a wide spectral distribution. The hue of a single blue line color patch was 381 nm. The reflectance curve from this sample was inversely shaped which was unusual. Future studies including this product should investigate the reflectance of multiple samples for confirmation of this anomaly. Black, white, and grey color patches were not represented as maximum reflectance values because reflectance is horizontally linear over a wide range of wavelengths for these color patches. Hue at maximum reflectance is not a descriptive value for black, white, or grey color patches.

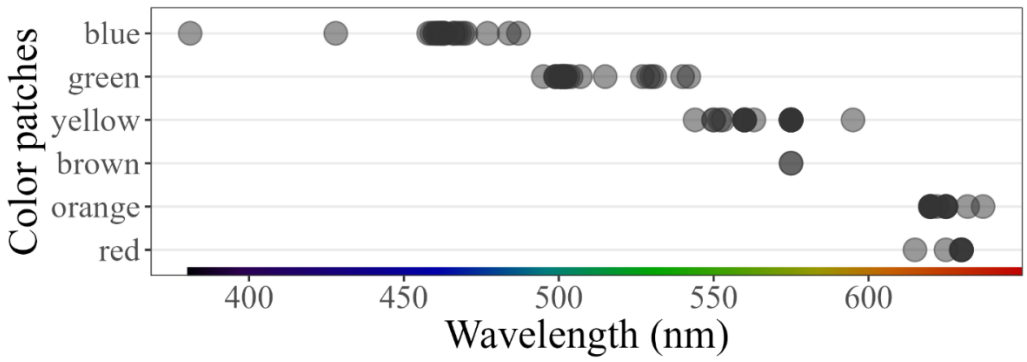


Figure 5. Maximum reflected wavelength (MRW) of 108 color patches from line and net trawl components.

Table 2. Maximum reflected wavelength (MRW) of trawl gear components and color patches

| Color patch | Component | Mean MRW | Minimum MRW | Maximum MRW | n |
|---|---|---|---|---|---|
| red | line | 627.5 | 615 | 630 | 6 |
| | net | 625.0 | 625 | 625 | 1 |
| orange | line | 624.9 | 620 | 637 | 9 |
| | net | 622.0 | 620 | 625 | 6 |
| yellow | line | 567.4 | 544 | 595 | 14 |
| | net | 565.7 | 552 | 575 | 11 |
| green | line | 506.3 | 495 | 540 | 18 |
| | net | 507.6 | 501 | 542 | 18 |
| blue | line | 454.1 | 381 | 477 | 10 |
| | net | 465.8 | 458 | 487 | 13 |
| brown | line | 575.0 | 575 | 575 | 1 |
| | net | 575.0 | 575 | 575 | 1 |

In the PCA clusters of color patches with similar wavelengths of maximum reflectance clustered together regardless of component type (Figure 6). PC1 accounts for 72% of the variation in spectral shape, and the first two principal component axes accounted for 92% of the variance in the shape of spectral reflectance curves (Figure 6). The variation describes the difference in the short-to-long wavelength ratio. Gray, white, and black color patches were grouped in the center. Orange and yellow color patches clustered and exhibited variation on both PC1 and PC2 axes. Brown color patches overlapped with yellow color patches on the top right portion of the yellow ellipse.

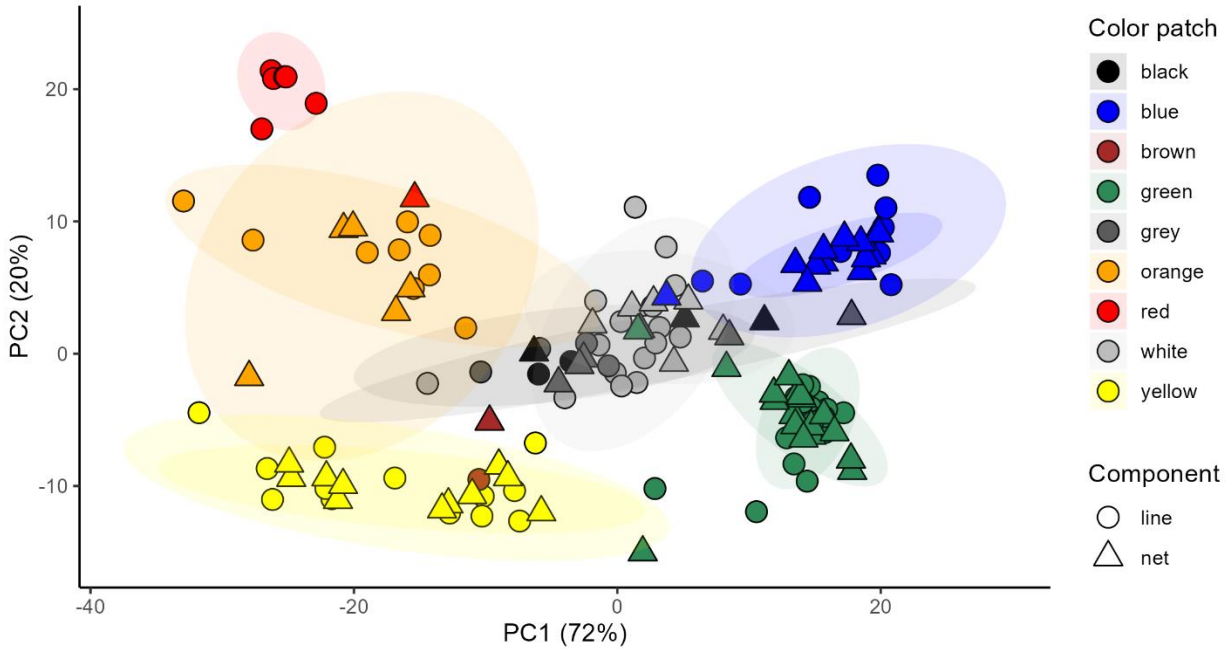


Figure 6. PCA depicting clustering of trawl component color patch samples based on maximum reflectance values in the range of 375–650 nm.

Reflectance curves for all samples were grouped by component and color patch. Visual pigment absorbance curves for walleye pollock and Chinook salmon were plotted in conjunction with the spectral reflectance curves (Figure 7). Interpretations of visual system activation are predicated on wavelength availability and intensity of luminescence at depth. Green, blue, white, grey, and black color patches reflected the greatest range of wavelengths that corresponded with the spectral range of visual pigments present in pollock and Chinook salmon. The red and orange color patches are unlikely to activate the cone photoreceptors of either species. Yellow and brown color patches are more likely to be detected by the Chinook salmon visual system than the walleye pollock system.

Red line

Walleye pollock visual pigments $x_{max}$

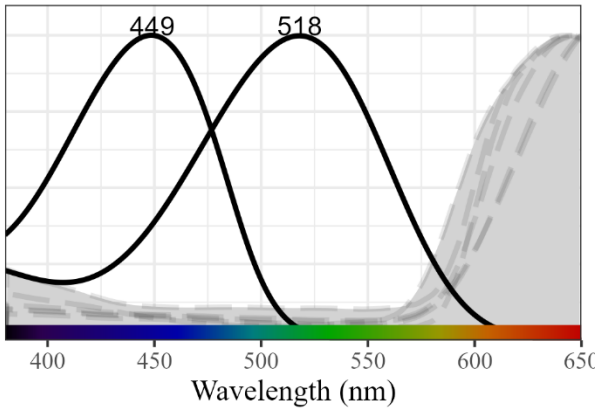


Red line

Chinook salmon visual pigments $x_{max}$

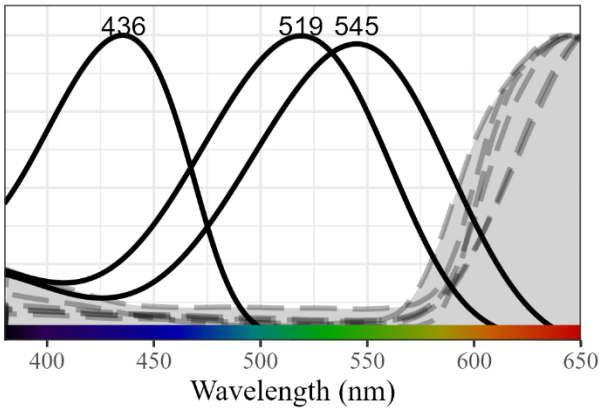


Red net

Walleye pollock visual pigments $x_{max}$

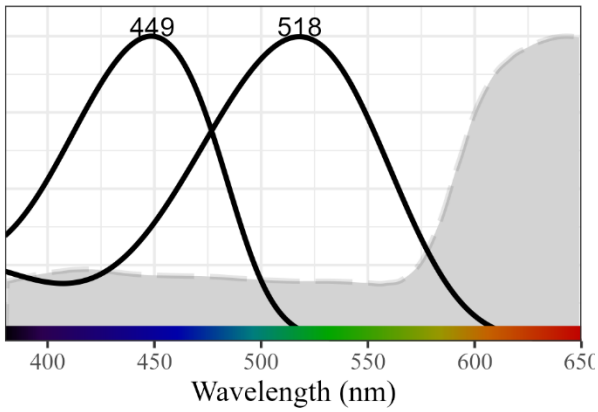


Red net

Chinook salmon visual pigments $x_{max}$

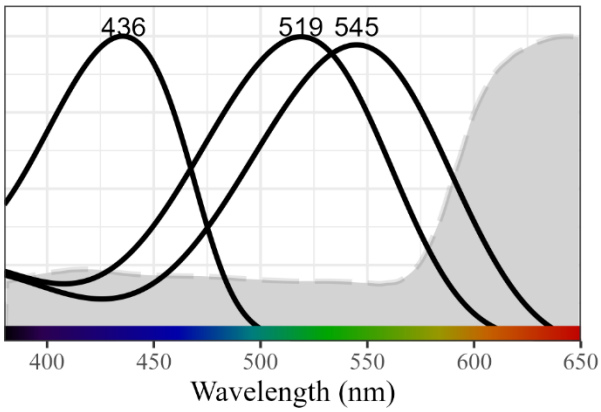

Orange line

Walleye pollock visual pigments $x_{max}$

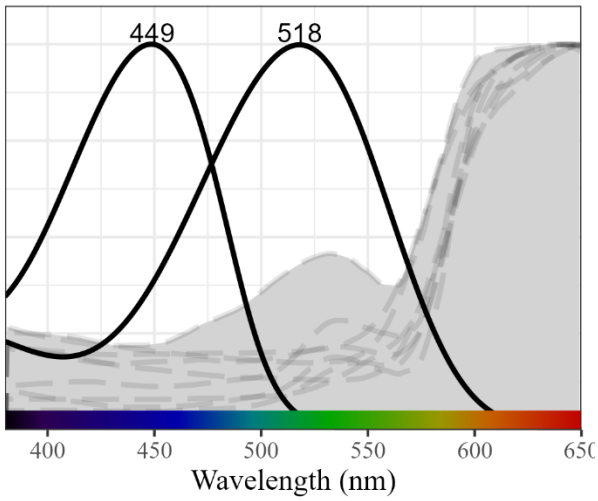


Orange line

Chinook salmon visual pigments $x_{max}$

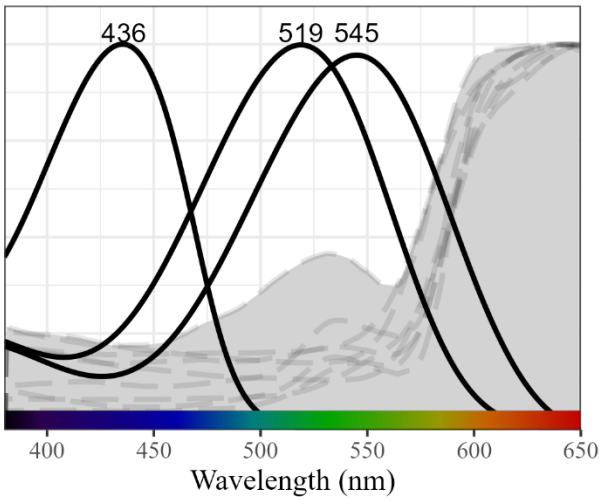


Orange net

Walleye pollock visual pigments $x_{max}$

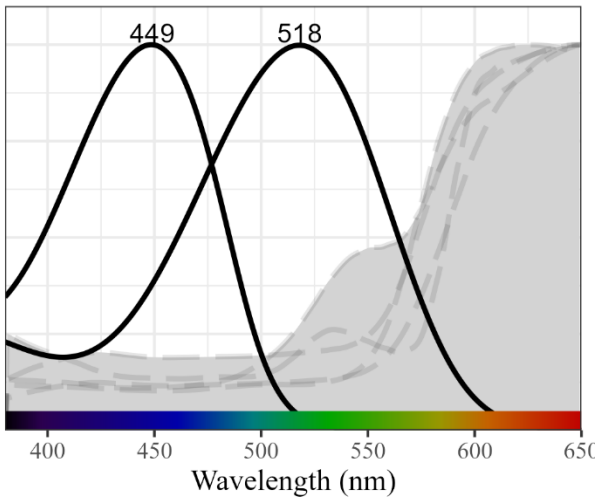


Orange net

Chinook salmon visual pigments $x_{max}$

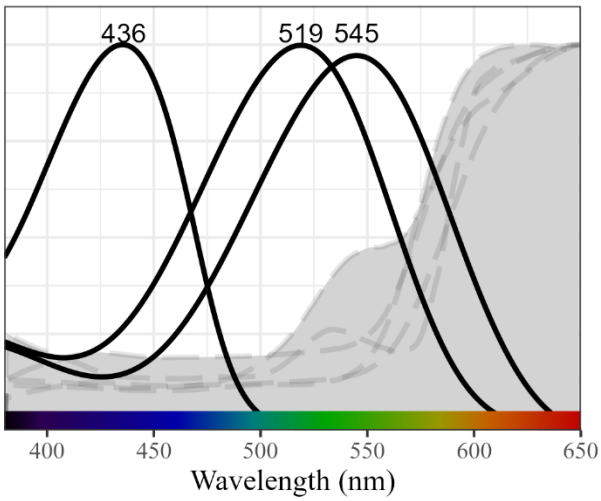

Yellow line

Walleye pollock visual pigments $x_{max}$

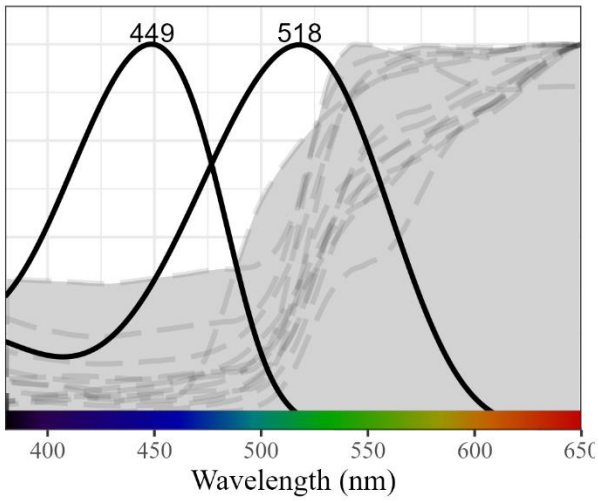


Yellow line

Chinook salmon visual pigments $x_{max}$

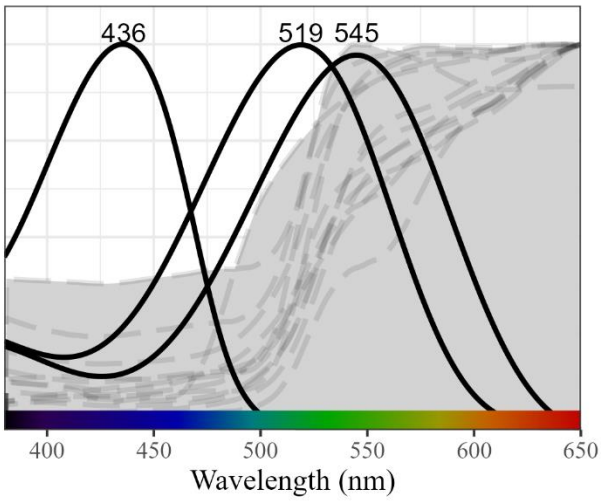


Yellow net

Walleye pollock visual pigments $x_{max}$

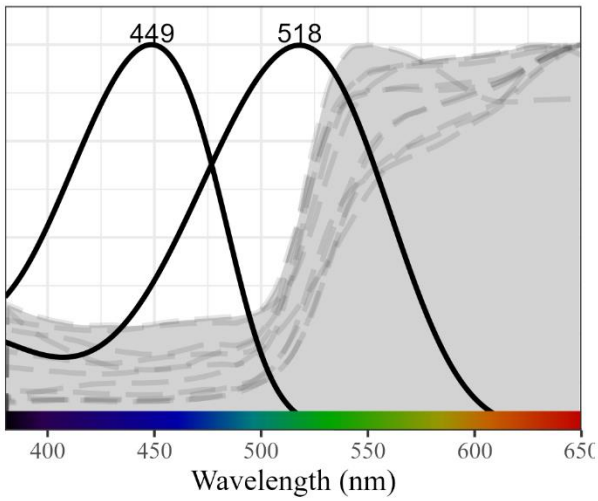


Yellow net

Chinook salmon visual pigments $x_{max}$

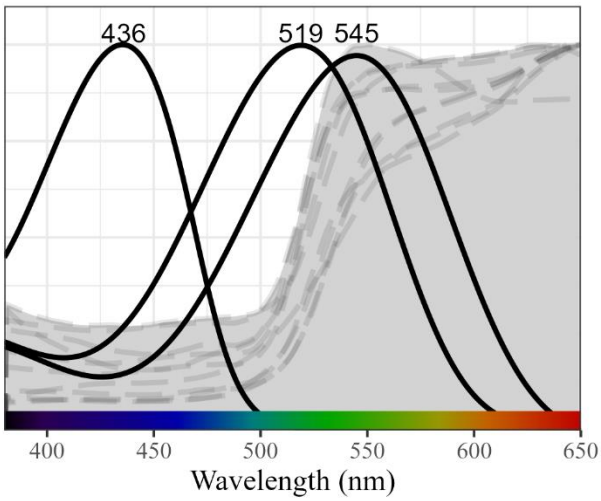

Green line

Walleye pollock visual pigments $x_{max}$

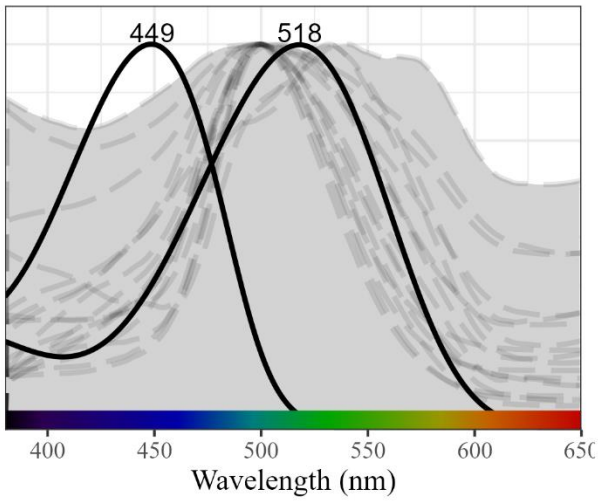


Green line

Chinook salmon visual pigments $x_{max}$

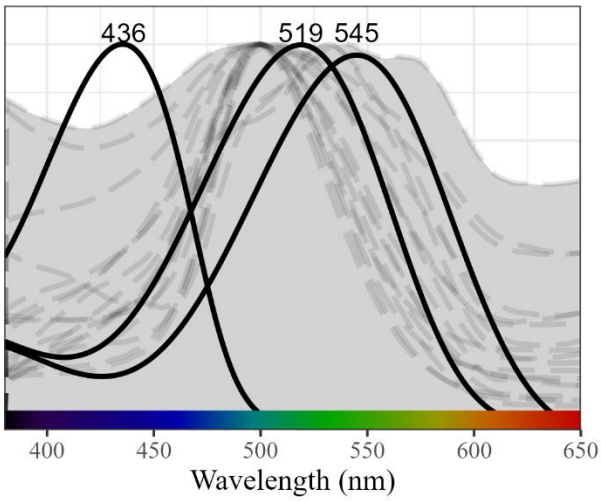


Green net

Walleye pollock visual pigments $x_{max}$

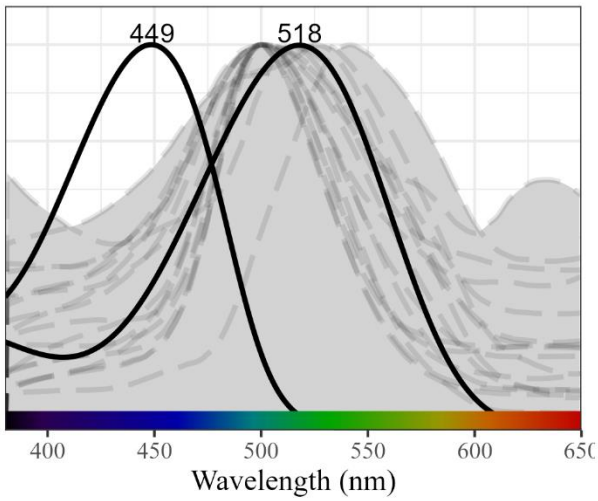


Green net

Chinook salmon visual pigments $x_{max}$

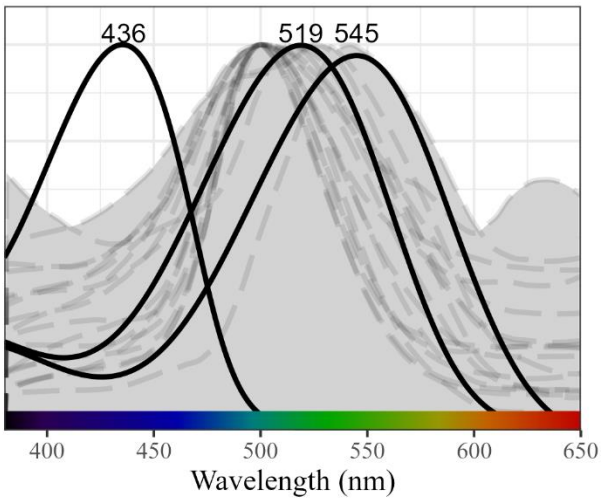

Blue line

Walleye pollock visual pigments $x_{max}$

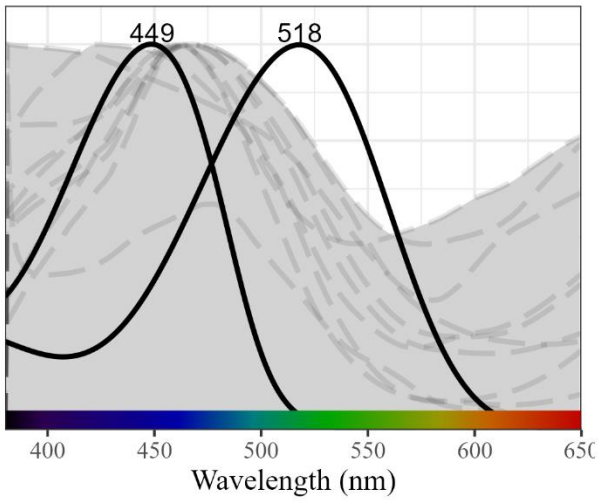


Blue line

Chinook salmon visual pigments $x_{max}$

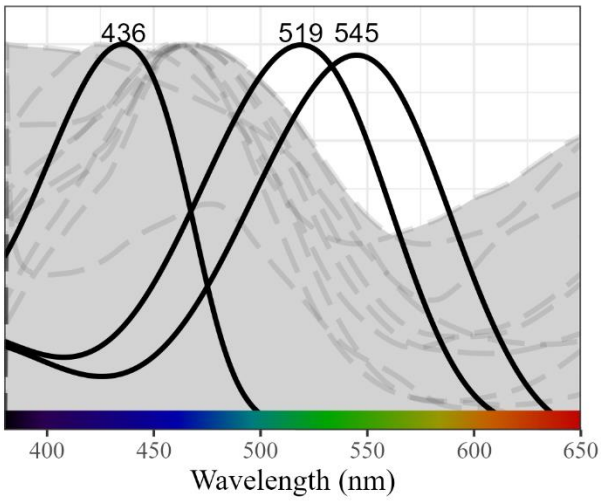


Blue net

Walleye pollock visual pigments $x_{max}$

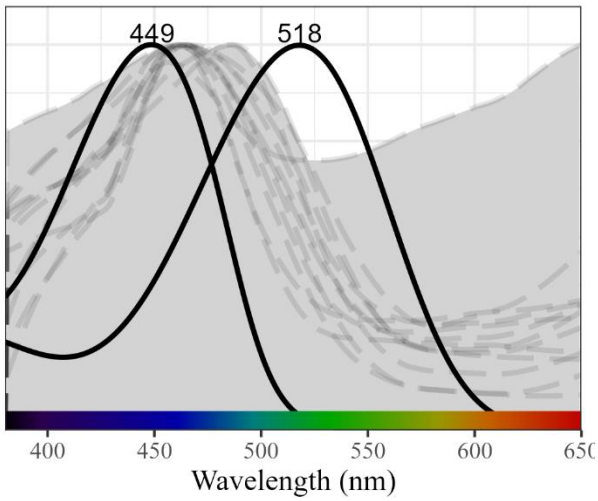


Blue net

Chinook salmon visual pigments $x_{max}$

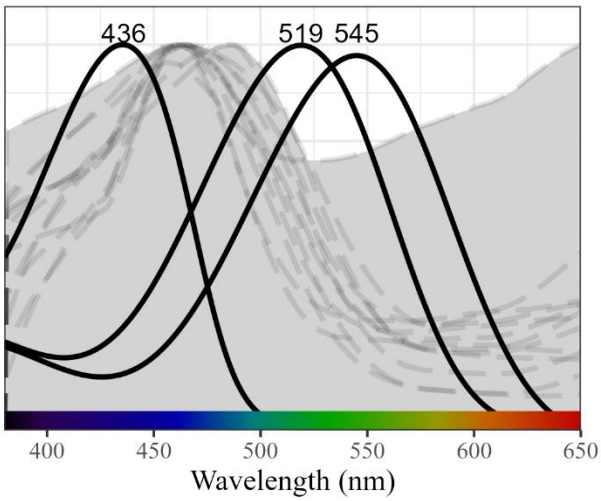

Brown line

Walleye pollock visual pigments $x_{max}$

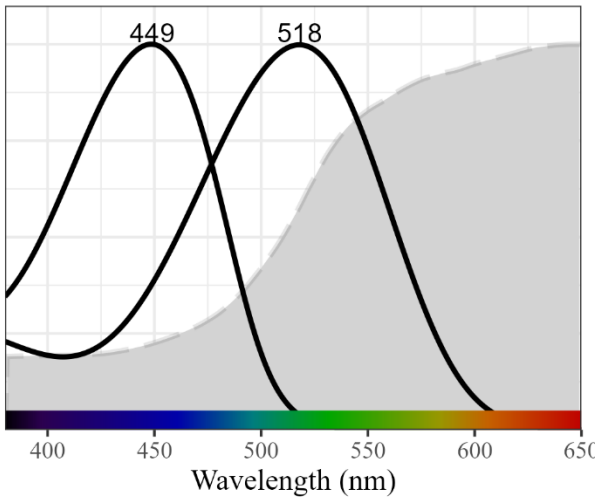


Brown line

Chinook salmon visual pigments $x_{max}$

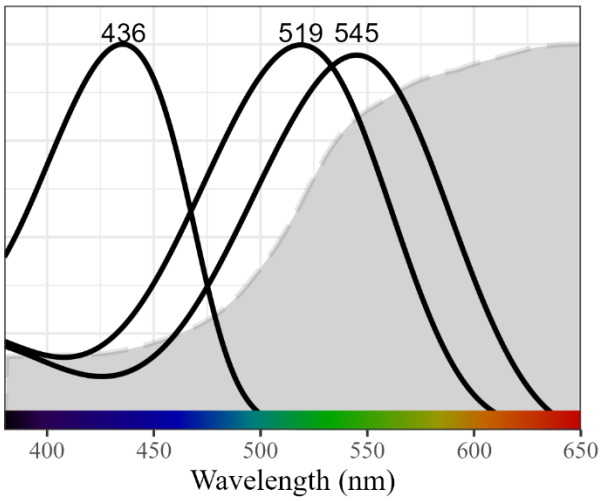


Brown net

Walleye pollock visual pigments $x_{max}$

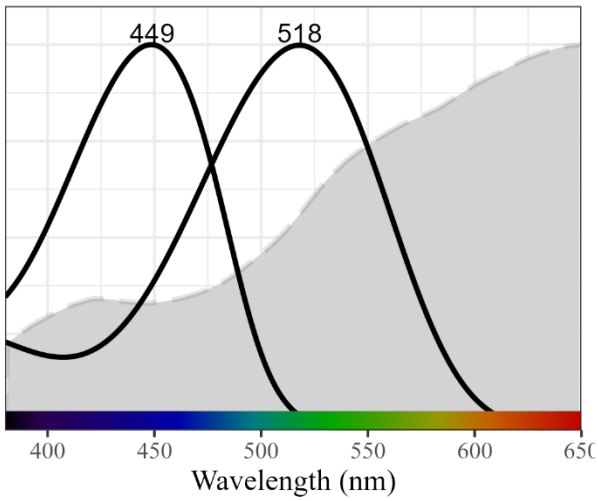


Brown net

Chinook salmon visual pigments $x_{max}$

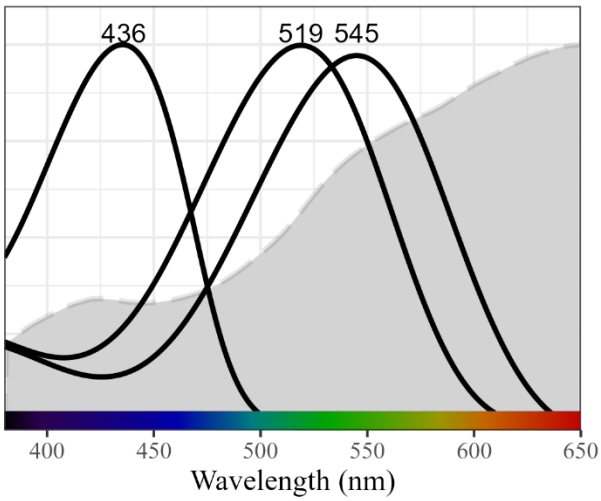

Black line

Walleye pollock visual pigments $x_{max}$

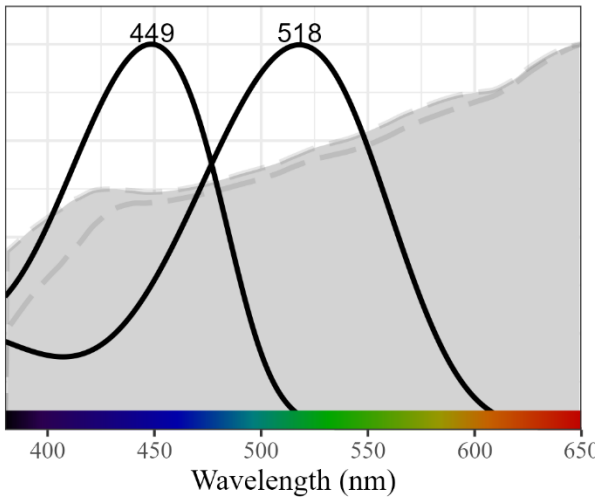


Black line

Chinook salmon visual pigments $x_{max}$

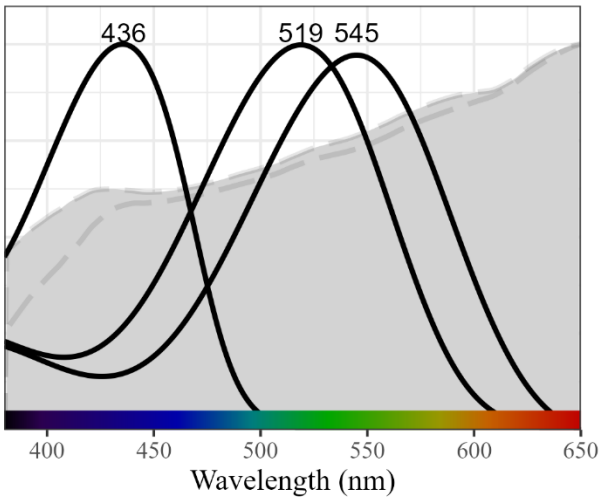


Black net

Walleye pollock visual pigments $x_{max}$

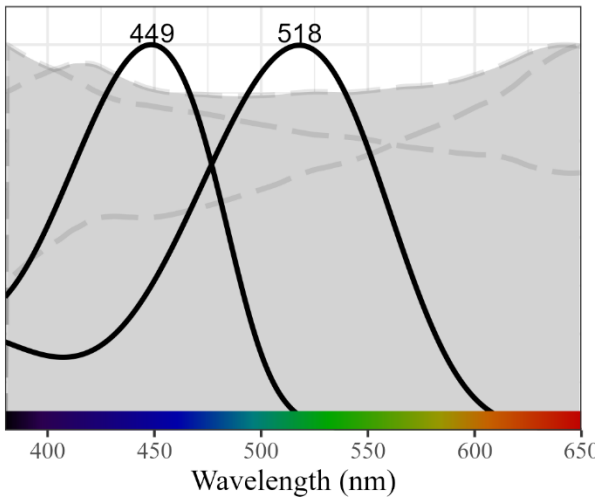


Black net

Chinook salmon visual pigments $x_{max}$

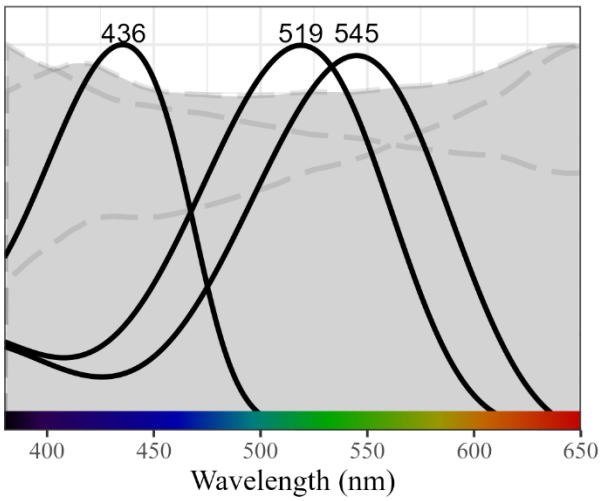

White line

Walleye pollock visual pigments $x_{max}$

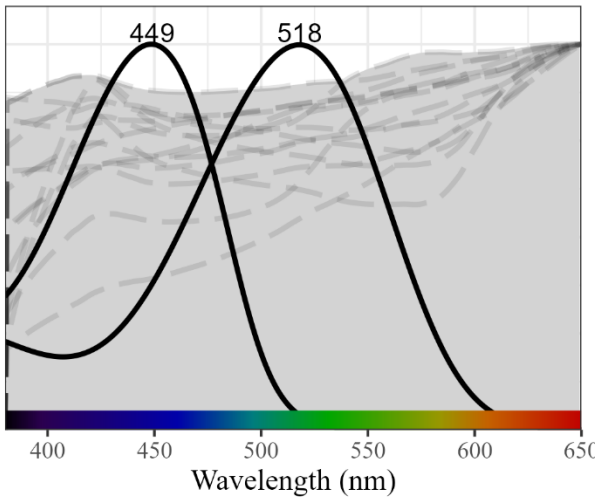


White line

Chinook salmon visual pigments $x_{max}$

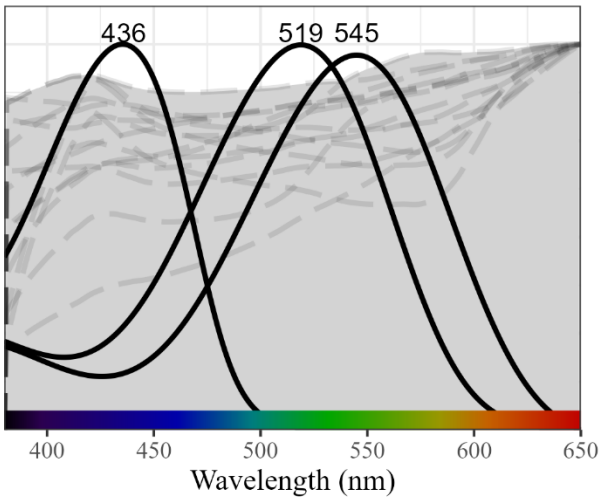


White net

Walleye pollock visual pigments $x_{max}$

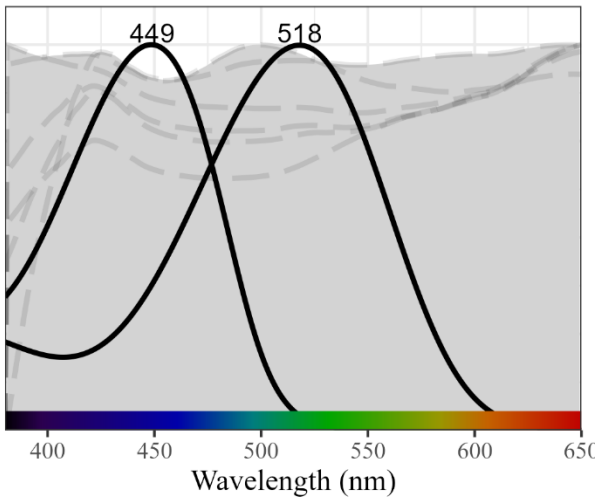


White net

Chinook salmon visual pigments $x_{max}$

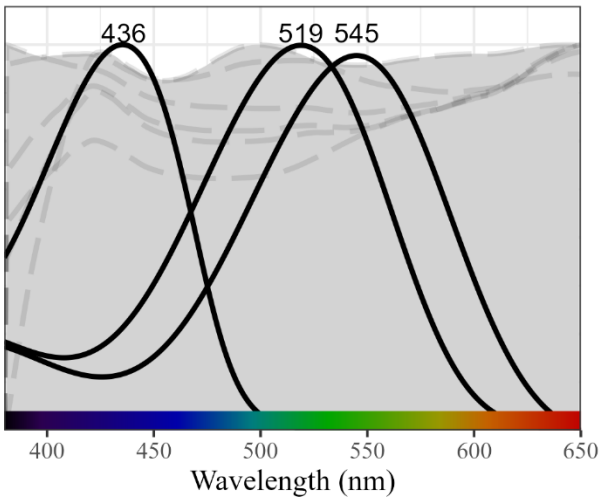

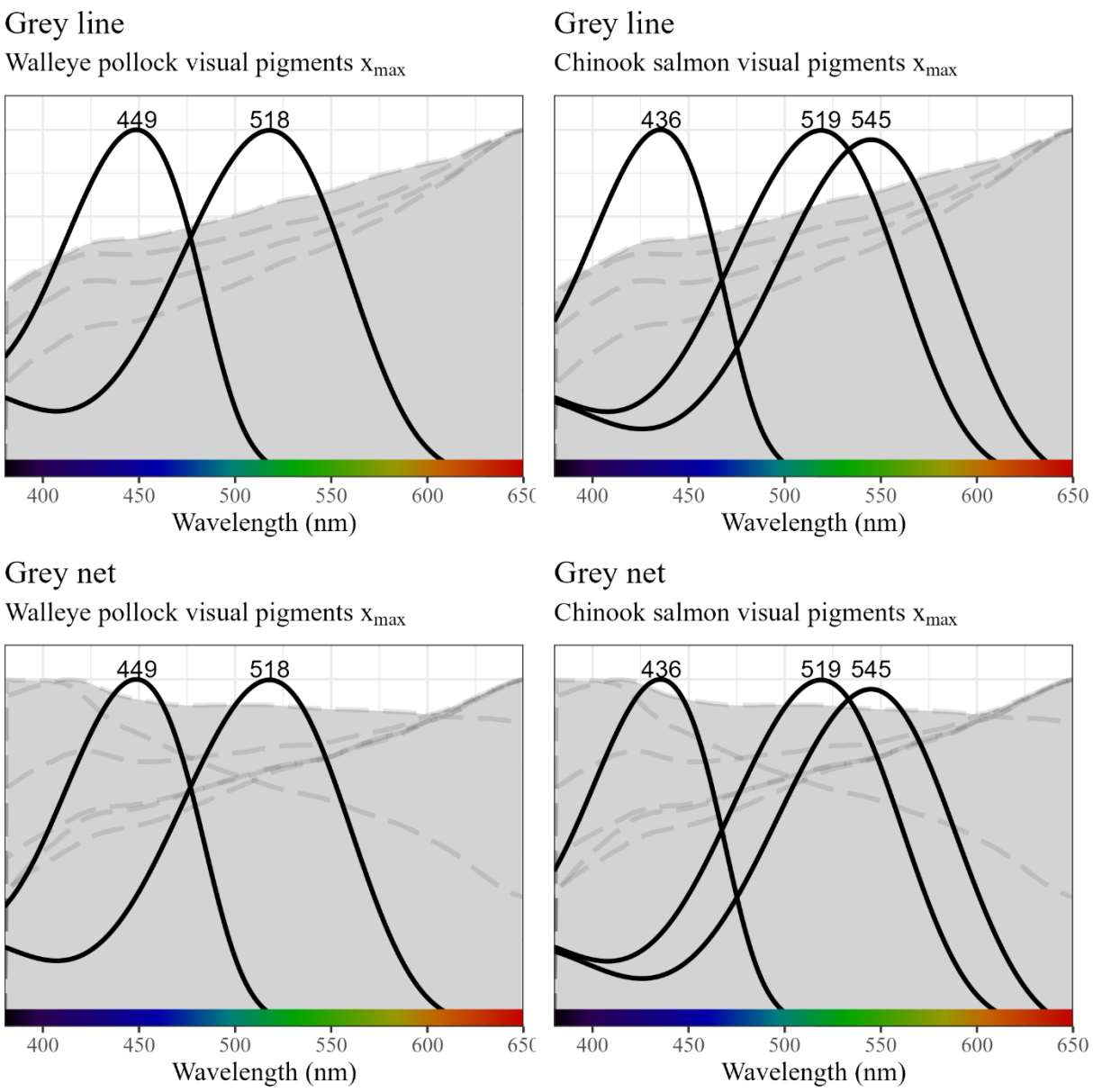


Figure 7. Spectral reflectance of trawl components (line or netting). Shaded areas include percent reflectance less than the maximum reflectance value at each wavelength. Reflectance curves (grey dashed lines) were plotted with visual pigment absorbance curves (solid black lines) for walleye pollock in the left column and Chinook salmon in the right column. The value above the absorbance curves is the $x_{max}$ for each visual pigment.

*Spectral irradiance*

The spectral irradiance profiles for the site selected depths characterize the irradiance as the unit of power per unit area for each wavelength. The similarities in the profile shapes and available spectral irradiance among the sites were consistent throughout the water column (Figure 8). In laboratory simulations, the light-intensity swimming threshold for juvenile pollock was 4.348 x $10^{-4}$ W/$m^2$/sec (Olla et al. 1997a). Intensity thresholds for adult Chinook salmon were available in lux (Hansen et al. 2013) and unable to be converted to irradiance without information on the wavelength or color of light. Light intensities from the bottom to 50 m above the bottom were present at detectable levels for both Chinook salmon and walleye pollock. As depth increased, the intensity and spectral availability of light decreased. The just-below-surface irradiance intensity was highest at 466 nm for sites A and C and 459 nm at site B **(**Error! Reference source not found. This was shifted toward longer wavelengths compared with typical oceanic-type water optical properties (Jerlov 1968). . The year the spectral irradiance data were collected was marked with unusual occurrences such as record low sea ice, high chlorophyll a concentrations, and increased spatiotemporal extent of coccolithophore blooms (Zador 2015). The wavelength with maximum intensity trending through the water column was ~ 498 nm for all three sites (Figure 8). The maximum intensity shifted slightly towards shorter wavelengths as depth increased. The range of spectral availability within 50 m from the bottom differed among station bottom depths (Figure 9).

Site A was the farthest west site near Zhemchug Canyon and 122 m deep. The spectral availability at Site A contained biologically relevant intensities ranging between 391 and 601 nm. Site B was the deepest site (157 m) near the Pribilof Canyon and had the most limited spectral

availability at biologically relevant intensity levels ranging from 441 to 534 nm. The most eastern station, Site C, was the shallowest site (97 m) and all wavelengths measured (380-750 nm) were present at biologically relevant intensities.

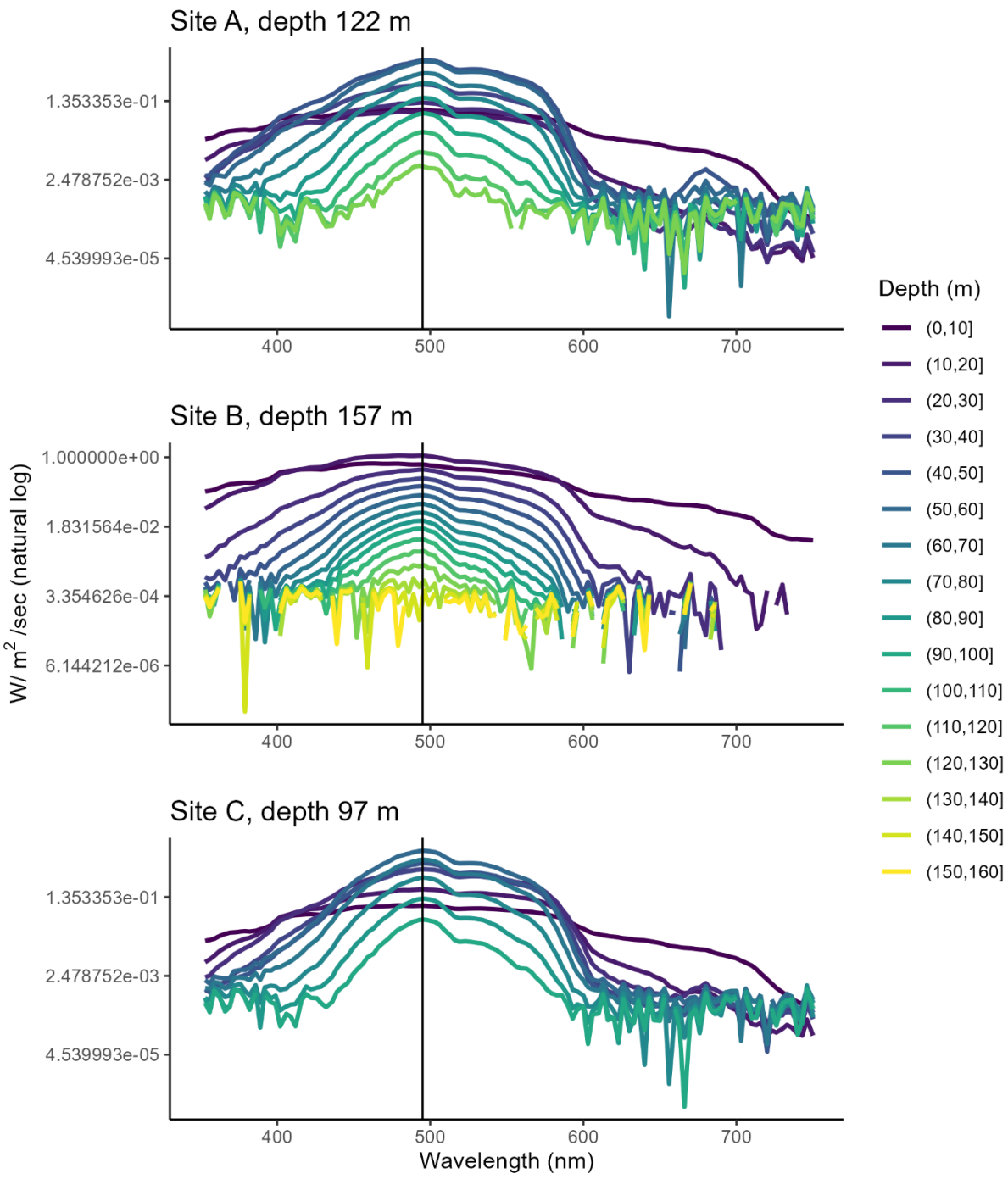


Figure 8. Spectral irradiance of 3 stations in the Bering Sea from surface to bottom. The vertical line indicates maximum transmittance at 498 nm.

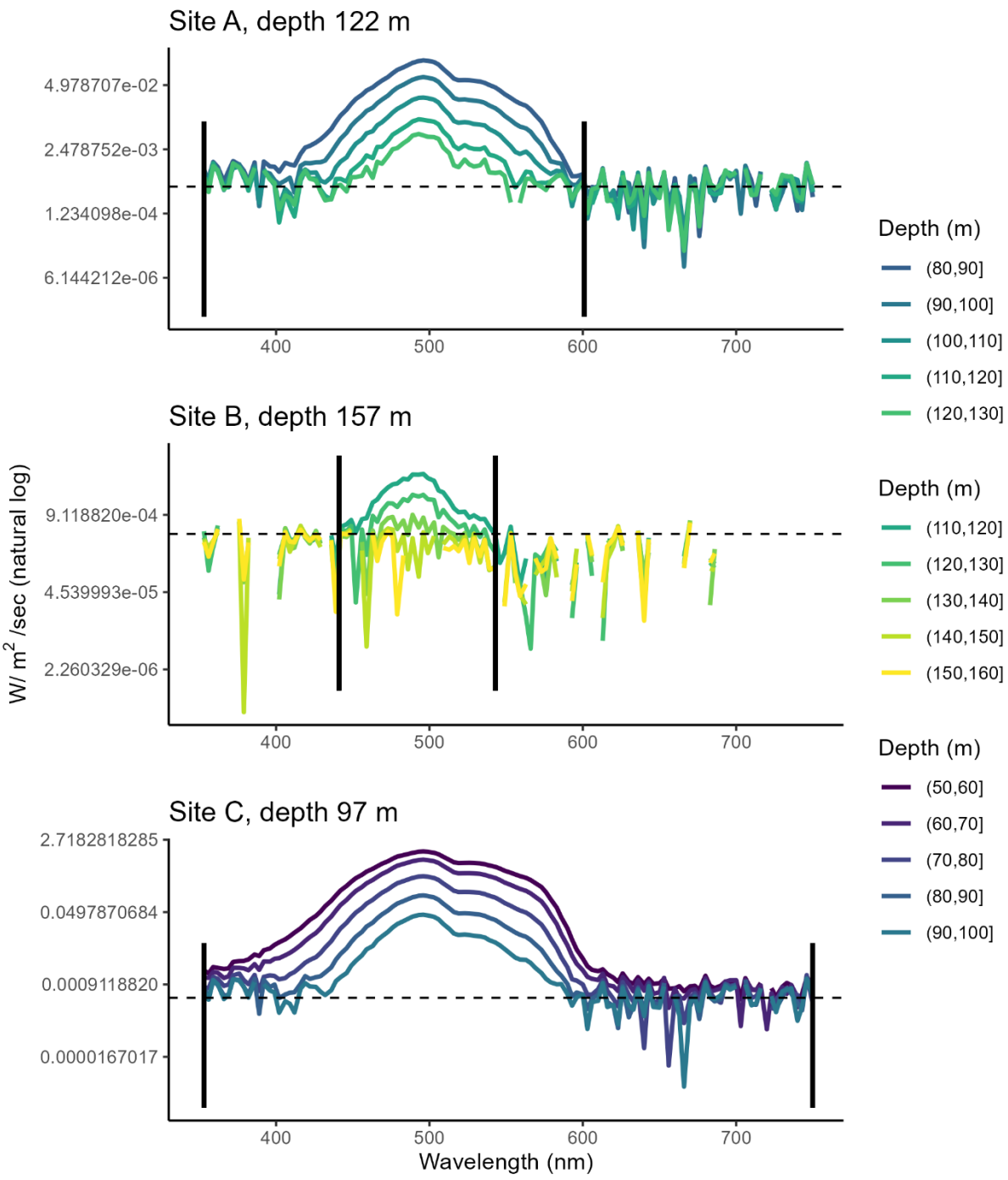


Figure 9. Spectral irradiance plot within 50 m of the bottom from 3 stations in the Bering Sea. The horizontal dashed line represents the minimum threshold of light intensity to swimming behavior for pollock and Chinook salmon. The solid vertical lines define the minimum and maximum limits of spectral availability at the biologically relevant intensity. Missing values are due to negative or 0 value irradiance measures.

*Theoretical color space modeling*

VPModel

VPModel predicted the best visual pigment pair, maximum depth, and maximum range at 15-m depth where the critical threshold occurred. The critical threshold is the point where 50% of the targets can be discriminated from the background spacelight. The maximum range is the distance from the 'visual receiver,' or eye. to the target. All targets were grouped as a parameter of the first set of models. The critical threshold was the maximum depth or range at which 5 of the 9 targets were distinguished from the background using the "best" predicted visual pigments. The depth or range of the critical threshold and predicted visual pigments were modeled with the just-below-surface irradiance data from three sites and two chlorophyll a concentrations representing warm (2014) and average (2022) water temperature conditions (Table 3).

Chlorophyll a concentrations did not influence the maximum horizontal detection range of the target at site B. The range of critical threshold at site C increased from 0.31 m to 0.56 m when chlorophyll a decreased. Chlorophyll a concentrations remained the same between 2014 and 2022 at Site A. The concentration decreased in 2022 at Sites B and C. The decrease in chlorophyll a shifted the scattering of light in the water towards shorter wavelengths (Figure 10). The maximum depth of the critical threshold increased at each site where chlorophyll a concentration decreased in 2022. The visual pigment ranges and critical threshold depth predicted by the model for site A, which was furthest away from a large land mass and had the same chlorophyll concentration during both years, were the same for both 2014 and 2022. The range of the first visual pigment encompassed the cyan portion of the spectrum (476-486 nm) and the second predicted visual pigment range was in the red to red-orange region (Table 1). The

edge of the first visual pigment range moved towards the shorter wavelengths and the range broadened when the chlorophyll a concentration decreased. The maximum depth where the critical threshold was predicted did not follow a noticeable pattern. Depth values were between 15.53 m and 20.36 m and did not appear to be associated with the chlorophyll a concentration.

Table 3. Predicted visual pigment (VP) pair ranges are required to discern 50% of the targets at maximum depth and maximum range of the critical threshold. All predictions were modeled using just-below-surface irradiance files for each site as well as the monthly averaged chlorophyll a concentration. In lieu of regional data, the DOM value was fixed at 0.99 mg/L.

| Site | July | Chl a ($mg/m^3$) | Max depth (m) | Max range (m) | VP1 range (nm) | VP2 range (nm) |
|---|---|---|---|---|---|---|
| A | 2014 | 1.5 | 16.90 | | 476-486 | 606-646 |
| | 2022 | 1.5 | 16.90 | | 476-486 | 606-646 |
| B | 2014 | 5.0 | 18.65 | | 456-496 | 571-646 |
| | 2022 | 2.0 | 20.36 | | 471-496 | 576-646 |
| C | 2014 | 1.0 | 15.53 | | 461-486 | 571-646 |
| | 2022 | 0.4 | 16.31 | | 451-491 | 471-646 |
| A | 2014 | 1.5 | | 1.30 | 471-611 | 576-646 |
| | 2022 | 1.5 | | 1.30 | 471-611 | 576-646 |
| B | 2014 | 5.0 | | 2.28 | 466-506 | 561-646 |
| | 2022 | 2.0 | | 2.28 | 461-506 | 546-646 |
| C | 2014 | 1.0 | | 0.31 | 461-491 | 566-646 |
| | 2022 | 0.4 | | 0.56 | 471-491 | 576-646 |

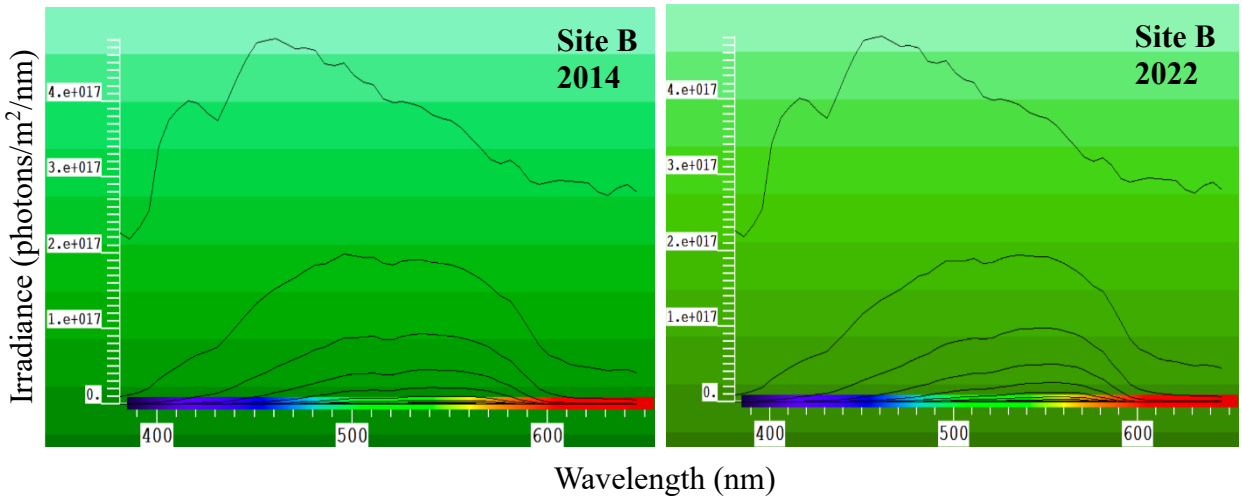


Figure 10. Downwelling spectral irradiance to 50 m depth and chlorophyll a concentration of 5.0 in 2014 and 2.0 mg/m$^3$ in 2022 at site B. The color gradient is indicative of human perceived water color. The brightness difference between years was eliminated through normalization of the spectral curves. The same just-below-surface spectral irradiance file and DOM concentration

The second set of models was conducted to determine the best visual pigments (VP1 and VP2) to chromatically discriminate single color targets from the background spacelight (Figure 11). The distance from the target and depth at the critical threshold of individual color patches against the background spacelight were calculated utilizing the same environmental and location parameters as the first set of models. The visual parameter was set to a single target to discern against the background space light; thus, the critical threshold was set at 100% for this module. The range at 15-m depth was greatest for the blue target at all sites. The predicted depth of the critical threshold was greatest for the blue target at sites A and B and the yellow target at site C. Maximum range and depth were shortest and shallowest for red, orange, and grey targets. Critical thresholds of range and depth were unable to be established at some or all site sites for red, black, white, and grey targets. The visual pigment pairs predicted to detect the targets at 15-m depth were similar for all colored targets. The first visual pigment ranged between 461 and 486 nm, and then the second pigment ranged between 569 and 646 nm. At maximum depth, the visual pigment pairs range between 465 and 526 nm and 571 and 646 nm. The maximum depth

of the critical threshold was consistently deepest at Site B, despite the higher concentration of chlorophyll a. Pigment pairs predicted for the critical threshold of the range at Site B were in a slightly longer wavelength range than Site A when values were available to compare.

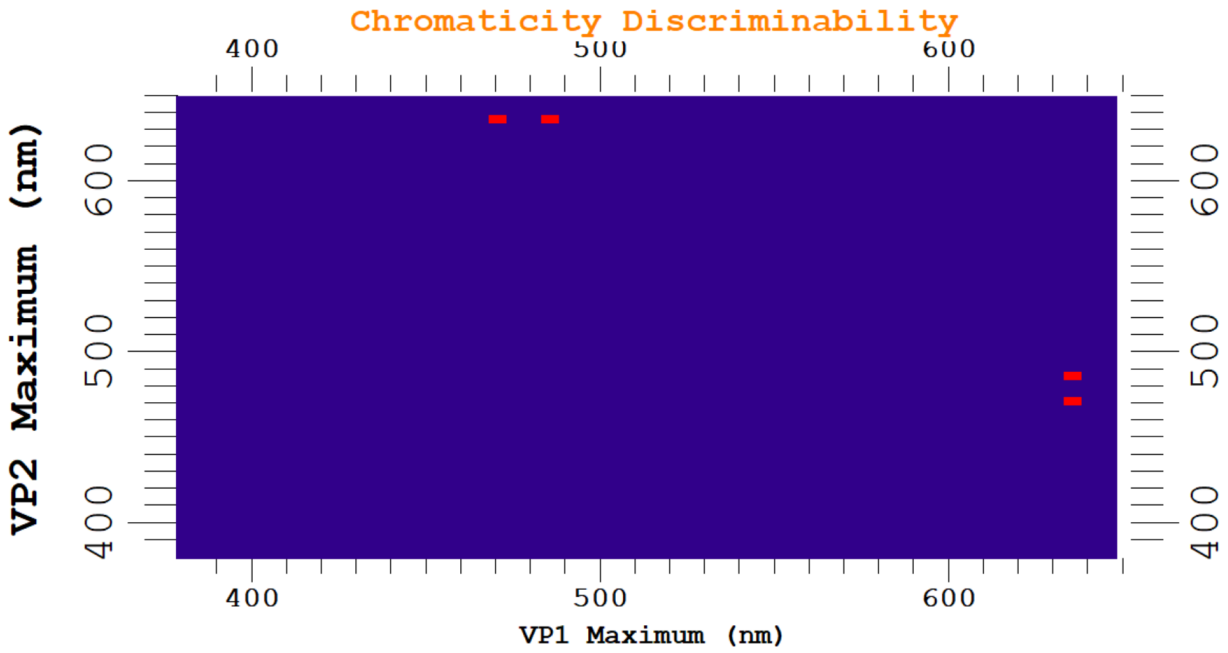


Figure 11. Example of chromaticity plot predicting the best pigment pairs (VP1 and VP2) to distinguish a blue target from the background. The red pixels are indicative of the wavelength(s) of the visual pigments needed to detect the target from the background.

Table 4. Predicted visual pigment pairs at 100% critical threshold for color patch recognition at maximum range from all the targets at 15 m below the surface and at maximum depth when the distance from the targets was 1 m. Data inputs were 1) spectral irradiance data for each site derived from just-below-surface spectral irradiance measurements, 2) averaged color patch spectral reflectance data for each color class of targets, 3) chlorophyll a concentrations, set as 1.5, 1.0, and 4.0 mg/m$^3$ for sites A, B, and C (2014 values corresponding with irradiance data), and 4) DOM, fixed at 0.99 mg/L. Photopic and scotopic thresholds were converted from values in Olla et al. 1997b. The critical threshold was set to 100% for these single targets.

| Color patch | Site | Max range | Max depth (1 m range from target) | VP1 | VP2 |
|---|---|---|---|---|---|
| Red | A | 0.12 | | 481-491 | 569-631 |
| | | | 11.82 | 521 | 641 |
| | B | 0.26 | | 491-516 | 616-646 |
| | | | 12.99 | 506-526 | 631 |
| | C | - | | - | - |
| | | | 9.28 | 501-526 | 611-646 |
| Orange | A | 1.30 | | 491 | 611-646 |
| | | | 16.90 | - | - |
| | B | 2.28 | | 496 | 606-616 |
| | | | 18.65 | 456-481 | 571-641 |
| | C | 0.70 | | 461 | 646 |
| | | | 13.10 | 476-481 | 611-646 |
| Yellow | A | 3.99 | | - | - |
| | | | 23.93 | 471, 486 | 636, 626 |
| | B | 6.54 | | 476 | 611 |
| | | | 37.73 | 476 | 626-641 |
| | C | 2.16 | | 476-486 | 601-616 |
| | | | 22.56 | 471 | 646 |
| Green | A | 3.34 | | 486 | 616 |
| | | | 19.08 | 486 | 636 |
| | B | 3.62 | | - | - |
| | | | 20.22 | 481 | 606,621 |
| | C | 0.27 | | - | - |
| | | | 13.97 | 486 | 616-636 |
| Blue | A | 5.47 | | 471-476 | 631 |
| | | | 21.97 | 466-481 | 606-646 |
| | B | 8.98 | | - | - |
| | | | 40.92 | - | - |

| | | | | | |
|---|---|---|---|---|---|
| | C | 2.93 | 19.43 | 471,481<br>471,486 | 621, 646<br>636 |
| Brown | A | 2.27 | 18.65 | 471<br>481 | 636<br>606 |
| | B | 4.72 | 25.68 | -<br>- | -<br>- |
| | C | 1.06 | 14.81 | -<br>466-476 | -<br>641 |
| Black | A | - | 5.18 | -<br>476 | -<br>626 |
| | B | - | 8.11 | -<br>- | -<br>- |
| | C | - | 2.65 | -<br>471-491 | -<br>611-646 |
| White | A | - | 4.20 | -<br>491 | -<br>636 |
| | B | - | 6.35 | -<br>481 | -<br>631 |
| | C | - | 2.25 | -<br>- | -<br>- |
| Grey | A | 0.56 | 5.57 | 461-471<br>481 | 611-646<br>621-646 |
| | B | - | 8.50 | -<br>- | -<br>- |
| | C | 3.07 | 3.08 | 476, 486<br>476, 486 | 626-641<br>626-646 |

Models Using *pavo*

Visual pigment absorbance curves for pollock and Chinook were defined and produced in *pavo* for comparison to VPModel® predictions. These curves were plotted against absorbance curves collected from photoreceptors (Figure 12). Curves generated from *pavo* were set at a maximum absorbance of 450 nm and 435 nm for pollock and Chinook blue visual pigments. The *pavo* blue absorbance curve was offset to slightly longer wavelengths than the photoreceptor curve on both the right and left limbs of the curve. The cyan absorbance curves, 518 nm for pollock and 517

nm for Chinook salmon, generated from *pavo* and the curve from the photoreceptors displayed the best overlapping fit. The green visual pigment curve produced by *pavo* matched the right limb of the photoreceptor absorbance curve for the green visual pigment possessed by Chinook salmon (548 nm); however, the left limb was shifted toward longer wavelengths. Overall, the absorbance curves produced by *pavo* matched the photoreceptor absorbance curves, although *pavo* curves were noticeably offset to longer wavelengths for blue and green visual pigment. For consistency, *pavo* absorbance curves were used to define the color space for pollock and Chinook salmon.

Color spaces for standard daylight (above water) and 50-m and 100-m depths at each site were produced to model differences in photoreceptor stimulation by a target. The color space modeled under standard daylight illumination (D65) depicted targets above water with the visual pigment spectral sensitivities for pollock and Chinook salmon to provide a frame of reference for above and below water irradiance regimes. The areas close to the edges of the triangle indicated high saturation of a hue (e.g., red is more saturated than pink). The further away from the edge of a trichromatic color space, the less saturated the hue of the reflectance spectrum of a target. The center of the color space represents the achromatic point where cones are stimulated equally.

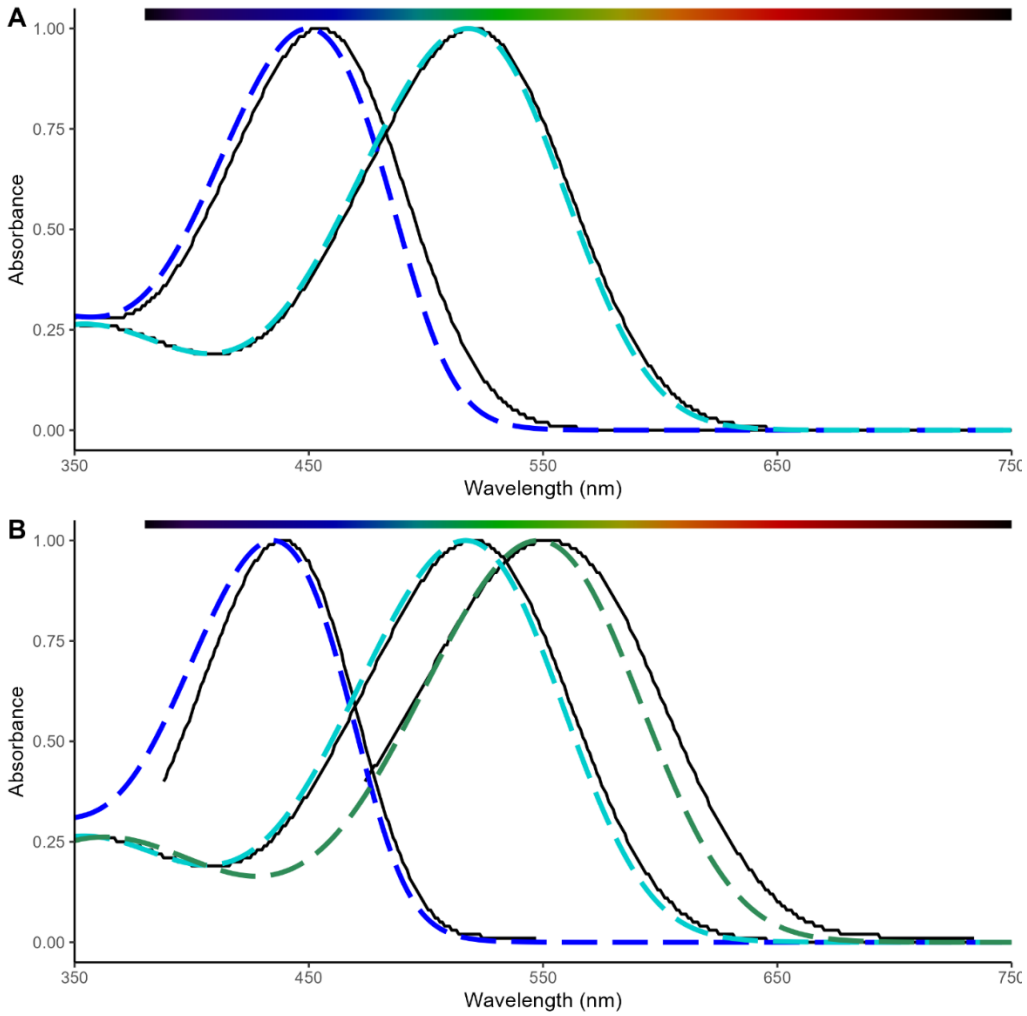


Figure 12. Walleye pollock (panel A) and Chinook salmon (panel B) A1 template curves for cone photoreceptor cells generated from VPModel® (solid lines) and the R package pavo (dashed lines). Pollock had 2 cone visual pigment absorbance curves with peak absorbance at 450 and 518 nm. Three cone visual pigments were found in Chinook salmon with peak absorbance at 435, 517, and 548 nm.

Within the pollock color space above water, all targets are shifted toward longer wavelengths (red). The 40-50 m and 90-100 m color spaces integrated spectral irradiance data at the corresponding depths and generally shifted the targets towards shorter wavelengths (blue) (Figure 13). The targets were located closer to the shorter wavelengths at the 40-50 m depth and gradually decreased in saturation as depth increased. The targets closest to the short wavelength

at 40-50 m were located further away from the short wavelength point in the 90-100 m depth bin. The deepest depth bin at each station was characterized by a reversal of the trend toward shorter wavelengths exhibited in shallower depths (Figure 14). The contrast range between targets was greatest at site A 40-50 m and site B 140-150 m. The further a target was from the center point at any given depth, the greater the contrast from the center point representing the background spacelight. Color spaces modeling 40-50 m depth bin at all sites indicated the least amount of contrast between the red and orange targets against the background. There was no apparent pattern between color patches and distance from the achromatic point within sites at the deepest depth bin.

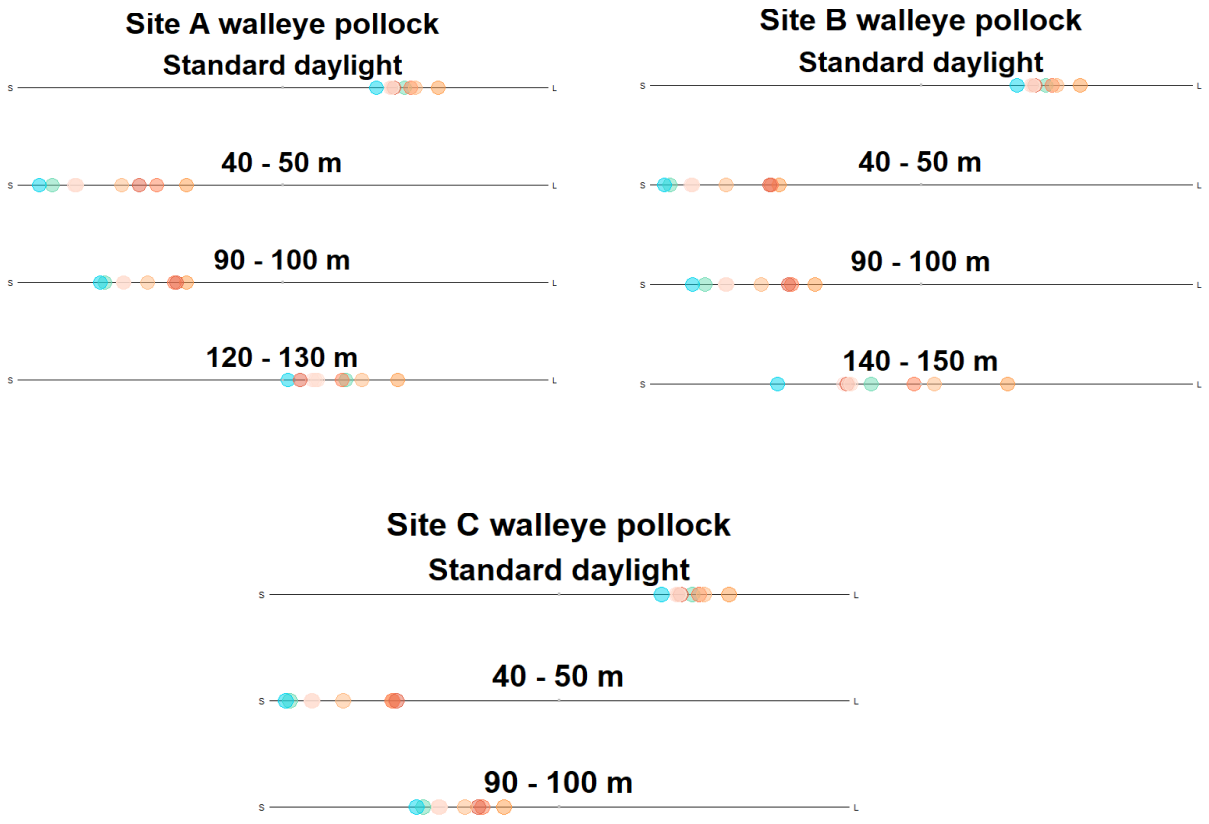


Figure 13. Dichromatic color spaces were constrained by walleye pollock visual pigment spectral sensitivities. Wavelengths are from left to right, short to long. Targets within each color space were modeled under different spectral irradiance regimes: standard daylight (D65) and spectral

irradiance at defined depth bins. The deepest depth bin represents the maximum depth of each station.

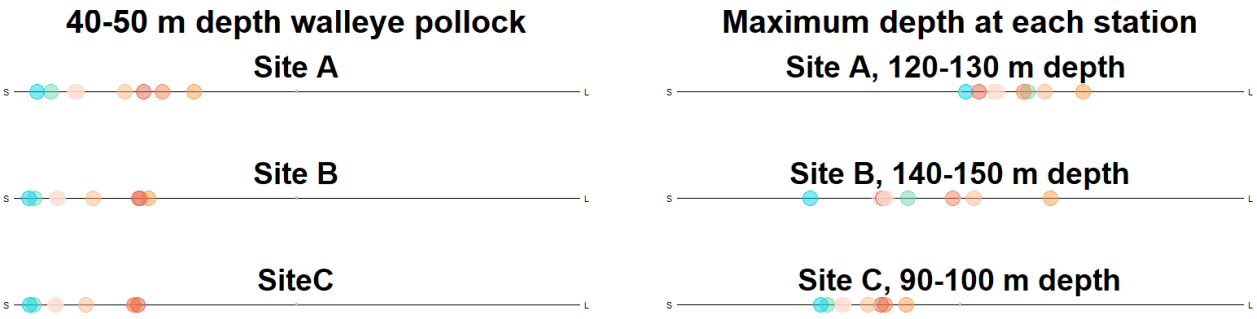


Figure 14. Walleye pollock color space for each station representing targets at 40-50 m depth and maximum depth irradiance spectra.

Similar patterns were observed in the color spaces defined by Chinook salmon spectral sensitivities. The standard daylight (above water) irradiance clustered the targets between the medium and long wavelength vertices (Figure 15). As depth increased, the 40-50-m bin shifted the targets to coordinate space approximately halfway between the short- and long-wavelength vertices at sites A and B. Targets at site C in the 40-50-m depth bin occupied color space closer to the long-wavelength vertex. The location within the color space of the average reflectance spectra for blue and green targets indicated these color patches were highly saturated in this depth bin. The color space with the spectral irradiance profile at the 90-100-m depth bin continued the shift in the target location closer to the long wavelength vertex at all sites. This shift was in response to the decrease in available spectral range as short wavelengths were filtered out of the water column. The target cluster within the color space representing the deepest depth bin at each site was repositioned to a more central location within the triangle. The deepest site (B) was characterized by movement toward the center of the triangle when compared to all other depths and sites (Figure 16). The targets positioned closest to the center of the

triangle had the least amount of contrast against the background space light. Red, orange, and yellow targets had the least amount of contrast to the background spacelight at the shallowest stations for Chinook salmon visual models. The color space depicting site A 120-130-m depth indicated the blue target and background color space were likely indistinguishable based on overlap.

The color spaces provided a quantitative map of how the color of the targets is perceived by species-specific visual systems. The target color patches closest to the center point of the segment or triangle are interpreted as achromatic neutral and closest to the background spacelight spectrum. Overlapping targets were unlikely to be distinguished from one another; however, they may be discerned against the background spacelight depending on the modeled depth.

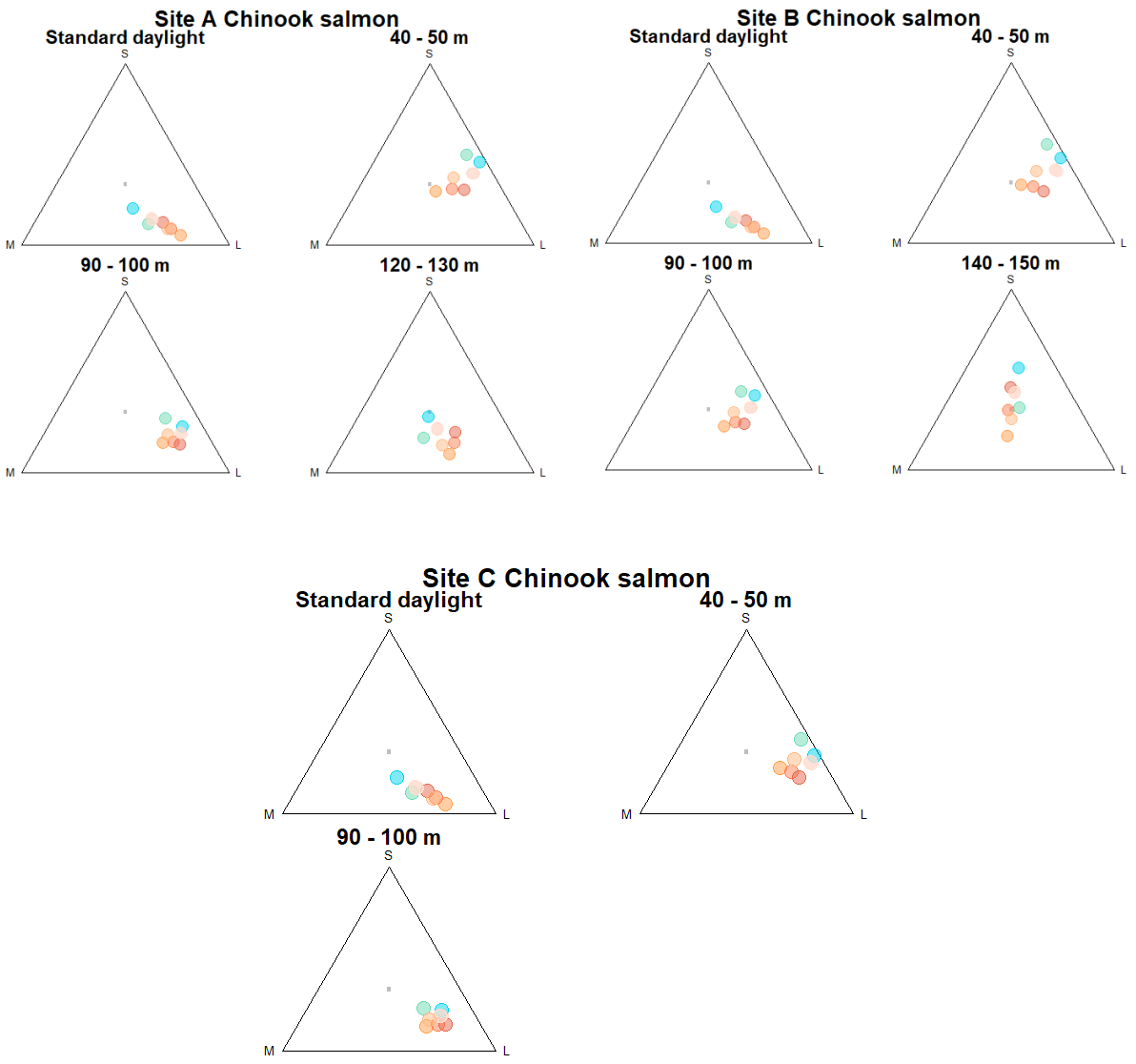


Figure 15. Trichromatic color space was defined by Chinook salmon visual pigment spectral sensitivities. Each vertex represents short (s), medium (m), or long (l) wavelengths. Targets (aggregated spectral reflectance curves of color patch classes) within each color space were modeled for 3 (site C) or 4 (sites A & B) different spectral irradiance regimes: standard daylight (D65) and spectral irradiance at defined depth bins. The deepest depth bin represents the maximum depth of each station.

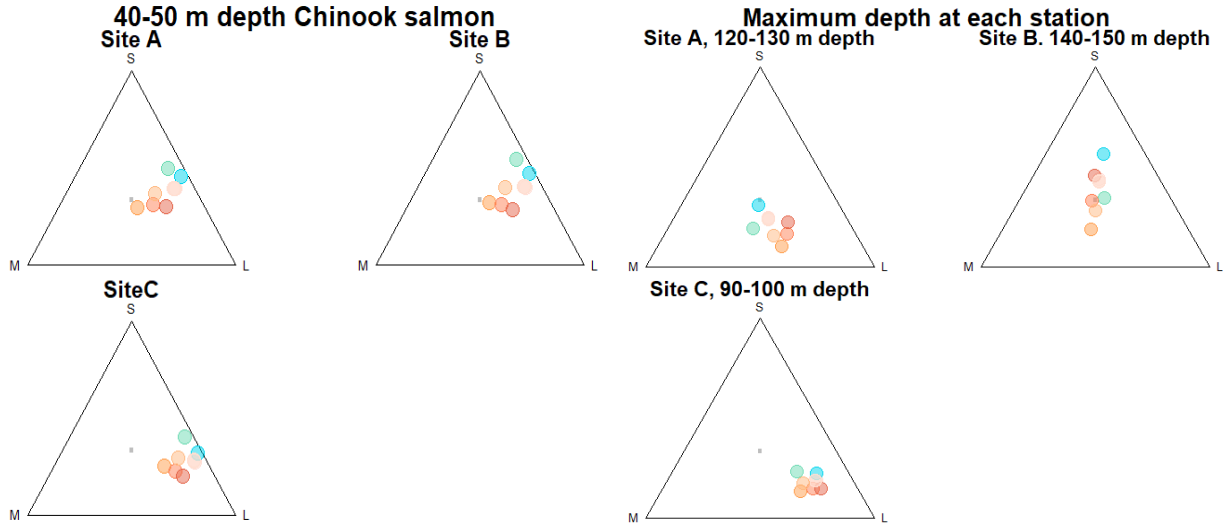


Figure 16. Chinook salmon color space for each station representing targets at 40-50 m depth and the maximum depth irradiance spectra at each site.

Chromatic contrast values between color patches were all <1 and not included in further analysis. Continued work addressing noise values for each receptor, photoreceptor density, illumination conditions, background spacelight spectrum, and achromatic photoreceptor stimulation in conjunction with the behavioral response is recommended.

## Discussion

*Microspectrophotometry*

Visual pigment studies conducted on marine fishes are generally within three environments: deep water, coastal, or tropical reef. Until recently, MSP machines lacked the stability to compensate for the motion and vibrations on board a vessel. Fishes would need to be caught, kept alive, and live-transported to shore (Jokela-Määttä et al. 2007). Advances in technology have made it possible, albeit not easy, to obtain MSP measurements while on board large vessels. This development in technology has decreased the cost and opened the marine offshore and midwater

fish communities to visual pigment analysis, although difficulties in obtaining MSP samples for this study were noted by the engineer (E. Loew, *pers. comm*.). Updated and specialized MSP equipment has been engineered to reduce the effect of vessel motion on the light filament for use in future studies.

Rod, cone, and non-identical twin cone photoreceptors were present in adult and juvenile walleye pollock and adult Chinook salmon. Visual pigment maximum absorbance wavelength values ranged from blue to blue-green in pollock and blue to green in Chinook salmon. The presence of rod and non-identical twin photoreceptors in walleye pollock is novel information, as previously only single and identical twin cones were detected in larval walleye pollock (Britt et al. 2001). In both species, the rod (507 nm) and blue-green cone (515-519 nm) spectral sensitivities closely match the light environment of Pacific coastal and estuarine areas (Novales Flamarique and Hawryshyn 1993), while the light environment at the Bering Sea site was shifted toward longer wavelengths. The spectral environment characteristics were likely to be different from years which experienced normal levels of sea ice and cooler temperatures.

Pollock and Chinook salmon rod maximum absorbance values were both centered around 507 nm in the green range of the visible spectrum. Walleye pollock had 2 distinct cone pigments in the blue and blue-green spectral classes. Chinook salmon had 3 distinct cone pigments in the blue, blue-green, and green spectral classes. In the general sense, when facing the surface, the blue-green sensitive pigment enables the fishes to discern contrasting objects against the blue-green spacelight, whereas the blue visual pigment enables bright objects to be distinguished (Levine and MacNichol 1982). The pigment roles are reversed when the eyes of the fish face

forward or downward. Chinook salmon spectral sensitivity spans a larger range than pollock due to the presence of a third visual pigment with maximum absorbance in the 545 nm (green) band located in single and non-identical twin cones. When a photon of light with a frequency corresponding to the green spectral range is absorbed by the chromophores with green visual pigment, the phototransduction cascade is activated. Levine and MacNichol (1982) hypothesize that evolutionary selection towards cones was in part due to the efficiency of cones in bright light environments and the advantage of greater contrasts between targets and spacelight over a broader spectral range. Trichromats, such as Chinook salmon, have developed an advantageous visual system that performs effectively in a wide range of environmental water conditions due to the broader spectral coverage of 3 visual pigments (Munz and McFarland 1973, Levine and MacNichol 1979, 1982) .

Samples included photoreceptor cells from multiple pieces of the retina. The wild-caught fish experienced lengthy exposure to bright light and air before placement in the lightproof container in most instances. These events likely affected the amount of visual pigment built up during dark adaptation, particularly for short wavelength opsins. During the collection of absorbance curve data from individual photoreceptor cells, the motion of the vessel affected the light filament, causing the light beam to move in and out of the cell sample. The samples where this occurred were discarded. Approximately 50% of all MSP records were used in the analysis. It is possible that the number of shortwave photoreceptor cell spectral classes was underrepresented or absent in these samples. Microspectrophotometry measures a subsample of the available photoreceptors. The missing or underrepresented spectral classes may be an artifact of sample size.

Ultraviolet shortwave (UVS) single cones have been measured in alevin, parr, and smolt stage salmonids including rainbow trout (*O. mykiss*), sockeye salmon (*O. nerka*), brown trout (*Salmo trutta),* and Atlantic salmon (*S. salar*) (Kuntz 1987, Novales Flamarique 2000, 2005, Allison et al. 2003). These cones disappear or are greatly reduced during the later life stages. Retinal mosaic results and electroretinography have indicated the possibility of UVS cone regeneration in adult rainbow trout, coho salmon (*O. kisutch*), Chinook and chum (*O. keta*) salmon (Beaudet et al. 1997, Novales Flamarique 2000); however, these findings have not been validated by microspectrophotometry or behavioral evidence. This study did not find evidence of UVS cones in wild-caught or hatchery adult Chinook salmon.

Despite the ease and relevance of discussing visual pigments in terms of maximum absorbance, it must be recognized that visual pigments have broad absorbance across the spectrum. Assuming the lens and cornea of these fishes did not filter out a range of wavelengths and the wavelengths are present in the aquatic environment; the potential range of spectral sensitivity can span from the UV wavelengths into the 625 nm range for walleye pollock and the 675 nm range for Chinook salmon. The spectral sensitivity range of the visual pigment for pollock included reactivity to stimuli reflecting in the blue through the orange range. Chinook salmon visual pigment sensitivities additionally expand into the red-orange spectrum. These physiological visual pigment ranges represent probabilities that a photon at a specified wavelength would stimulate a photoreceptor to send a signal through the visual system to be processed by higher cognitive functions. Behavioral experiments can build on this information to determine what is a biologically significant visual stimulus, such as colored trawl materials.

*Spectral reflectance*

Walleye pollock and Chinook salmon visual systems have the visual capability to detect most fishing gear. The shape, color, and contrast of fishing gear is a novel stimulus to fish. Predicting the resulting behavioral response of the higher cognitive processes occurring after the signal passes through the retina was not within the scope of this study. This study attempted to determine which spectral reflectance curves stimulate photoreceptor activation in pollock and Chinook salmon, and most of the colors tested are within the range of visual capability. Reds and oranges are unlikely to stimulate walleye pollock and Chinook salmon visual pigments. Pollock are less likely to discern yellow material than Chinook salmon. Chinook salmon blue-green and green cones are highly likely to be activated by green color patches, and both species should be able to discriminate blue color patches. The maximum reflected wavelength of the trawl gear materials included short, medium, and long wavelength hues as well as reflectance values equally distributed among wavelengths in the grey, white, and black color patch reflectance curves. The hues of these targets were generally not found at the depths where fishing occurs which may influence the behavior of fishes. Information on what the two fish species are physiologically capable of seeing could inform behavioral experiments by defining physiological visual limitations.

The target reflectance was determined by the available light in the environment. Without the attenuation, absorption, and particle scatter effects of water on light availability, targets reflecting blue, green, grey, white, and yellow were the most likely to reflect photons in the wavelength ranges which would stimulate walleye pollock and Chinook salmon visual pigments. The remaining red and orange targets were least likely to activate both fish visual systems. Under

ideal light and clear water conditions, adult pollock (> 50 cm total length) detected 2 cm targets at an approximately 5-m viewing range (Zhang and Arimoto 1993). In waters that are not clear, the light transmission was progressively filtered by suspended particles and the scattering effect of water molecules which reduced the available wavelengths. The reduction in wavelength range at depths where fishing was conducted resulted in a monochromatic background spacelight. The contrast of a target against the background spacelight was theorized to be more important than the brightness of the target (Wardle 1983).

Contrast thresholds varied among species, target classification, ambient light, and water clarity. The term contrast was applied to both the scotopic and photopic portions of the visual system. The contrast hypothesis as applied to the scotopic system is supported for both species. Pollock and Chinook salmon contain rod pigments that "match" the background (507 nm) and was used to discern an object from the background based on brightness. The visual pigments of Chinook salmon also support the offset hypothesis (Lythgoe 1972) referred to in the context of the photopic visual system where one visual pigment matches the background and a second pigment is offset 10-30 nm (i.e. 519 nm and 545 nm, Table 1). The maximum absorbance values of these two pigments indicated the physiological ability of Chinook salmon to discriminate objects based on their spectral reflectance in the Bering Sea environment. The spectral reflectance from the generalized color patches of trawl components which activated the photoreceptors of pollock and Chinook salmon was physiologically detected from the background.

Reflectance curves of individual materials may interact differently with the visual pigment absorbance curves than the averaged curves used in this model. Characteristics of materials that

may affect results include polymer type or composition, percent area covered by the color patch in multicolor material, contrast patterns, saturation of hue, and brightness. A second consideration not examined in this study was the transmission and filtering of light through ocular media. Absorption properties of ocular media (cornea, lens, humors) can filter the spectrum of light, reducing the wavelengths that reach the retina. If certain wavelengths are absorbed in near totality, vision in the spectral range corresponding to these wavelengths is unlikely (Losey et al. 2003). Data on ocular media characteristics for Chinook salmon and walleye pollock were not available. Adding these data to the model may shift the spectral availability of light passing through the lens.

*Spectral irradiance*

The light environment is spatially and temporally variable on both large and small scales. the diversity of aquatic environments in depth, clarity, and color, all restrict the spectral availability of light. Oceanic light measurements and characterization of the light environment have focused on large bodies of accessible waters at differing depths (Tyler and Preisendorfer 1962, Jerlov 1968). Light environments in shallow systems in channels south of Vancouver Island at water column depths ranging from 23 m to the surface at 3 m intervals (Novales Flamarique and Hawryshyn 1993) . Information on the underwater spectral light environment of Arctic water bodies is lacking in the literature (Cohen et al. 2015). Incorporating a spectral composition of the Bering Sea underwater environment in models with the visual pigment spectral sensitivity of pollock and Chinook allowed the determination of the proportion of biologically available light. This snapshot in time represented one of many photic environments encountered by walleye pollock and Chinook salmon in the Bering Sea.

Spectral conditions are impacted by ecosystem processes and variables such as temperature, ice formation, nutrient availability, and turbidity. The intensity, depth, and spectral signature able to penetrate the water column are constrained by regional and local physical properties. The spectral irradiance data were collected during the summer of 2014. This period was the initial start of a warm stanza (2014-2017) in the Bering Sea (Stevenson and Lauth 2019). Warm stanzas are characterized by low sea ice formation in the winter and warm temperatures in the summer. Surface temperatures ranged from 2.6 to11.9°C in 2014 (average 1982–2021 6.7°C), and bottom temperatures ranged from -1.6 to 7.8°C (average 1982–2022 2.5°C) (Conner et al. 2017, Markowitz et al. 2022). Bottom temperatures were atypically warm (>3°C) at all stations included in this study. Warm summer temperatures were typically preceded by a winter of low sea ice (Hunt et al. 2022). Low sea ice cover and thickness were also associated with greater light intensities and a wider spectral range of light becoming available to open surface waters. Increased primary productivity was associated with low sea ice as more surface water was exposed to greater intensity and spectral range of light (Arrigo et al. 2008, Brown and Arrigo 2012). Chlorophyll a concentrations peaked in 2014 and have decreased in subsequent years (Siddon 2022). Water bodies with high chlorophyll a concentrations undergo a shift in available spectral irradiance signatures from blue to green. Downwelling irradiance is significantly affected by phytoplankton abundance as chlorophyll a absorbs blue and red wavelengths, which increases the green backscatter (Yentsch 1960). Downwelling irradiance is a measure of light moving vertically through the water column. The vertical spectral availability was characterized by reduced range as depth increased at each site.

Pollock and Chinook salmon eyes are laterally placed; therefore, light enters the eye primarily along the vertical axis. Light viewed horizontally under the surface is more monochromatic than light viewed along a vertical sightline near the surface (McFarland and Loew 1983). The horizontal light spectral signature was calculated within VPModel®.

Maximum spectral availability shifted slightly toward longer wavelengths as depth increased. The limited available transmitted wavelengths overlap with the rod and cone spectral sensitivities exhibited by both species. The matching of available wavelengths and spectral sensitivities supports both the contrast and sensitivity hypotheses. The wavelength range with the greatest intensity at the deepest depth was around 480-520 nm. Previous studies have documented that juvenile pollock require a minimum light intensity of >0.002 μmol photons/$m^2$/sec (4.348 x $10^{-4}$ W/$m^2$) to detect visual targets (Olla et al. 1997a), and juvenile Chinook salmon can detect prey at light at a similar level (4.02 x $10^{-4}$ W/$m^2$) when turbidity is 0 NTU (Mazur and Beauchamp 2003, Hansen et al. 2013).

Available intensity and spectra of light can be altered by bioluminescence and artificial light sources. Bioluminescence, when present, generates ~5% of overall light intensity over a wide spectral range and can significantly increase the visibility of fishing gear (Arimoto et al. 2010). The expanding spectral range at the maximum depths of sites A and B are indicative of bioluminescence present in the layer. At low ambient light levels (depths > 200 m) without bioluminescence, pollock and possibly Chinook would be unable to orient and escape a net regardless of spectral availability (Zhang and Arimoto 1993, Olla et al. 2000). Artificially

enhancing light intensity and spectral availability by adding light to a trawl is likely to alter the response of fishes to trawl gear at these depths (Lomeli and Wakefield 2012, 2019).

*Theoretical color space*

Vision-based foragers and predators are constrained by the light environment during the search and capture of prey. During periods of decreased sea ice, fish exhibit an increase in visual searching for prey as opposed to predations through scent or vibration detections (Langbehn and Varpe 2017). The alterations in the visual landscape transform on short- and long-term spatiotemporal scales. Modeling the spectral distribution and physiological visual characteristics provides an avenue to predict how fish interact and adapt to the changing light environment.

Color space models were developed to predict how color is perceived by an organism. The visual pigment range, photoreceptor class, and illumination present in an environment were included as variables to produce a graphical representation of how an organism's visual capabilities interact with stimuli (Kuehni 2003). Modeling the visual parameters may provide links to a better understanding of the behavioral ecology of an organism. VPModel® and *pavo* are considered basic psychophysical color spaces (Renoult et al. 2017). While basic psychophysical models cannot provide information on higher visual discrimination capabilities or high-level perceptual mechanisms, these models provide insight into the visual ecology of organisms that are difficult to obtain, exist in remote areas, or experience environmental conditions that are not easily replicated in a laboratory setting.

VPModel®

The input parameters of the model included just-below-surface irradiance data, chlorophyll A and DOM concentrations, and spectral reflectance curves of single or multiple targets. The product of these modules was critical threshold contrast predictions of the range and depth of targets against the background spacelight. The background spacelight values were interpolated from the supplied irradiance data within VPModel®. The chlorophyll a concentrations selected as inputs were representative of conditions from warm (2014) and average (2022) temperature regimes. DOM concentrations have a significant effect on spectral distribution. This analysis used the concentration 0.99 mg/L to represent ocean water for all models. Changing the concentration to 0.10 mg/L shifted the spectral distribution from the green portion of the spectrum into the blue portion (Appendix D).

There is a high probability that site C would have higher DOM than sites A and B due to the closer proximity toward land. However, with no evidence, models were run with the same DOM value to avoid using unconfirmed environmental parameters. The spectral reflectance curves of the targets were chosen to imitate colors commonly used to build trawl gear. The visual pigment and critical thresholds produced by these models provide a theoretical representation of the biological light environment that exists for walleye pollock and Chinook salmon.

The projected spectral availability of the light environment at sites B and C was dissimilar between 2014 and 2022. The higher chlorophyll a concentration during 2014 indicated a shift of the spectral distribution toward shorter wavelengths. The comparison between years at each site showed an increase in maximum depth at the critical threshold when chlorophyll a decreased.

The increased depth signifies an expansion of the available range of depths in the water column to visual foragers and predators. The visual pigment pairs predicted to best distinguish 50% targets were similar for all conditions tested. The first visual pigment range was within the cyan and green spectral limits, and the second visual pigment was within the yellow and orange portion of the visible light spectrum. The background spacelight spectral signature indicated by the irradiance data is within the range of the predicted first visual pigment. The second visual pigment was composed of long wavelength ranges. These medium and long wavelength range paired visual pigments support the contrast hypothesis, which proposes a matching and an offset visual pigment are best for detecting chromatic differences.

The second suite of models was run on single targets defining a color-patch predicted similar maximum absorbance wavelengths of the first visual pigment for all targets except red. The critical thresholds for the range and depth of the red target were the shortest (<0.3 m) and shallowest (<15 m) at all sites. Long wavelengths are filtered out of the water column at shallow depths more than shorter wavelengths. The presence of long wavelengths at shallower depths may account for the difference in the first visual pigment pair from all other targets. The second visual pigment pair was in the long wavelength portion of the spectrum. The deepest depth when the critical threshold was attained was for the blue target at site B. Short wavelengths travel deeper into the water column than long wavelengths, enabling blue targets to reflect more light particles at deeper depths stimulating chromatic contrast.

Distinguishing chromatic contrast requires more metabolic energy than contrast as a function of luminosity, as cone visual pigments are more energetically expensive to produce, (MacLeod and

Boynton 1979, McFarland and Loew 1983, 1983, Loew and Zhang 2005). The stimulation of the cone photoreceptor requires more energy than rods. Luminosity contrast thresholds and selection of best visual pigment pairs were not within the scope of this project although VPModel contains the capability to model this type of data.

*pavo*

Model inputs for *pavo* included the visual pigment absorbance curves specific to walleye pollock and Chinook salmon. The illumination of the modeled light environment used irradiance data collected at specific depths. The background spacelight data was not collected as part of this data set and the critical threshold between targets and the background were unable to be calculated. This visual model program contained opportunities for other data input such as achromatic (rod) densities, optical filter curves, different methods of calculating quantum catch, and application of the von Kries transformation. While these analyses were not within the scope of this project, additional inputs would add clarity to receptor noise models and potentially add strength to the model outputs. This project modeled the chromaticity of targets in a theoretical color space defined by species-specific visual pigment absorbance curves.

Differences in the overlap of *pavo* and photoreceptor absorbance curves could be explained by the chromophore group used to produce the visual pigment absorbance curve versus the chromophore group(s) present in the photoreceptor. The $A_1$ chromophore group (11-*cis* retinal) is associated with open water aquatic organisms, whereas, the $A_2$ is correlated with aquatic environments where the spectrum is red-shifted such as streams and coastal areas. The $A_2$ (11-*cis* 3,4 didehydroretinal) group broadens the bandwidth of the absorbance curve and red-shifts the

spectral sensitivity. Some organisms, such as salmonids, can incorporate both $A_1$ and $A_2$ into the outer segment (Novales Flamarique 2005). The ratio of the chromophore group can vary throughout life stages and seasonality. Adult Chinook salmon may integrate both chromophore groups into their photoreceptors. Currently, *pavo* does not allow the user to define an $A_2$ template or a ratio when generating absorbance curves with the function *sensmodel*. This study did not investigate $A_1/A_2$ ratios and used *pavo* to produce pure $A_1$ absorbance curves using the defined peak absorption from the MSP portion of this project. Future investigations could incorporate the available retinal mosaic data for adult salmonids (Beaudet, Flamarique, and Hawryshyn, 1997). The receptor-noise limited (RNL) model could use photoreceptor densities from future studies to calculate noise-weighted perceptual distances between targets in conjunction with psychological and behavioral data producing a more advanced version of a psychophysical color space model.

The absorbance curves defined the di- and tri-chromatic color space models produced for pollock and Chinook salmon. The color space representing increasing depths assimilated the spectral range and intensity of ambient light. As light passes through the water column, the spectral range is reduced due to scattering and particle absorption. The reduction in spectral range increased the saturation of blue and green targets at shallower depths, and this saturation decreased as depth increased. The color spaces depicting the deepest depths, particularly site A, indicated an increase in the available spectral range, possibly due to the presence of bioluminescence.

Physiologically relevant spectral range was present at biologically relevant intensity levels which would stimulate photoreceptors of both species. Behavioral visual responses are linked to physiological traits and responses to ecologically pertinent targets. Evolutionary adapted visual

responses to targets are not likely to include man-made materials and shapes such as fishing gear although aspects of gear likely induce behavioral response due to sensory perception. Although vision is only one of the sensory systems utilized by fishes to detect objects, predicting visually-mediated responses to fishing gear based on retinal physiology can assist with a mechanistic approach to fisheries bycatch mitigation experiments and overall efforts.

*Walleye pollock and Chinook salmon response to light and color*

As noted by many visual and behavioral ecologists, models can generate hypotheses about a species perception of color (Lythgoe and Partridge 1991, Aksnes and Giske 1993, Eiane et al. 1997, Aksnes and Utne 1997, Loew and Zhang 2005, Delhey et al. 2015, Wilkins et al. 2016, Gawryszewski 2018). However, contextual validation through behavioral studies is necessary to fully understand each species' color perception. The secondary neural processes taking place after visual information has left the retina directly impact the responses and behavior of fishes to objects encountered in their environment. The underwater ambient light environment is spatially and temporally variable. The light landscape can be affected artificially by attaching lights of different intensities or spectral signatures to fishing gear. This approach to reducing bycatch has been successfully utilized by longline fisheries to attract target fish species (Southwood et al. 2008) and promote avoidance of gear from bycatch species typically caught in gill nets (Senko 2022). Using light as a bycatch detractor or attracter of Chinook salmon toward escapement panels in trawls was found to be moderately successful in the Pacific coast hake fishery (Lomeli and Wakefield 2019). It is my hope that the physiological data collected by this study and the models produced will provide a path forward to increase the success of Chinook salmon escapement within the Alaska pollock fishery.

Pelagic salmonids are visual predators (Ali 1959). The presence of 3 cone visual pigments enhances salmonid ability to discern targets from the background illumination. Incorporating light into a salmon excluder device could be beneficial depending on the irradiance spectrum of the artificial illumination and the luminosity, chromaticity, and saturation of trawl components considering the turbidity of the environment. In laboratory studies, decreased reaction distances of juvenile Chinook salmon were strongly associated with high turbidity and low light levels (Hansen et al. 2013). Light experiments and observations in conjunction with bycatch reduction devices (BRD) have populated the literature (Walsh and Hickey 1993, Glass and Wardle 1995, Olla et al. 1997a, Hunt 2015, Bradburn and Keller 2015, Lomeli and Wakefield 2019, McCarthy et al. 2020, 2020, Southworth et al. 2020, Yochum et al. 2021). These studies have concluded that light affects the success of BRDs. There are competing conclusions over whether light stimulates a positive or negative phototactic effect on salmonids.

The presence of light increased swimming speed as a fright response in a laboratory environment (Yochum et al. 2022). Adult Chinook salmon maintained a closer distance to blue, green, and red non-strobing lights than white light in laboratory studies (Yochum et al. 2022), while smolts have been found to exhibit negative phototactic behavior to red light (Hansen et al. 2018). Laboratory experiments and field video analysis suggest juvenile and adult pollock react to trawls if the light intensity is $\geq$0.017 W/m$^2$ (Olla et al. 1997a, 2000). Bycatch reduction techniques in fisheries that regularly catch massive quantities of a targeted species require a combination of environmental (spectral availability and intensity), physiological, and behavioral information tailored to differences between targeted and bycatch species to be effective.

Focusing on the differences in visual pigment spectral range could direct bycatch reduction efforts to reduce Chinook salmon incidental catch in the walleye pollock fishery. Based on the potential range of spectral sensitivity in pollock and Chinook salmon, it would be possible to construct a light setup turned to an intensity and wavelength range to elicit a phototactic response in adult Chinook salmon. The results of this study suggest focusing on a light source with a maximum intensity of a maximum of 0.10 Watts/$m^2$ and targets designed to stimulate Chinook salmon visual systems that reflect wavelengths >550 and <600 nm as well as turning the intensity to levels that promote increased reactivity distances (Hansen et al. 2013).

**References**

Aksnes, D. L., and J. Giske. 1993. A theoretical model of aquatic visual feeding. Ecological Modelling 67:233–250.

Aksnes, D. L., and A. C. W. Utne. 1997. A revised model of visual range in fish. Sarsia 82:137–147.

Ali, M. A. 1959. The ocular structure, retinomotor and photo-behavioral responses of juvenile Pacific salmon. Canadian Journal of Zoology 37:965–996.

Allison, W. T., S. G. Dann, J. Vidar Helvik, C. Bradley, H. D. Moyer, and C. W. Hawryshyn. 2003. Ontogeny of ultraviolet-sensitive cones in the retina of rainbow trout (*Oncorhynchus mykiss*). Journal of Comparative Neurology 461:294–306.

Andersson, S. 1999. Morphology of UV reflectance in a whistling-thrush: Implications for the study of structural colour signalling in birds. Journal of Avian Biology 30:193–204.

Arimoto, T., C. W. Glass, and X. Zhang. 2010. Fish vision and its role in fish capture. Pages 25–44 *in* P. He, editor. Behavior of marine fishes. Wiley-Blackwell, Oxford, UK.

Arrigo, K. R., G. van Dijken, and S. Pabi. 2008. Impact of a shrinking Arctic ice cover on marine primary production. Geophysical Research Letters 35:L19603, doi:10.1029/2008GL035028.

Beamish, R. 2022. The need to see a bigger picture to understand the ups and downs of Pacific salmon abundances. ICES Journal of Marine Science 79:1005–1014.

Beaudet, L., I. N. Flamarique, and C. W. Hawryshyn. 1997. Cone photoreceptor topography in the retina of sexually mature Pacific salmonid fishes. Journal of Comparative Neurology 383:49–59.

Bowmaker, J. K. 1990. Visual pigments of fishes. Pages 81–107 *in* Djamgoz M. B. A. and R. H. Douglas, editors. The visual system of fish. Springer, Dordrecht.

Bradburn, M. J., and A. A. Keller. 2015. Impact of light on catch rate of four demersal fish species during the 2009–2010 U.S. west coast groundfish bottom trawl survey. Fisheries Research 164:193–200.

Bridges, C. D. 1972. The rhodopsin-porphyropsin visual system. Pages 417–480 *in* H. J. A. Dartnall, editor. Handbook of Sensory Physiology VII/I. Spring- Verlag.

Britt, L. L. 2009. Ontogenetic changes in the visual ecology of northeast Pacific marine fishes. PhD Dissertation, University of Washington, Seattle, WA.

Britt, L. L., E. R. Loew, and W. N. McFarland. 2001. Visual pigments of PNW fish larvae. The Journal of Experimental Biology 204:2581–2587.

Brown, Z. W., and K. R. Arrigo. 2012. Contrasting trends in sea ice and primary production in the Bering Sea and Arctic Ocean. ICES Journal of Marine Science 69:1180–1193.

Catalá, T. S., S. Shorte, and T. Dittmar. 2021. Marine dissolved organic matter: a vast and unexplored molecular space. Applied Microbiology and Biotechnology 105:7225–7239.

Chittka, L., and R. Menzel. 1992. The evolutionary adaptation of flower colours and the insect pollinators' colour vision. Journal of Comparative Physiology A 171:171–181.

Cohen, J. 1964. Dependency of the spectral reflectance curves of the Munsell-color chips. Psychonomic Science 1:369–370.

Cohen, J. H., J. Berge, M. A. Moline, A. J. Sørensen, K. Last, S. Falk-Petersen, P. E. Renaud, E. S. Leu, J. Grenvald, F. Cottier, H. Cronin, S. Menze, P. Norgren, Ø. Varpe, M. Daase, G. Darnis, and G. Johnsen. 2015. Is ambient light during the high Arctic polar night sufficient to act as a visual cue for zooplankton? PLOS ONE 10:e0126247.

Conner, J., D. E. Stevenson, and R. R. Lauth. 2017. Results of the 2014 eastern Bering Sea continental shelf bottom trawl survey of groundfish and invertebrate resources. Pages 1–154. NOAA Technical Memorandum, U.S. Department of Commerce.

Dartnall, H. J. A. 1953. The interpretation of spectral sensitivity curves. British Medical Bulletin 9:24–30.

Dartnall, H. J. A. 1975. Assessing the fitness of visual pigments for their photic environments. Pages 543–563 *in* M. A. Ali, editor. Vision in Fishes. Plenum Press, Boston, MA.

Delhey, K., V. Delhey, B. Kempenaers, and A. Peters. 2015. A practical framework to analyze variation in animal colors using visual models. Behavioral Ecology 26:367–375.

Eiane, K., D. L. Aksnes, and J. Giske. 1997. The significance of optical properties in competition among visual and tactile planktivores: A theoretical study. Ecological Modelling 98:123–136.

Endler, J. A. 1990. On the measurement and classification of colour in studies of animal colour patterns. Biological Journal of the Linnean Society 41:315–352.

Gawryszewski, F. M. 2018. Color vision models: Some simulations, a general n-dimensional model, and the colour vision R package. Ecology and Evolution 8:8159–8170.

Glass, C. W., and C. S. Wardle. 1995. Studies on the use of visual stimuli to control fish escape from codends. II. The effect of a black tunnel on the reaction behaviour of fish in otter trawl codends. Fisheries Research 23:165–174.

Govardovskii, V. I., N. Fyhrquist, T. Reuter, D. G. Kuzmin, and K. Donner. 2000. In search of the visual pigment template. Visual Neuroscience 17:509–528.

Guthrie III, C. M., Hv. T. Nguyen, K. Karpan, J. T. Watson, and Larson. 2021. Genetic stock composition analysis of Chinook salmon (*Oncorhynchus tshawytscha*) bycatch samples

from the 2019 Bering Sea pollock trawl fishery. Page 33. NOAA Technical Memorandum, U.S. Department of Commerce.

Hansen, A. G., D. A. Beauchamp, and E. R. Schoen. 2013. Visual prey detection responses of piscivorous trout and salmon: Effects of light, turbidity, and prey size. Transactions of the American Fisheries Society 142:854–867.

Hansen, M. J., D. E. Cocherell, S. J. Cooke, P. H. Patrick, M. Sills, and N. A. Fangue. 2018. Behavioural guidance of Chinook salmon smolts: the variable effects of LED spectral wavelength and strobing frequency. Conservation Physiology 6:coy032; doi:10.1093/conphys/coy032.

Hirawake, T., J. Oida, Y. Yamashita, H. Waga, H. Abe, J. Nishioka, D. Nomura, H. Ueno, and A. Ooki. 2021. Water mass distribution in the northern Bering and southern Chukchi seas using light absorption of chromophoric dissolved organic matter. Progress in Oceanography 197:102641, doi:10.1016/j.pocean.2021.102641.

Honkalehto, T., and A. McCarthy. 2015. Results of the acoustic-trawl survey of walleye pollock (*Gadus chalcogrammus*) on the U.S. and Russian Bering Sea shelf in June - August 2014 (DY1407). Page 63. AFSC Processed Report, Alaska Fisheries Science Center, NOAA, National Marine Fisheries Service., 7600 Sand Point Way NE, Seattle WA 98115.

Hunt, D. E. 2015. The effect of visual capacity and swimming ability of fish on the performance of light-based bycatch reduction devices in prawn trawls. University of Tasmania, Hobart, Australia.

Hunt, G. L., Jr., E. M. Yasumiishi, L. B. Eisner, P. J. Stabeno, and M. B. Decker. 2022. Climate warming and the loss of sea ice: the impact of sea-ice variability on the southeastern Bering Sea pelagic ecosystem. ICES Journal of Marine Science 79:937–953.

Ianelli, J., B. Fissel, S. Stienessen, T. Honkalehto, E. Siddon, and C. Allen-Akselrud. 2021. Chapter 1: Assessment of the Walleye Pollock Stock in the Eastern Bering Sea. Page 171. Economic status of the groundfish fisheries off Alaska, NOAA.

Ianelli, J., S. Stienessen, T. Honkalehto, E. Siddon, and C. Allen-Akselrud. 2022. Chapter 1: Assessment of the walleye pollock stock in the Eastern Bering Sea. Pages 1–160. Economic status of the groundfish fisheries off Alaska, NOAA., Alaska Fisheries Science Center, National Marine Fisheries Service National Oceanic and Atmospheric Administration, Seattle, WA.

Jerlov, N. G. 1968. Optical oceanography. American Elsevier Publ Co Inc, NY.

Jokela-Määttä, M., T. Smura, A. Aaltonen, P. Ala-Laurila, and K. Donner. 2007. Visual pigments of Baltic Sea fishes of marine and limnic origin. Visual Neuroscience 24:389–398.

Krapivin, V. F., F. A. Mkrtchan, C. A. Varotsos, and Y. Xue. 2021. Operational diagnosis of Arctic waters with instrumental technology and information modeling. Water, Air, & Soil Pollution 232:137.

Kuehni, R. G. 2003. Color Space and its Divisions. John Wiley & Sons, Hoboken.

Kuntz, Y. W. 1987. Tracts of putative ultraviolet receptors in the retina of the two-year-old brown trout (*Salmo trutta*) and the Atlantic salmon (*Salmo salar*). Experientia 43:1202–1204.

Langbehn, T. J., and Ø. Varpe. 2017. Sea-ice loss boosts visual search: fish foraging and changing pelagic interactions in polar oceans. Global Change Biology 23:5318–5330.

Levine, J. S., and E. F. MacNichol. 1979. Visual pigments in teleost fishes: Effects of habitat, microhabitat, and behavior on visual system evolution. Sensory processes 3:95–131.

Levine, J. S., and E. F. MacNichol. 1982. Color vision in fishes. Scientific American 246:140–149.

Liebman, P. A. 1972. Microspectrophotometry of photoreceptors. Pages 481–528 *in* H. J. A. Dartnall, editor. Photochemistry of vision. Springer, Berlin.

Loew, E. R. 1982. A field-portable microspectrophotometer. Pages 647–655 *in* S. Fleischer and L. Packer, editors. Methods in Enzymology: Biomembranes - Part H: Visual pigments and purple membranes - I. Academic Press.

Loew, E. R. 1994. A third, ultraviolet-sensitive, visual pigment in the Tokay gecko (*Gekko gekko*). Vision Research 34:1427–1431.

Loew, E. R., and J. N. Lythgoe. 1978. The ecology of cone pigments in teleost fishes. Vision Research 18:715–722.

Loew, E. R., and H. Zhang. 2005. The propagation of visual signals in the aquatic environment: An interactive Windows®-based model. Page *in* F. Ladich, S. P. Collin, P. Moller, and B. G. Kapoor, editors. Communication in Fishes. Science Publishers, Enfield, NH, USA.

Lomeli, M. J. M., and W. W. Wakefield. 2012. Efforts to reduce Chinook salmon (*Oncorhynchus tshawytscha*) and rockfish (*Sebastes spp.*) bycatch in the U.S. west coast Pacific hake (*Merluccius productus*) fishery. Fisheries Research 119–120:128–132.

Lomeli, M. J. M., and W. W. Wakefield. 2019. The effect of artificial illumination on Chinook salmon behavior and their escapement out of a midwater trawl bycatch reduction device. Fisheries Research 218:112–119.

Losey, G. S., W. N. McFarland, E. R. Loew, J. P. Zamzow, P. A. Nelson, and N. J. Marshall. 2003. Visual biology of Hawaiian coral reef fishes. I. Ocular transmission and visual pigments. Copeia 2003:433–454.

Lythgoe, J. N. 1966. Visual pigments and underwater vision. Pages 375–391 *in* R. Bainbridge, G. C. Evans, and O. Rackham, editors. Light as an ecological factor. Blackwell, Oxford.

Lythgoe, J. N. 1968. Visual pigments and visual range underwater. Vision Research 8:997–1011.

Lythgoe, J. N. 1972. The adaptation of visual pigments to the photic environment. Pages 566–603 *in* H. J. A. Dartnall, editor. The handbook of sensory physiology. Springer, Berlin.

Lythgoe, J. N. 1984. Visual pigments and environmental light. Vision Research 24:1539–1550.

Lythgoe, J. N., W. R. A. Muntz, J. C. Partridge, J. Shand, and D. McB. Williams. 1994. The ecology of the visual pigments of snappers (Lutjanidae) on the Great Barrier Reef. Journal of Comparative Physiology A 174:461–467.

Lythgoe, J. N., and J. C. Partridge. 1991. The modelling of optimal visual pigments of dichromatic teleosts in green coastal waters. Vision Research 31:361–371.

MacLeod, D. I. A., and R. M. Boynton. 1979. Chromaticity diagram showing cone excitation by stimuli of equal luminance. Journal of the Optical Society of America A:1183–1186.

MacNichol, E. F. 1986. A unifying presentation of photopigment spectra. Vision Research 26:1543–1556.

Magnuson-Stevens Fishery Conservation and Management Act. 2007. . Page 178.

Maia, R., H. Gruson, J. A. Endler, and T. E. White. 2019. pavo 2: New tools for the spectral and spatial analysis of colour in r. Methods in Ecology and Evolution 10:1097–1107.

Markowitz, E. H., E. J. Dawson, N. E. Charriere, B. K. Prohaska, S. K. Rohan, and L. L. Britt. 2022. Results of the 2021 eastern and northern Bering Sea continental shelf bottom trawl survey of groundfish and invertebrate fauna. Page 227. U.S Department of Commerce.

Marshall, N. J. 2000. The visual ecology of reef fish colours. Pages 83–120 *in* Y. Espmark, T. Amundsen, and G. Rosenquist, editors. Animal signals: Signalling and signal design in animal communication. Tapir Academic Press, Trondheim, Norway.

Mazur, M. M., and D. A. Beauchamp. 2003. A comparison of visual prey detection among species of piscivorous salmonids: Effects of light and low turbidities. Environmental Biology of Fishes 67:397–405.

McCarthy, A., T. Honkalehto, N. Lauffenburger, and A. De Robertis. 2020. Results of the acoustic-trawl survey of walleye pollock (*Gadus chalcogrammus*) on the U.S. Bering Sea Shelf in June - August 2018 (DY1807). Page 83. AFSC Processed Report, Alaska Fisheries Science Center, NOAA, National Marine Fisheries Service., 7600 Sand Point Way NE, Seattle WA 98115.

McFarland, W. N., and E. R. Loew. 1983. Wave produced changes in underwater light and their relations to vision. Pages 173–184 *in* D. L. G. Noakes, editor. Predators and prey in fishes: proceedings of the 3rd biennial conference on the Ethology and Behavioral Ecology of Fishes, held at Normal, Illinois, U.S.A., May 19-22, 1981. W. Junk ; Distributors for the United States and Canada, Kluwer Boston, The Hague ; Boston : Hingham, MA, U.S.A.

McFarland, W. N., and F. W. Munz. 1975. Part III: The evolution of photopic visual pigments in fishes. Vision Research 15:1071–1080.

Munz, F. W., and W. N. McFarland. 1973. The significance of spectral position in the rhodopsins of tropical marine fishes. Vision Research 13:1829-IN1.

Naik, P., E. J. D'Sa, H. do R. Gomes, J. I. Goés, and C. B. Mouw. 2013. Light absorption properties of southeastern Bering Sea waters: Analysis, parameterization and implications for remote sensing | Elsevier Enhanced Reader. Remote Sensing of Environment 134:120–134.

NOAA. 2023, April 25. Chlorophyll from NASA VIIRS Near-Real-Time 2012-2022. Chlorophyll from NASA VIIRS Near-Real-Time. https://polarwatch.noaa.gov/catalog/.

NOAA Fisheries: Landings. 2023. . https://www.fisheries.noaa.gov/foss/f?p=215:200:5163805155355:Mail::::

Novales Flamarique, I. 2000. The ontogeny of ultraviolet sensitivity, cone disappearance and regeneration in the sockeye salmon *Oncorhynchus nerka*. Journal of Experimental Biology 203:1161–1172.

Novales Flamarique, I. 2005. Temporal shifts in visual pigment absorbance in the retina of Pacific salmon. Journal of Comparative Physiology A 191:37–49.

Novales Flamarique, I. N., and C. W. Hawryshyn. 1993. Spectral characteristics of salmonid migratory routes from southern Vancouver Island (British Columbia). Canadian Journal of Fisheries and Aquatic Sciences 50:1706–1716.

Oksanen, J., G. L. Simpson, F. Guillaume Blanchet, R. Kindt, P. Legendre, P. R. Minchin, R. B. O'Hara, P. Solymos, M. H. H. Stevens, E. Szoecs, H. Wagner, M. Barbour, M. Bedward, B. Bolker, D. Borcard, G. Carvalho, M. Chirico, M. De Caceres, S. Durand, H. B. A. Evangelista, R. FitzJohn, M. Friendly, B. Furneaux, G. Hannigan, M. O. Hill, L. Lahti, D. McGlinn, M.-H. Ouellette, E. R. Cunha, T. Smith, A. Stier, C. J. F. Ter Braak, and J. Weedon. 2022. vegan:: community ecology package.

Olla, B. L., M. W. Davis, and C. Rose. 2000. Differences in orientation and swimming of walleye pollock (*Theragra chalcogramma*) in a trawl net under light and dark conditions: Concordance between field and laboratory observations. Fisheries Research 41:261–266.

Olla, B. L., M. W. Davis, and C. B. Schreck. 1997a. Effects of simulated trawling on sablefish and walleye pollock: the role of light intensity, net velocity and towing duration. Journal of Fish Biology 50:1181–1194.

Olla, B. L., M. W. Davis, and C. B. Schreck. 1997b. Effects of simulated trawling on sablefish and walleye pollock: the role of light intensity, net velocity and towing duration. Journal of Fish Biology 50:1181–1194.

Press, W. H., B. P. Flannery, S. A. Teukolsky, and W. T. Vetterling. 1987. Numerical Recipes in Pascal. Cambridge University Press, Cambridge.

R Core Team. 2023. R: A language and environment for statistical computing. R Foundation for Statistical Computing, https://www.Rproject.org/.

Renoult, J. P., A. Kelber, and H. M. Schaefer. 2017. Colour spaces in ecology and evolutionary biology. Biological Reviews 92:292–315.

RGB Photoronics GmbH. 2020, December 15. Waves spectrometer. Broadcom, Kelheim.

Rohan, S. K., S. Kotwicki, K. A. Kearney, J. A. Schulien, E. A. Laman, E. D. Cokelet, D. A. Beauchamp, L. L. Britt, K. Y. Aydin, and S. G. Zador. 2021. Using bottom trawls to monitor subsurface water clarity in marine ecosystems. Progress in Oceanography 194:102554, doi: https://doi.org/10.1016/j.pocean.2021.102554.

Sasaki, H., S. Saitoh, and M. Kishino. 2001. Bio-optical properties of seawater in the Western Subarctic Gyre and Alaskan Gyre in the subarctic North Pacific and the Southern Bering Sea during the summer of 1997. Journal of Oceanography 57:275–284.

Senko, J. F. 2022. Net illumination reduces fisheries bycatch, maintains catch value, and increases operational efficiency. Current Biology 32:911–918.

Siddon, E. 2022. Ecosystem status report 2022: Eastern Bering Sea, stock assessment and fishery evaluation report. Page 227. North Paci c Fishery Management Council, 1007 West 3rd Ave., Suite 400, Anchorage, Alaska 99501.

Southwood, A., K. Fritsches, R. Brill, and Y. Swimmer. 2008. REVIEW: Sound, chemical, and light detection in sea turtles and pelagic fishes: sensory-based approaches to bycatch reduction in longline fisheries. Endangered Species Research 5:225–238.

Southworth, L. K., F. C. Ratcliffe, I. S. M. Bloor, J. Emmerson, D. Watson, D. Beard, and M. J. Kaiser. 2020. Artificial light improves escapement of fish from a trawl net. Journal of the Marine Biological Association of the United Kingdom 100:267–275.

Stevenson, D. E., and R. R. Lauth. 2019. Bottom trawl surveys in the northern Bering Sea indicate recent shifts in the distribution of marine species. Polar Biology 42:407–421.

Stienessen, S. C., T. Honkalehto, N. E. Lauffenburger, P. H. Ressler, and L. L. Britt. 2022. Acoustic vessel-of-opportunity (AVO) index for midwater Bering Sea walleye pollock, 2021. Page 24. AFSC Processed Report, Alaska Fisheries Science Center, NOAA, National Marine Fisheries Service., 7600 Sand Point Way NE, Seattle WA 98115.

Stram, D., and J. N. Ianelli. 2009. Eastern Bering Sea pollock trawl fisheries: Variation in salmon bycatch over time and space. Pages 827–850 American Fisheries Society Symposium.

Stram, D. L., and J. N. Ianelli. 2015. Evaluating the efficacy of salmon bycatch measures using fishery-dependent data. ICES Journal of Marine Science 72:1173–1180.

Tyler, J. E., and R. W. Preisendorfer. 1962. IV. Transmission of energy within the sea 8. Light. Pages 397–448 *in* M. N. Hill, editor. The sea, Volume 1: Physical Oceanography. Harvard University Press, Cambridge, Mass, United States.

Vorobyev, M., J. Marshall, D. Osorio, N. Hempel de Ibarra, and R. Menzel. 2001. Colourful objects through animal eyes. Color Research & Application 26:S214–S217.

Vorobyev, M., and D. Osorio. 1998. Receptor noise as a determinant of colour thresholds. Proceedings of the Royal Society of London. Series B: Biological Sciences 265:351–358.

Walker, R. V., and K. W. Myers. 2009. Behavior of Yukon River Chinook salmon in the Bering Sea as inferred from archival tag data. North Pacific Anadromous Fish Commission Bulletin 5:121–130.

Walker, R. V., V. V. Sviridov, S. Urawa, and T. Azumaya. 2007. Spatio-temporal variation in vertical distributions of Pacific salmon in the ocean. North Pacific Anadromous Fish Commission Bulletin 4:193–201.

Wallace, A. R. 1891. Natural selection and tropical nature: Essays on descriptive and theoretical biology. 2nd edition. Macmillan and Company., London.

Walls, G. L. 1942. The vertebrate eye and its adaptive radiation. Cranbrook Institute of Science., Bloomfield Hills, Michigan.

Walsh, S. J., and W. M. Hickey. 1993. Behavioural reactions of demersal fish to bottom trawls at various light conditions. Pages 68–76 ICES Marine Science Symposium.

Wardle, C. S. 1983. Fish reaction to towed fishing gears. Pages 168–195 *in* A. G. MacDonald and I. G. Priede, editors. Experimental Biology at Sea. Academic Press, London.

Welch, D. W., A. D. Porter, and E. L. Rechisky. 2021. A synthesis of the coast-wide decline in survival of West Coast Chinook Salmon (*Oncorhynchus tshawytscha*, Salmonidae). Fish and Fisheries 22:194–211.

Wilkins, L., N. J. Marshall, S. Johnsen, and D. Osorio. 2016. Modelling fish colour constancy, and the implications for vision and signalling in water. Journal of Experimental Biology 219:1884–1892.

Yao, Y., T. Li, X. Zhu, and X. Wang. 2022. Characteristics of water masses and bio-optical properties of the Bering Sea shelf during 2007–2009. Acta Oceanologica Sinica 41:140–153.

Yentsch, C. 1960. The influence of phytoplankton pigments on the colour of seawater. Deep Sea Research 53:1–9.

Yochum, N., D. R. Bryan, L. L. Britt, B. A. Berejikian, R. Haehn, S. McEntire, R. Towler, J. Atkins, B. Gadberry, and P. Irvin. 2022. Evaluating Chinook salmon (*Oncorhynchus tshawytscha*) response to artificial light in support of bycatch mitigation. Canadian Journal of Fisheries and Aquatic Sciences 79:912–924.

Yochum, N., M. Stone, K. Breddermann, B. A. Berejikian, J. R. Gauvin, and D. J. Irvine. 2021. Evaluating the role of bycatch reduction device design and fish behavior on Pacific salmon (*Oncorhynchus spp.*) escapement rates from a pelagic trawl. Fisheries Research 236:105830.

Zador, S. G. 2015. Ecosystem considerations 2015 Status of Alaska's marine ecosystems report. North Pacific Fishery Management Council, 1007 West 3rd Ave., Suite 400, Anchorage, Alaska 99501.

Zhang, H. 1997. Why do animals have the color vision systems that they have? Cornell University, Ithica, NY.

Zhang, X. M., and T. Arimoto. 1993. Visual physiology of walleye pollock (*Theragra chalcogramma*) in relation to capture by trawl nets. Pages 113–116 ICES Marine Science Symposium.

**Appendix A.**

The mean and standard deviation (SD) of xmax for each fish specimen. The individual fish on each day were iteratively numbered according to the date they were processed.

| Species | Date | Specimen | Cell type | Spectral group | Mean $x_{max}$ | SD | Min $x_{max}$ | Max $x_{max}$ | Spectral class | Number of samples |
|---|---|---|---|---|---|---|---|---|---|---|
| *Gadus chalcogrammus* | 3/20/2018 | 2 | c | SWC | 447.00 | 0.00 | 447 | 447 | blue | 2 |
| | 3/18/2018 | 1 | c | SWC | 450.00 | 0.00 | 450 | 450 | blue | 2 |
| | 3/22/2018 | 1 | c | SWC | 451.00 | 4.24 | 448 | 454 | blue | 2 |
| | 3/20/2018 | 2 | c | MWC | 518.83 | 4.20 | 503 | 522 | blue-green (cyan) | 18 |
| | 3/18/2018 | 1 | c | MWC | 519.00 | 2.55 | 515 | 521 | blue-green (cyan) | 5 |
| | 3/18/2018 | 1 | t | SWC | 514.64 | 3.61 | 506 | 520 | blue-green (cyan) | 22 |
| | 3/22/2018 | 1 | t | SWC | 515.56 | 3.47 | 508 | 520 | blue-green (cyan) | 9 |
| | 3/20/2018 | 2 | t | SWC | 518.86 | 1.77 | 516 | 521 | blue-green (cyan) | 7 |
| | 3/18/2018 | 1 | r | rod | 505.20 | 2.86 | 502 | 509 | blue-green (cyan) | 5 |
| | 3/20/2018 | 2 | r | rod | 511.67 | 7.51 | 503 | 516 | blue-green (cyan) | 3 |
| *Oncorhynchus tshawytscha* (cont.) | 4/25/2019 | 2 | c | SWC | 435.75 | 2.22 | 433 | 438 | blue | 4 |
| | 3/18/2018 | 1 | c | SWC | 439.00 | | 439 | 439 | blue | 1 |
| | 3/21/2018 | 1 | c | MWC | 518.00 | | 518 | 518 | blue-green (cyan) | 1 |
| | 4/25/2019 | 1 | c | MWC | 518.40 | 4.56 | 515 | 526 | blue-green (cyan) | 5 |

| Species | Date | Specimen | Cell type | Spectral group | Mean $x_{max}$ | SD | Min $x_{max}$ | Max $x_{max}$ | Spectral class | Number of samples |
|---|---|---|---|---|---|---|---|---|---|---|
| *Oncorhynchus tshawytscha* | 3/19/2018 | 2 | c | MWC | 521.67 | 8.39 | 512 | 527 | blue-green (cyan) | 3 |
| | 4/25/2019 | 2 | c | MWC | 544.00 | | 544 | 544 | green | 1 |
| | 4/25/2019 | 1 | c | MWC | 545.33 | 7.02 | 538 | 552 | green | 3 |
| | 4/25/2019 | 2 | t | SWC | 432.00 | | 432 | 432 | blue | 1 |
| | 3/18/2018 | 1 | t | SWC | 515.50 | 2.12 | 514 | 517 | blue-green (cyan) | 2 |
| | 4/25/2019 | 2 | t | SWC | 517.00 | 3.16 | 512 | 520 | blue-green (cyan) | 5 |
| | 3/21/2018 | 1 | t | SWC | 519.00 | 7.07 | 514 | 524 | blue-green (cyan) | 2 |
| | 3/19/2018 | 2 | t | SWC | 521.00 | 4.58 | 517 | 526 | blue-green (cyan) | 3 |
| | 4/25/2019 | 1 | t | SWC | 530.00 | | 530 | 530 | blue-green (cyan) | 1 |
| | 4/25/2019 | 1 | t | SWC | 535.00 | | 535 | 535 | green | 1 |
| | 4/25/2019 | 2 | t | SWC | 549.33 | 4.16 | 546 | 554 | green | 3 |
| | 3/18/2018 | 1 | r | rod | 496.00 | | 496 | 496 | blue-green (cyan) | 1 |
| | 3/21/2018 | 1 | r | rod | 504.00 | 2.83 | 502 | 506 | blue-green (cyan) | 2 |
| | 4/25/2019 | 3 | r | rod | 509.00 | | 509 | 509 | blue-green (cyan) | 1 |
| | 4/25/2019 | 1 | r | rod | 514.50 | 6.36 | 510 | 519 | blue-green (cyan) | 2 |

**Appendix B.**

Comprehensive list of trawl line and netting used in the spectral reflectance analysis.

| ID | Trade name | Manu-facturer | Country of origin | Dealer | New/ Used | Com-ponent | Primary color | 2nd color | 3rd color | Material |
|---|---|---|---|---|---|---|---|---|---|---|
| 1 | Perlon | Hampidjan | Lithuania | Hampidjan-Canada | new | line | yellow | white | | polysulphone/poly ethylene blend |
| 2 | Magnet Compact | Hampidjan | Lithuania | Hampidjan-Canada | new | mesh | yellow | orange | | polyethylene braided twine net |
| 3 | Tiptolon | Lankhorst | Netherlands | Dantrawl | new | line | yellow | green | | PE/PP copolymer, 12-strand braided rope, 32mm |
| 4 | Euroline Premium | Euronete | Portugal, India, Brazil, France | Dantrawl | new | mesh | yellow | green | | PE braided twine, used in netting |
| 5 | Euroline Premium | Euronete | Portugal, India, Brazil, France | Dantrawl | new | mesh | yellow | green | | PE braided twine, used in netting |
| 6 | Euroline Premium Plus | Euronete | Portugal, India, Brazil, France | Net Systems, Dantrawl | new | mesh | yellow | green | | PE braided, knotted, 16 carrier twine |
| 7 | Euroline Premium Plus | Euronete | Portugal, India, | LFS | new | mesh | yellow | gold | | polyethylene, 4.5mm braided twine |

| ID | Trade name | Manu-facturer | Country of origin | Dealer | New/ Used | Com-ponent | Primary color | 2nd color | 3rd color | Material |
|---|---|---|---|---|---|---|---|---|---|---|
| | | | Brazil, France | | | | | | | |
| 8 | Euroline Premium Plus | Euronete | Portugal, India, Brazil, France | Dantrawl | new | mesh | yellow | gold | | PE braided twine, used in netting |
| 9 | Euro Premium Plus | Lankhorst | Netherlands | LFS | new | mesh | yellow | blue | | polyethylene, braided 4.5mm double |
| 10 | polymax Ultra | Redes-Salinas | Spain | LFS | new | mesh | yellow | blue | | polyethylene, braided 6mm single strand netting |
| 11 | polyethylene 6mm | King Chou Marine | Taiwan | Amack Inc. | new | mesh | yellow | green | | polyethylene 6mm x 77.5 mm 59, double |
| 12 | Magnet Yellow | Hampidjan | Lithuania | Hampidjan-Canada | new | mesh | yellow | blue | white | polyethylene braided netting |
| 13 | polyethylene braided | Fortune Net and Twine | Philippines | Fortune Net and Twine | new | mesh | yellow | | | polyethylene braided knotted net |
| 14 | Advant | Hampidjan | Lithuania | Hampidjan-Canada, Swan Net | new | line | yellow | | | Dyneema braided twine Thin |

| ID | Trade name | Manu-facturer | Country of origin | Dealer | New/ Used | Com-ponent | Primary color | 2nd color | 3rd color | Material |
|---|---|---|---|---|---|---|---|---|---|---|
| 15 | Braided polyethylene trawl net | Diamond Nets | USA | Net Systems | new | mesh | orange | green | | polyethylene braided knotted twine |
| 16 | Poly Twine | | Mexico | NET Systems | new | line | orange | blue | | PE braided twine, used in netting |
| 17 | polymax | Redes-Salinas | Spain | LFS | new | mesh | orange | blue | | polyethylene, 16 strand braided, 4mm double |
| 18 | Poly Twine | Euronete | Portugal, India, Brazil, France | Net Systems, Dantrawl | new | line | orange | | | polyethylene braided twine |
| 19 | Standard Orange | Garware Technical Fibres | India | Garware Technical Fibres | new | mesh | orange | | | polyethylene braided netting |
| 20 | Magnet Compact | Hampidjan | Lithuania | Hampidjan-Canada | new | line | yellow | orange | | PE braided twine, used in netting |
| 21 | Advant | Hampidjan | Lithuania | Hampidjan-Canada | new | line | yellow | | | Dyneema braided twine Thick |
| 22 | Floatrope | Hampidjan | Lithuania | Swan Net | new | line | yellow | | | PE jacket, braided 8-strand, PA core |
| 23 | Polypropylene 24mm | King Chou Marine | Taiwan | Amack Inc. | new | line | green | | | polypropylene medium hard lay rope 24mm |

| ID | Trade name | Manu-facturer | Country of origin | Dealer | New/ Used | Com-ponent | Primary color | 2nd color | 3rd color | Material |
|---|---|---|---|---|---|---|---|---|---|---|
| 24 | Nylex Rope | Hampidjan | Lithuania | Hampidjan-Canada | new | line | green | | | PA (nylon) 12-strand used in netting |
| 25 | Floatrope | Hampidjan | Lithuania | Swan Net | new | line | green | | | PE jacket, braided 8-strand, PA core |
| 26 | Nylex | Hampidjan | Lithuania | Swan Net | new | line | red | | | PA (nylon) 12-strand used in netting |
| 27 | Olivine | Garware | India | NET Systems | new | line | green | orange | | PE braided twine |
| 28 | Magnet Green | Hampidjan | Lithuania | Hampidjan-Canada | new | mesh | green | white | | polyethylene braided single strand netting |
| 29 | Magnet Green | Hampidjan | Lithuania | Hampidjan-Canada | new | mesh | green | white | | polyethylene braided double strand netting |
| 30 | polyethylene 5mm | King Chou Marine | Taiwan | Amack Inc. | new | mesh | green | red | | polyethylene 5mm x 75 mm 59, double |
| 31 | Magnet Compact | Hampidjan | Lithuania | Hampidjan-Canada | new | line | green | orange | | polyethylene braided twine thick |
| 32 | polyethylene 4mm | King Chou Marine | Taiwan | Amack Inc. | new | mesh | green | | | polyethylene 4mm x 77.5 mm 59, single |

| ID | Trade name | Manu-facturer | Country of origin | Dealer | New/ Used | Com-ponent | Primary color | 2nd color | 3rd color | Material |
|---|---|---|---|---|---|---|---|---|---|---|
| 33 | polyethylene braided | Fortune Net and Twine | Philippines | Fortune Net and Twine | new | mesh | green | | | polyethylene braided knotted net |
| 34 | Magnet standard | Hampidjan | Lithuania | Hampidjan-Canada | new | mesh | green | | | polyethylene 4mm braided single net |
| 35 | Magnet Green Standard | Hampidjan | Lithuania | Hampidjan-Canada | new | mesh | green | | | polyethylene braided double strand netting |
| 36 | Green PE | Redes-Salinas | Spain | LFS | new | mesh | green | | | polyethylene, braided, 5mm double netting |
| 37 | Twisted knotted nylon trawl net | Diamond Nets | USA | Net Systems | new | mesh | green | | | nylon twisted dyed twine |
| 38 | Standard Green | Garware Technical Fibres | India | Garware Technical Fibres | new | mesh | green | | | polyethylene braided netting |
| 39 | Poly Twine | Cotesi | Portugal | Dantrawl | new | line | green | | | PE braided twine, used in netting |
| 40 | Poly Twine | Euronete | Portugal | Net Systems, Dantrawl | new | line | green | | | PE braided twine, used in netting |
| 41 | polyethylene braided | Fortune Net and Twine | Philippines | Fortune Net and Twine | new | mesh | aqua | | | polyethylene braided knotted net |

| ID | Trade name | Manu-facturer | Country of origin | Dealer | New/ Used | Com-ponent | Primary color | 2nd color | 3rd color | Material |
|---|---|---|---|---|---|---|---|---|---|---|
| 42 | Utzon | Hampidjan | Lithuania | Hampidjan-Canada | new | line | green | | | braided nylon twine |
| 43 | Kraft rope | Hampidjan | Lithuania | Hampidjan-Canada | new | line | green | blue | | twisted polyethylene |
| 44 | DynIce | Hampidjan | Lithuania | Hampidjan-Canada | new | line | white | | | Dyneema 10mm |
| 45 | Premium Double Braid | Continental Western | USA | Net Systems | new | line | white | | | PA (nylon) braided twine, used in lashing |
| 46 | Magnet Gray Thick | Hampidjan | Lithuania | Swan Net | new | mesh | grey | white | blue | PE braided twine, used in netting |
| 47 | Coverbraided DynIce 75 | Hampidjan | Lithuania | Hampidjan-Canada | new | line | grey | | | DynIce rope wrapped in Dyneema braided twine |
| 48 | Dynet | Hampidjan | Lithuania | Hampidjan-Canada | new | mesh | grey | | | Dyneema knotless netting |
| 49 | DynIce | Hampidjan | Lithuania | Hampidjan-Canada | new | line | grey | | | Dyneema 12 strand braided rope |
| 50 | Utra Cross Silver | Nichimo | Japan | Net Systems | new | mesh | grey | | | Dyneema knotless 4-strand netting |
| 51 | Dynet | Hampidjan | Lithuania | Hampidjan-Canada | new | mesh | grey | | | Dyneema double knot braided net |

| ID | Trade name | Manu-facturer | Country of origin | Dealer | New/ Used | Com-ponent | Primary color | 2nd color | 3rd color | Material |
|---|---|---|---|---|---|---|---|---|---|---|
| 52 | polyethylene twisted | Fortune Net and Twine | Phillippines | Fortune Net and Twine | new | mesh | black | yellow | | polyethylene twisted knotted net |
| 53 | polyethylene braided | Fortune Net and Twine | Phillippines | Fortune Net and Twine | new | mesh | black | | | polyethylene braided knotted double strand net |
| 54 | polyethylene twisted | Fortune Net and Twine | Phillippines | Fortune Net and Twine | new | mesh | black | | | polyethylene twisted knotted net |
| 55 | Premium Double Braid | Continental Western | USA | Net Systems | new | line | black | | | PA (nylon) braided twine, used in lashing |
| 56 | Bluesteel | Continental Western | USA | Dantrawl | new | line | blue | blue | | PP/PE copolymer, 3-strand twisted rope, 14mm |
| 57 | Chaffer Hula | Continental Western | USA | Dantrawl | new | line | blue | | | PP/PE copolymer rope |
| 58 | Magnet Red | Hampidjan | Lithuania | Hampidjan-Canada | new | line | red | blue | white | polyethylene braided twine very thin |
| 59 | Sapphire | Garware Technical Fibres | India | NET Systems | new | mesh | blue | yellow | | PE braided twine, used in netting |
| 60 | polymax | Redes-Salinas | Spain | LFS | new | mesh | blue | | | polyethylene, braided 4mm single strand net |

| ID | Trade name | Manu-facturer | Country of origin | Dealer | New/ Used | Com-ponent | Primary color | 2nd color | 3rd color | Material |
|---|---|---|---|---|---|---|---|---|---|---|
| 61 | polyethylene 4mm | King Chou Marine | Taiwan | Amack Inc. | new | mesh | blue | | | polyethylene 4mm x 77.5 mm 59, single |
| 62 | polyethylene 4mm Double | King Chou Marine | Taiwan | Amack Inc. | new | mesh | blue | | | polyethylene 4mm x 77.5 mm 59, double |
| 63 | Perlon | Hampidjan | Lithuania | Hampidjan-Canada | new | line | green | white | | polysulphone/polyethylene blend |
| 64 | Perlon | Hampidjan | Lithuania | Hampidjan-Canada | new | line | red | white | | polysulphone/polyethylene blend |
| 65 | Floatrope | Hampidjan | Lithuania | Hampidjan-Canada | new | line | red | | | PE Jacket, braided 8-strand, PA core |
| 66 | Nylex | Hampidjan | Lithuania | Hampidjan-Canada | new | line | blue | | | PA (nylon) 12-strand used in netting |
| 67 | Kraft rope | Hampidjan | Lithuania | Hampidjan-Canada | new | line | white | blue | | twisted polyethylene |
| 68 | Magnet Gray medium | Hampidjan | Lithuania | Swan Net | new | mesh | gray | white | blue | PE braided twine, used in netting |
| 69 | Magnet Gray thin | Hampidjan | Lithuania | Swan Net | new | mesh | gray | white | blue | PE braided twine, used in netting |
| 70 | Sapphire | Garware Technical Fibres | India | Garware Technical Fibres | new | mesh | blue | yellow | | PE braided twine, used in netting |

| ID | Trade name | Manu-facturer | Country of origin | Dealer | New/ Used | Com-ponent | Primary color | 2nd color | 3rd color | Material |
|---|---|---|---|---|---|---|---|---|---|---|
| 71 | Utzon | Hampidjan | Lithuania | Hampidjan-Canada | new | line | yellow | | | braided nylon twine |
| 72 | Magnet Red | Hampidjan | Lithuania | Hampidjan-Canada | new | line | red | blue | white | polyethylene braided twine thick |
| 73 | Utzon | Hampidjan | Lithuania | Hampidjan-Canada | new | line | white | | | braided nylon twine thick |
| 74 | Utzon | Hampidjan | Lithuania | Hampidjan-Canada | new | line | white | | | braided nylon twine thin |
| 75 | Utzon | Hampidjan | Lithuania | Hampidjan-Canada | new | line | white | | | Twisted nylon twine thick |
| 76 | Olivine | Garware Technical Fibres | India | NET Systems | new | mesh | green | orange | | PE braided netting |
| 77 | Utzon | Hampidjan | Lithuania | Hampidjan-Canada | new | line | red | | | braided nylon twine thin |
| 78 | Utzon | Hampidjan | Lithuania | Hampidjan-Canada | new | line | blue | | | braided nylon twine thin |
| 79 | Coverbraided DynIce 75 | Hampidjan | Lithuania | Hampidjan-Canada | new | line | black | | | DynIce rope wrapped in Dyneema braided twine |
| 80 | Dynet Braid 60 | Hampidjan | Lithuania | Hampidjan-Canada | new | line | grey | | | Dyneema braided twine thick |
| 81 | Dynet Braid 60 | Hampidjan | Lithuania | Hampidjan-Canada | new | line | grey | | | Dyneema braided twine medium |

| ID | Trade name | Manu-facturer | Country of origin | Dealer | New/ Used | Com-ponent | Primary color | 2nd color | 3rd color | Material |
|---|---|---|---|---|---|---|---|---|---|---|
| 82 | Dynet Braid 60 | Hampidjan | Lithuania | Hampidjan-Canada | new | line | grey | | | Dyneema braided twine thin |
| 83 | Magnet Compact | Hampidjan | Lithuania | Hampidjan-Canada | new | line | green | orange | | polyethylene braided twine thin |
| 84 | Utzon | Hampidjan | Lithuania | Hampidjan-Canada | new | line | orange | | | braided nylon twine thin |
| 90 | Euroline Premium | Euronete | Portugal, India, Brazil, France | Net Systems, Dantrawl | used | mesh | yellow | green | | PE Braided, knotted, 16 carrier twine |
| 91 | polyethylene 4mm | King Chou Marine | Taiwan | Amack Inc. | used | mesh | green | | | polyethylene 4mm x 77.5 mm 59, single |
| 92 | Magnet Yellow | Hampidjan | Lithuania | Hampidjan-Canada, Swan Net | used | mesh | yellow | blue | white | polyethylene braided netting |
| 93 | Sapphire | Garware Technical Fibres | India | Garware Technical Fibres | used | mesh | blue | | | PE braided twine, used in netting |
| 94 | Twisted knotted nylon trawl net | Diamond Nets | USA | Diamond Nets | used | mesh | green | | | nylon twisted dyed twine |
| 95 | Braided polyethyl | Diamond Nets | USA | Diamond Nets | used | mesh | orange | green | | polyethylene braided knotted twine |

| ID | Trade name | Manu-facturer | Country of origin | Dealer | New/ Used | Com-ponent | Primary color | 2nd color | 3rd color | Material |
|---|---|---|---|---|---|---|---|---|---|---|
| | ene trawl net | | | | | | | | | |
| 96 | polyethylene braided | Fortune Net and Twine | Phillippines | Fortune Net and Twine | used | mesh | green | | | polyethylene braided knotted net |

**Appendix C.**

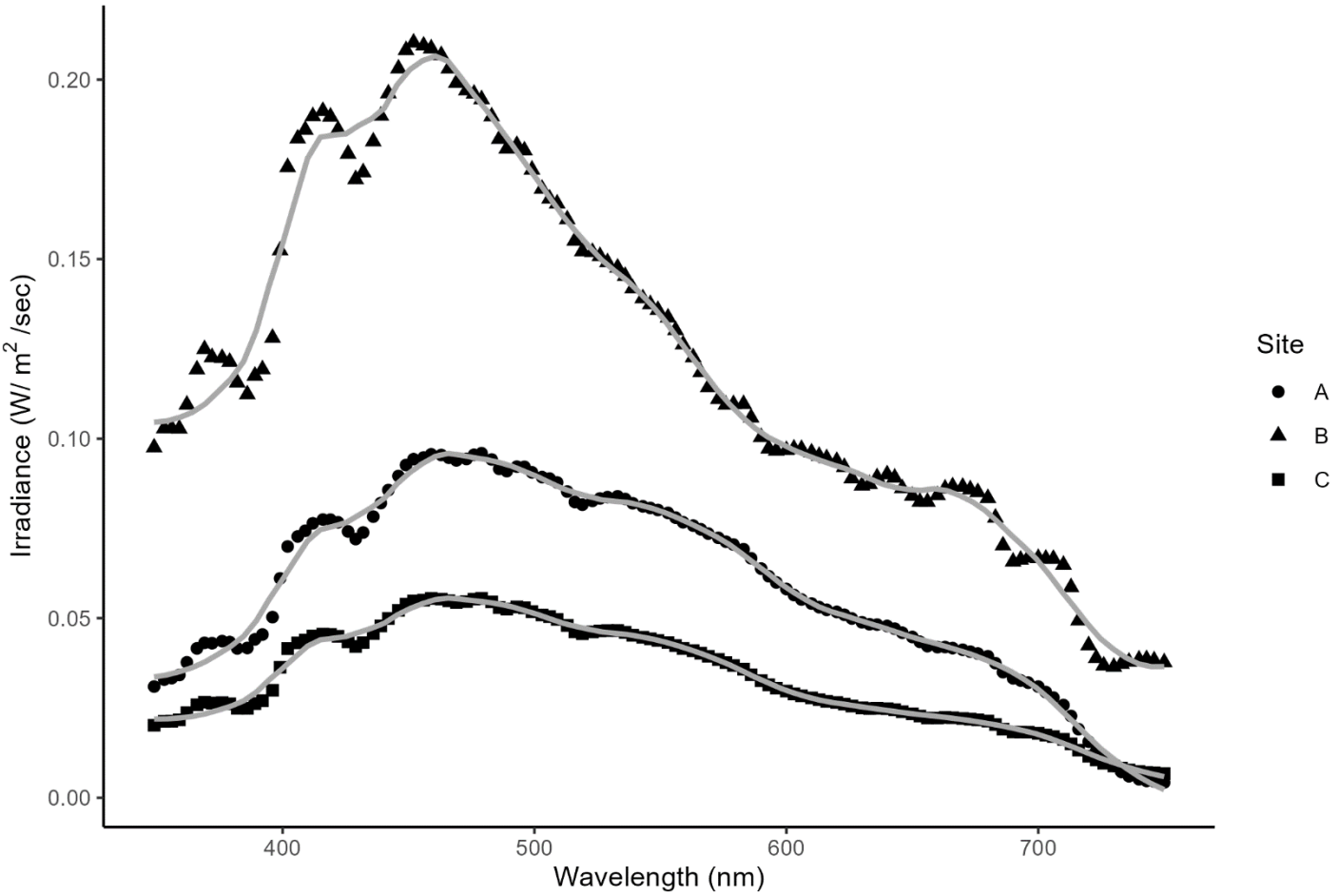


Just-below-surface irradiance for the study sites. Black shapes represent irradiance values at sites A, B, and C. The grey line is a LOESS smoothing (span = 0.2). The wavelength with the highest irradiance at sites A and C was 466 nm and 493 nm at site B.

**Appendix D.**

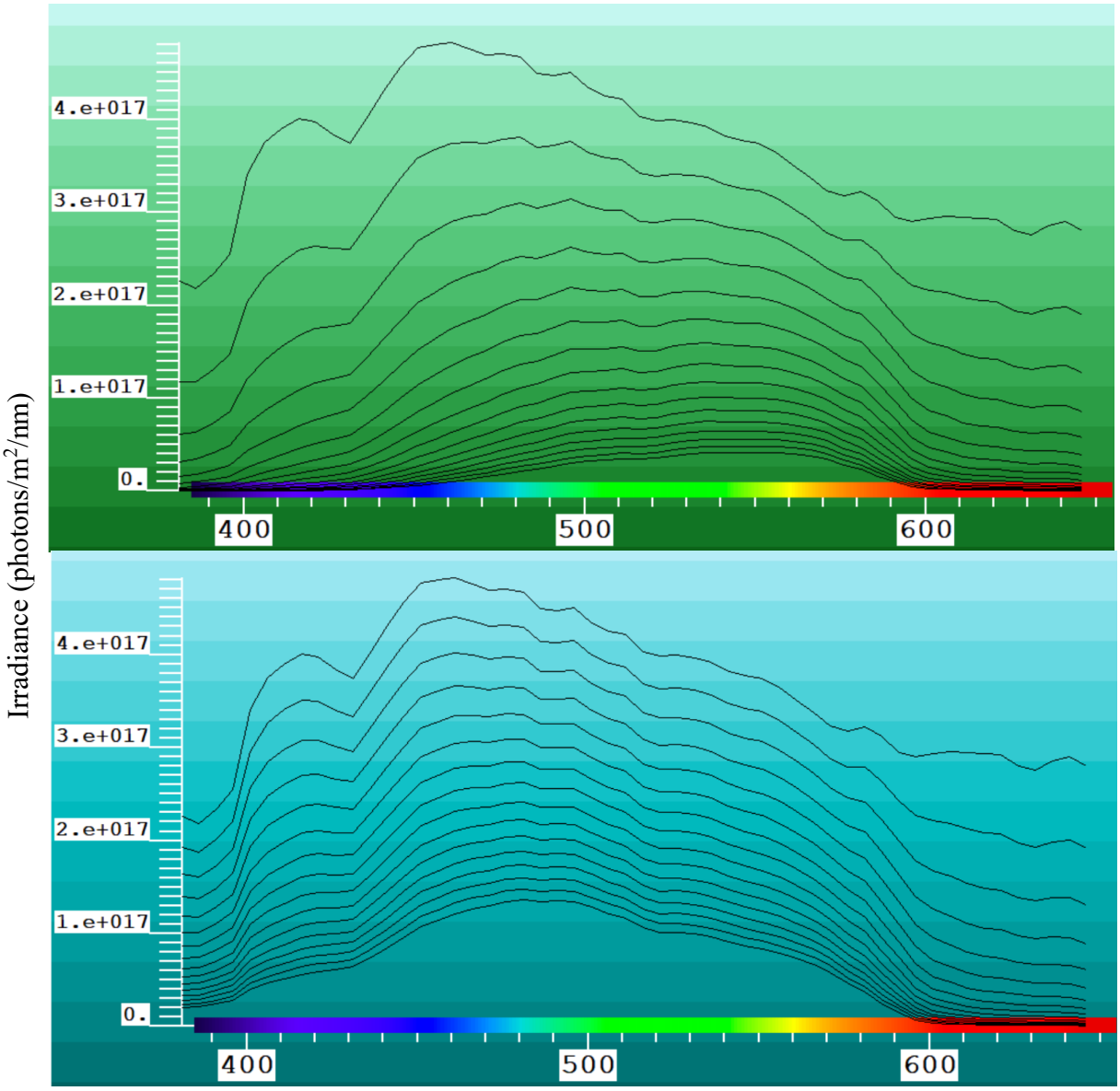


Projection of spectral irradiance from VPModel® with the same chlorophyll a value (5) and DOM values of 0.99 and 0.1 using the just-below-surface irradiance of Site B.